CalVal Jason
CLS.DOS/NT/05.241
Version : 1rev1, January 30, 2006
Nomenclature : SALP-RP-MA-EA-21314-CLS

Ramonville, January 30, 2006

Jason-1 validation and cross calibration activities

Contract No 03/CNES/1340/00-DSO310 - lot2.C

	AUTHORS	COMPANY	DATE	INITIALS
WRITTEN BY	M. Ablain	CLS		
	S. Philipps	CLS		
APPROVED BY	J. Dorandeu	CLS		
QUALITY VISA	M. Destouesse	CLS		
APPLICATION AUTHORISED BY	N.Picot	CNES		

CLS - 8-10 Rue Hermès - Parc Technologique du Canal - 31520 Ramonville St-Agne - FRANCE
Telephone 33 5 61 39 47 00 / Fax 33 5 61 75 10 14

DISTRIBUTION LIST

COMPANY	NAMES	COPIES
CLS/DOS	M.ABLAIN	1 electonic copy
	J.DORANDEU	1 electonic copy
	S.PHILIPPS	1 electonic copy
	V.ROSMORDUC	1 electonic copy
DOC/CLS	DOCUMENTATION	1 electonic copy
CNES	N.PICOT	1 copy + 1 electonic copy
CNES	D.SCHOLLER	1 copy + 1 electonic copy
CNES	J.LAMBIN	1 electonic copy
CNES	S.COUTIN-FAYE	1 electonic copy
CNES	P.SNINI	1 electonic copy
CNES	J.NOUBEL	1 electonic copy

CHRONOLOGY ISSUE

Control Initials	ISSUE	DATE	REASON FOR CHANGE
			Creation

LIST OF ACRONYMS

TBC	To Be Confirmed

List of Tables

List of Figures

Contents

APPLICABLE DOCUMENTS / REFERENCE DOCUMENTS

1 Introduction

This document presents the synthesis report concerning validation activities of Jason-1 GDRs under SALP contract (N° 03/CNES/1340/00-DSO310 Lot2.C) supported by CNES at the CLS Space Oceanography Division. It is divided into three parts: CAL/VAL Jason-1 activities(Lot2.C) - Jason-1 / T/P cross-calibration (Lot2.C) - Validation of GPS and tri-technique CNES orbits (lot4-BC 5761-4-14).

Since the beginning of the mission, Jason-1 data have been analysed and monitored in order to assess the quality of Jason-1 GDR products (AVISO and PODAAC User handbook, [41]) for oceanographic applications. This report is basically concerned with long-term monitoring of the Jason-1 altimeter system, from all GDR products available to date, that is for 4 years of data (cycles 1 to 135). This includes careful monitoring of all altimeter and radiometer parameters, performance assessment, geophysical evaluation and cross-calibration with T/P measurements. Moreover specific studies are presented in this document :

- the performance impact of the new geophysical corrections which be available in the new GDRs realease in 2006, such tidal, atmospheric and MOG2D corrections.
- the impact of a precise orbit based on a GRACE gravity model and tri-technic method,
- the comparisons between the mean sea level and the sea surface temperature for all operational altimeter missions.

This work is routinely performed at CLS and in this frame, besides continuous analyses in terms of altimeter data quality, Jason-1 GDR Quality Assessment Reports (e.g. Ablain et al. 2005 [4]) are produced and associated to data dissemination. Even if only low order statistics are mainly presented here, other analyses including histograms, plots and maps are continuously produced and used in the quality assessment process. The work performed in terms of data quality assessment also includes cross-calibration with other missions, among which the comparison to the T/P mission is essential.

Indeed, it is now well recognized that the usefulness of any altimeter data only makes sense in a multi-mission context, given the growing importance of scientific needs and applications, in particular for operational oceanography. One major objective of the Jason-1 mission is to continue the T/P high precision altimetry and to allow combination with other missions (ENVISAT, GFO). This kind of comparisons between different altimeter missions flying together provides a large number of estimations and consequently efficient long term monitoring of instrument measurements. Of course, other sources of comparisons are also needed, using independent datasets (e.g. Queffeulou et al. 2004 [44], Ray and Beckley 2003 [47], Arnault et al. 2004 [6], Provost et al. 2004 [42]).

2 Processing status

2.1 GDR and CAL/VAL Processing

Jason-1 GDRs from cycle 1 to 135, are used in this report. They have been processed with the same version of the CMA ground processing software (Jason-1 product version "a"). From cycle 136 onward, new Jason-1 products are available, see section 2.3. A report has been carried out for each cycle and is available for the GDR users. The purpose of this document is to report the major features of the data quality from the Jason-1 mission. Moreover, the document is associated with comparison results from T/P GDRs. All these cycle reports are available on AVISO website: http://www.jason.oceanobs.com. In addition to these reports, several meeting (CAVE) have been performed per year to inform the Jason-1 GDR's users about the main results and the studies in progress.

2.2 CAL/VAL status

2.2.1 Missing measurements

This section presents a summary of major satellite events that occurred from cycle 1 to 135. Table 1 gives a status about the number of missing passes (or partly missing) and the associated events for each cycle.
Gyro calibration, Star Tracker unavailability and ground processing issues were the main events which produced missing data from cycle 1 to 64 (2002 and 2003) recalling that ground processing issue will be resolved for the next GDR release.
During year 2004 (cycle 65 to 109), 2 safe hold mode incidents have produced 15 days of missing data due to a wheel anomaly. As result of this incident, only 3 wheels have been available but this has had no impact on scientific applications.
During year 2005 (110-135), most of incidents are due to SEU on C Band (see section 2.4. Few passes have only been impacted every time. Moreover some passes have been edited due to mispointing values out of the thresholds especially at the end of the period. This is mainly due to the star-tracker unavailability.

Jason-1 Cycles	Number of Missing passes	Number of partly missing passes	Events
001	12	0	Science telemetry unavailability
002	16	0	On board Doris anomaly
003	0	1	Gyro-calibration
004	2	5	Gyro-calibration and Science telemetry unavailability
006	1	4	Altimeter echo data unavailability
008	5	0	Ground processing issue

.../...

Jason-1 Cycles	Number of Missing passes	Number of partly missing passes	Events
009	9	3	Poseidon-2 altimeter SEU and Gyro-calibration
010	0	2	Gyro-calibration
014	2	1	Ground processing issue
015	2	1	Ground processing issue
016	1	1	Ground processing issue
019	2	1	Ground processing issue
021	0	1	Star tracker unavailability
023	0	1	Ground processing issue
026	0	2	Gyro-calibration
027	0	2	Gyro-calibration
029	4	2	Ground processing issue
031	1	1	Ground processing issue and Star tracker unavailability
032	38	1	DORIS data unavailability and ground processing issue
035	1	2	Ground processing issue
038	0	4	Ground processing issue
039	0	1	Gyro-calibration
042	8	2	Poseidon-2 altimeter SEU and ground processing issue
045	0	3	Gyro-calibration
046	0	1	Poseidon-2 altimeter SEU
048	0	1	Gyro-calibration
055	1	1	Ground processing issue
061	1	2	Ground processing issue
062	2	1	Ground processing issue
064	0	2	Exceptional calibrations
075	4	0	Poseidon-2 altimeter SEU

.../...

Jason-1 Cycles	Number of Missing passes	Number of partly missing passes	Events
077	69	0	Safe hold mode (15/02/04 to 21/02/04)
078	82	0	Safe hold mode (15/02/04 to 21/02/04)
080	0	1	Calibration over ocean
082	54	0	Failure in module 3 of on board ...
087	0	1	Calibration over ocean
091	25	0	DORIS instrument switch to redundancy and altimeter incident (no C band information)
094	0	1	Under investigation : altimeter incident or star tracker unavailability
099	0	1	Under investigation : altimeter incident or star tracker unavailability
101	0	1	Under investigation : altimeter incident or star tracker unavailability
102	2	0	Altimeter SEU (no C band information)
103	4	1	Altimeter SEU (no C band information)
104	0	1	No data between 21:29:18 and 21:30:07 on November 8th pass 189
106	3	2	Altimeter SEU (no C band information)
108	5	0	Altimeter SEU (no C band information)
114	3	1	Altimeter SEU (no C band information)
115	6	2	2 altimeter SEU incidents (C band) and altimeter initialization procedure.
118	6	2	Altimeter SEU (no C band information)
131	0	7	TRSR2 "elephant packets" anomaly
132	0	1	Altimeter SEU (no C band information)

.../...

Jason-1 Cycles	Number of Missing passes	Number of partly missing passes	Events
133	0	2	Altimeter SEU (no C band information)

Table 1: *M*issing pass status

2.2.2 Edited measurements

Table 2 indicates the cycles which have a larger amount of removed data due to editing criteria (see section 3.2.1). Most of the occurrences correspond to Star Tracker unavailability.
Notice that since cycle 78, the satellite operates with only 3 wheels: the maneuver impact (burn maneuver, yaw transition) is greater than before on the attitude control. Consequently, some measurements can be edited due to higher mispointing values when a maneuver occurs. Further improvements in ground retracking algorithm have been set up in place and this will be resolved in the next GDR release.

Jason-1 Cycles	Comments
003	Pass 1 is removed due to bad orbit quality. The burn maneuver is not correctly taken into accounts on this pass.
006	Pass 56 (in the Pacific ocean) is partly edited due to the bad quality of data. Indeed, the altimetric parameters values are out of the thresholds.
008	All the altimetric parameters are edited for 10% of pass 210 due to the bad quality of all the altimetric parameters as a result of a Star Tracker incident leading to a quite high off nadir angle. A part of pass 087 is edited by the square of the mispointing angle criterion due to a Star Tracker incident.
010	All the altimetric parameters are edited for 15% of pass 210. This is due to the Star Tracker unavailability as for cycle 6.
021	Small part of pass 254 is edited after checking the square of the mispointing angle criterion.
053	Some mispointing angle values are out of threshold. This is due to a satellite maneuver on this pass.
069	Passes 209 to 211 are edited due to the JMR set to default value. This is linked to the safe hold mode on cycle 69 : the JMR has been set on 2 hours after the altimeter.
078	Passes 83 to 85 are edited due to the JMR set to default value. This is linked to the safe hold mode on cycle 88 : the JMR has been set on 2 hours after the altimeter.
084	Pass 84 is partly edited (great mispointing values) due to a yaw flip.
	.../...

Jason-1 Cycles	Comments
089	Pass 167 is partly edited (great mispointing values) due to a yaw flip.
096	Pass 36 is partly edited (great mispointing values) due to a yaw flip.
098	Pass 98 is partly edited (great mispointing values) due to the star-tarcker unavailability.
098	Pass 115 is partly edited (great mispointing values) due to the star-tarcker unavailability.
101	Pass 254 is partly edited (great mispointing values) due to a burn maneuver
102	Pass 37 is partly edited (great mispointing values) due to a yaw flip maneuver
107	Pass 138 is partly edited (great mispointing values) due to a yaw flip maneuver
109	Pass 219 and 220 are partly edited (great mispointing values). Star-tracker is out of the SCAO loop during 2 hours (dark current monitoring).
113	Pass 213 is partly edited (great mispointing values) due to a yaw flip maneuver
119	Pass 190 is partly edited (great mispointing values) due to the star-tarcker unavailability.
122	Passes 142 to 143 were partially edited (great mispointing values). Star-tracker is out of the SCAO loop.
124	Passes 3 and 4 were partially edited (great mispointing values) due to a burn maneuver.
125	Pass 89 is partly edited (great mispointing values) due to a yaw flip maneuver.
131	Pass 190 is partly edited (great mispointing values) due to a yaw flip maneuver.
133	Pass 21 is partly edited (great mispointing values) due to the star-tracker unavailability.
134	Passes 83, 153, 177, 233 and 235 are partly edited (great mispointing values) due to the star-tracker unavailability.
135	Many passes are partly edited (great mispointing values) due to the star-tracker unavailability.

Table 2: *E*dited measurement status

2.3 Jason-1 product version "b"

2.3.1 Models and Standards History

Two versions of the Jason-1 Interim Geophysical Data Records (IGDRs) and Geophysical Data Records (GDRs) have been generated to date. These two versions are identified by the version numbers "a" and "b" in the name of the data products. For example, version "a" GDRs are named "JA1_GDR_2Pa" and version "b" GDRs are named "JA1_GDR_2Pb". Both versions adopt an identical data record format as described in Jason-1 User Handbook and differ only in the models and standards that they adopt. Version "a" I/GDRs were the first version released soon after launch. Version "b" I/GDRs were first implemented operationally from the start of cycle 140 for the IGDRs and cycle 136 for the GDRs. Reprocessing to generate version "b" GDRs for cycles 1-135 will be performed to generated a consistent data set next year (2006). The table below 3 summarizes the models and standards that are adopted in these two versions of the Jason I/GDRs. More details on some of these models are provided in Jason-1 User Handbook document.

Model	Product Version "a"	Product Version "b"
Orbit	JGM3 Gravity Field DORIS tracking data for IGDRs DORIS+SLR tracking data for GDRs	EIGEN-CG03C Gravity Field DORIS tracking data for IGDRs DORIS+SLR+GPS tracking data for GDRs
Altimeter Retracking	MLE3 + 1st order Brown model (mis pointed estimated separately)	MLE4 + 2nd order Brown model : MLE4 simultaneously retrieves the 4 parameters that can be inverted from the altimeter waveforms: epoch, SWH, Sigma0 and mispointing angle. This algorithm is more robust for large off-nadir angles (up to 0.8°).
Altimeter Instrument Corrections	Consistent with MLE3 retracking algorithm.	Consistent with MLE4 retracking algorithm.
Jason Microwave Radiometer Parameters	Using calibration parameters derived from cycles 1-30.	Using calibration parameters derived from cycles 1-115.
Dry Troposphere Range Correction	From ECMWF atmospheric pressures.	From ECMWF atmospheric pressures and model for S1 and S2 atmospheric tides.
Wet Troposphere Range Correction from Model	From ECMWF model	From ECMWF model.
		.../...

Model	Product Version "a"	Product Version "b"
Back up model for Ku-band ionospheric range correction.	Derived from DORIS measurements.	Derived from DORIS measurements.
Sea State Bias Model	Empirical model derived from cycles 19-30 of version "a" data.	Empirical model derived from cycles 11-100 of MLE3 altimeter data with version "b" geophysical models.
Mean Sea Surface Model	GSFC00.1	CLS01
Along Track Mean Sea Surface Model	None (set to default)	None (set to default)
Geoid	EGM96	EGM96
Bathymetry Model	DTM2000.1	DTM2000.1
Inverse Barometer Correction	Computed from ECMWF atmospheric pressures	Computed from ECMWF atmospheric pressures after removing model for S1 and S2 atmospheric tides.
Non-tidal High-frequency Dealiasing Correction	None (set to default)	Mog2D ocean model on GDRs, none (set to default) on IGDRs. Ocean model forced by ECMWF atmospheric pressures after removing model for S1 and S2 atmospheric tides.
Tide Solution 1	GOT99	GOT00.2 + S1 ocean tide . S1 load tide ignored.
Tide Solution 2	FES99	FES2004 + S1 and M4 ocean tides. S1 and M4 load tides ignored.
Equilibrium long-period ocean tide model.	From Cartwright and Taylor tidal potential.	From Cartwright and Taylor tidal potential.
Non-equilibrium long-period ocean tide model.	None (set to default)	Mm, Mf, Mtm, and Msqm from FES2004.
Solid Earth Tide Model	From Cartwright and Taylor tidal potential.	From Cartwright and Taylor tidal potential.
Pole Tide Model	Equilibrium model	Equilibrium model.
Wind Speed from Model	ECMWF model	ECMWF model
Altimeter Wind Speed	Table derived from TOPEX/POSEIDON data.	Table derived from version "a" Jason-1 GDR data.

.../...

Model	Product Version "a"	Product Version "b"
Rain Flag	Derived from TOPEX/POSEIDON data.	Derived from version "a" Jason-1 GDRs.
Ice Flag	Climatology table	Climatology table

Table 3: *M*odels and standards adopted for the Jason-1 product version "a" and product version "b"

2.3.2 Impact of product version "b" for the SSH calculation

2.3.2.1 Editing procedure

The new MLE4 retracking algorithm based on a second-order altimeter echo model is more robust for large off-nadir angles (up to 0.8 degrees). For product version "a" (previous CMA version 6.3), the maximum threshold on square off-nadir angle proposed in Jason-1 User Handbook document was set to 0.16 deg^2. Henceforth, this threshold is too restrictive and has to be set to 0.64 deg^2.

However, this editing criteria had the side effect of removing some bad measurements impacted by rain cells, sigma0 blooms or ice. With the new threshold (0.64 deg^2), these measurements are not rejected any more even though the estimated SSH is not accurate for such waveforms.
Therefore 2 new criteria have to be added to check for data quality:

- Standard deviation on Ku sigma0 $\leq$ 1 dB
- Number measurements of Ku sigma0 $\geq$ 10

The Jason-1 User Handbook suggests the following editing criteria for the version "a" GDRs:

- -0.2 $deg^2 \leq$ square of off-nadir angle from waveforms (off_nadir_angle_ku_wvf) $\leq$ 0.16 deg^2
- sigma0_rms_ku $<$ 0.22 dB (optional criterion)

For the version "b" GDRs these two edit criteria should be replaced by:

- -0.2 $deg^2 \leq$ square of off-nadir angle from waveforms (off_nadir_angle_ku_wvf) $\leq$ 0.64 deg^2
- and sigma0_rms_ku $\leq$ 1.0 dB
- and sig0_numval_ku $\geq$ 10

With these new criteria, the editing gives similar results for both product versions. Most of anomalous SSH measurements are rejected. Please note that some of them are still not detected, in particular close to sea ice. This is due to the ice flag which is not perfect.

2.3.2.2 Impact on mean SSH

Some evolutions have a direct impact on the SSH estimation. The global bias between version "a" and "b" of the products is 1.9 cm :

$$\overline{SSH_{CMA_{7.1}}} = \overline{SSH_{CMA_{6.3}}} - 1.9cm$$

This comes from two main components:

- A very slight effect of the MLE4 retracking and of the new instrumental tables (0.1 cm).
- The improved SSB correction is shifted in average by 2.0 cm in comparison with the previous one

$$\overline{SSB_{CMA_{7.1}}} = \overline{SSB_{CMA_{6.3}}} + 2.0cm$$

For several scientific applications (mean sea level trend, ...), it is important to take this difference in mean SSH into account until all the GDRs cycles are provided with the new ground processing version.

2.3.2.3 Impact on mean SWH and sigma0

MLE4 retracking algorithms has no impact on SWH mean value.
Impact of MLE4 retracking algorithms on sigma0_ku mean value is 0.1 dB (sigma0_ku becoming higher). Please note that the rms on 20 Hz Ku sigma0 has increased as a consequence of the MLE4 inversion scheme.

2.3.2.4 Jason-1 Radiometer wet troposphere correction

The Jason-1 Microwave Radiometer (JMR) has been re-calibrated using data from repeat cycles 1-115. Version "b" GDRs contain the re-calibrated JMR data and some improved algorithms to derive JMR brightness temperatures. The re-calibrated JMR data remove the anomalous jumps observed in the JMR path delays on the version "a" GDRs. As a result of this recalibration a bias of approximately 0.9 cm in the JMR wet path delays exists between the version "a" GDRs from cycle 135 and the version "b" GDRs from cycle 136. This bias will then also affect mean SSH at this transition when JMR wet path delays are used to compute SSH.

A JMR replacement product that contains re-calibrated JMR wet path delay measurements for cycles that are being reprocessed into version "b" GDRs (e.g. cycles < 136) will be released soon. This replacement product can be used to ensure a stable sea surface height time series for precision applications such as mean sea level monitoring. In the meantime, it is preferable to use the EWCMF model wet troposphere correction.

2.4 Data quality during C band SEU

2.4.1 Presentation

During an SEU (Single Event Upset), radiation of particles changes the memory of the onboard computer causing loss of the radiometer measurements in C band. Therefore the ionospheric correction based on dual frequency measurements is impossible. Generally the corresponding GDRs wont be delivered.
The aim of this work is to study the quality of the data in the Ku band in order to be able to diffuse the GDRs even if no ionospheric correction is possible.
For this study we used 22 SEU passes coming from cycles 091 (passes 127 to 129), 102 (passes 187 to 189), 103 (passes 28 to 31), 108 (passes 14 to 18), and 115 (passes 19 to 21 and 28 to 31).

The cycles containing GDRs with SEU were reprocessed in the frame of a study by a Calval type chain. A flag containing the information of SEU was updated in the database and for the case of SEU the ionospheric correction based on dual frequency measurements was replaced by the model ionospheric correction GIM.

2.4.2 Quality of altimeter parameters during SEU

We first verified that the measured altimetric parameters during SEU were fine. The Figure 1 shows the histogram of the square of the off nadir angle from waveforms for the SEU incidences (left). In the right the histogram of passes from cycle 115 without SEU are shown. The histograms are very similar.

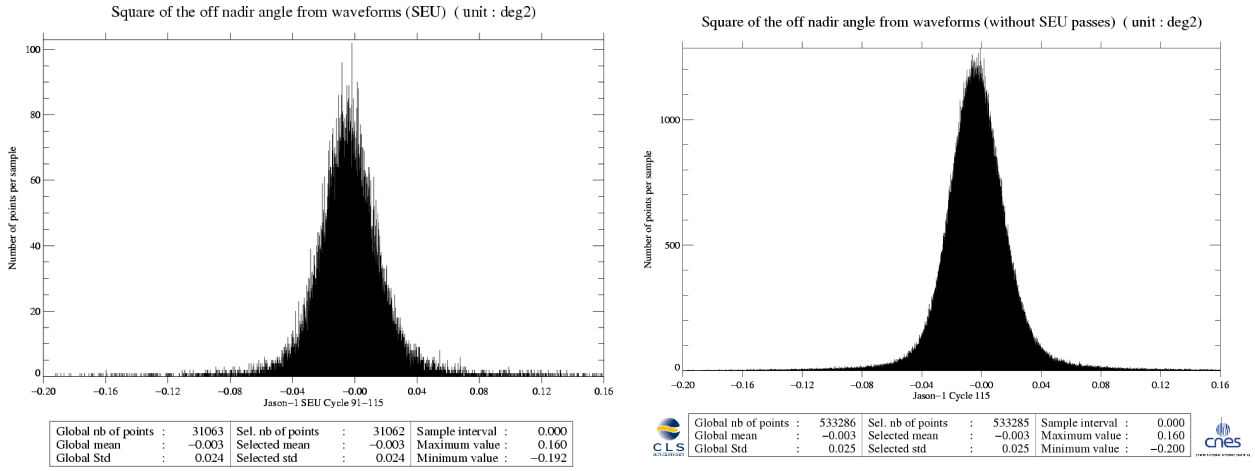

Figure 1: *Square of the off nadir angle from waveforms for the SEU incidences (cycles 091,102,103,108,115) (left) and for the passes without SEU of cycle 115 (right).*

The table 4 shows some statistical values for several altimetric parameters both for the SEU passes and (for comparison) passes from cycle 117 (which had no SEU incidences).
The values are quite similar, so we can conclude that the altimetric parameters during an SEU incident are good.

Parameter	Mean SEU/Cycle117	Rms SEU/Cycle117	Max SEU/Cycle117	Min SEU/Cycle117
ATT_FO_CARRE	-0.0 / -0.0	0.0 / 0.0	0.1 / 0.1	-0.1 / -0.2
SIG0	13.6 / 13.7	1.3 / 1.6	23.3 / 23.4	9.5 / 9.3
SWH	262.1 / 270.2	122.4 / 125.8	957.9 / 1099.1	0.8 / 0.0
ECT_SWH	52.7 / 52.9	11.2 / 11.3	520.1 / 765.0	0.0 / 0.0
DALT	1346.5 / 1347.0	5.3 / 5.4	1356.3 / 1355.9	1339.1 / 1338.8
NB_DALT	19.6 / 19.5	0.7 / 0.8	20.0 / 20.0	10.0 / 0.0
ECT_DALT	7.3 / 7.4	1.9 / 1.9	19.8 / 20.0	1.4 / 0.8
TRO_HUM_RAD	-14.3 / -13.6	9.7 / 9.2	-0.1 / -0.0	-47.5 / 49.3

Table 4: *S*tatistical values (Mean, Rms, Max, Min) of several altimetric parameters during passes with SEU and a cycle (117) without SEU.

2.4.3 Quality of SSH during SEU

Since cycle 115 was the cycle with the most SEU passes, table 5 shows the crossover differences for the 7 passes with SEU incident of cycle 115, for the 247 passes without SEU, and for all (254) passes. The crossover differences computed with the SEU values are slightly worse (are more biased) than crossover differences computed without SEU values. Nevertheless these values are still useful. Figure 2 shows a zoom of the evolution of SSH computed for passes with and without SEU. The SSH of the SEU pass is not noisier than the SSH of the other passes.

Selection	Number of Points (SEU/withoutSEU/Total	Mean (SEU/withoutSEU/Total	Rms (SEU/withoutSEU/Total)
No selection	335 / 7891 / 8223	1.02 / -0.26 / -0.26	8.01 / 6.92 / 6.98
Geographical Selection	117 / 2766 / 2880	-1.12 / -0.05 / -0.10	4.76 / 6.00 / 5.89

Table 5: *S*tatistical values of crossover differences for cycle 115 for no selection and geographical selection. 3 cases: SEU passes, passes without SEU, all passes.

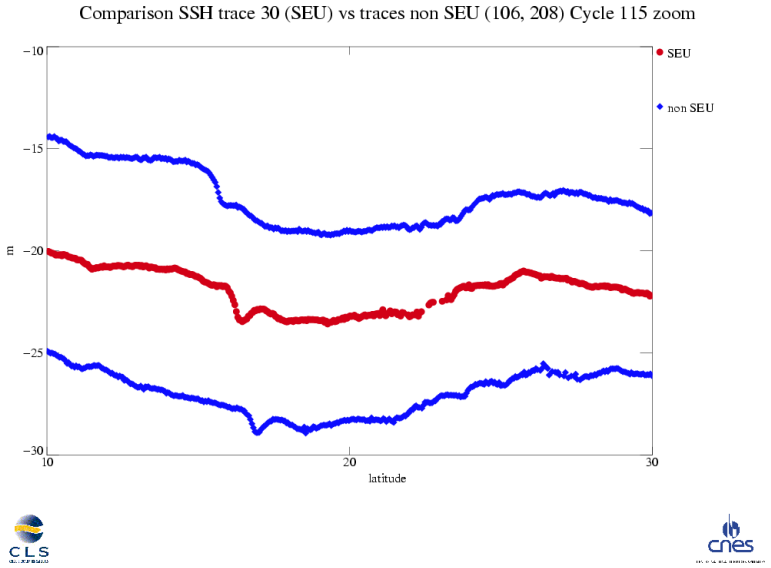

Figure 2: *Comparison of SSH of pass with SEU incidences (in red, pass 30 cycle 115) vs SSH of passes without SEU incidences (in blue, passes 106 and 208, cycle 115).*

3 Data coverage and edited measurements

3.1 Missing measurements

3.1.1 Over ocean

Determination of missing measurements relative to the theoretically expected orbit ground pattern is used to detect missing telemetry in Jason-1 datasets due to altimetry events for instance. This procedure is applied cycle per cycle and leads to results plotted on the left figure 3. It represents the percentage of missing measurements relative to the theory, when limited to ocean surfaces. The mean value is about 3.7% but this figure is not significant due to several events where the measurements are missing. All these events are described on table 1.
On figure 3 on the right, the percentage of missing measurements is plotted without taking into account the cycles where instrumental events or other anomalies occurred. Moreover shallow waters and high latitudes have been removed. This allows us to detect small data gaps in open ocean. The mean value is about 0.02%. This weak percentage of missing measurements is mainly explained by the rain cells, ice sea or sigma0 blooms. These sea states can disturb significantly the Ku band waveform shape leading to a non significant measure.

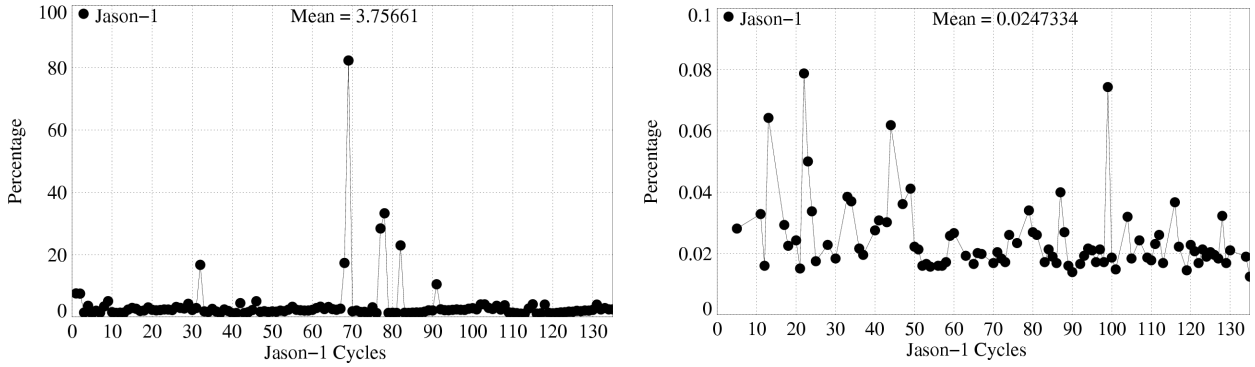

Figure 3: *Cycle per cycle percentage of missing measurements over ocean*

3.1.2 Over land and ocean

Figure 4 shows the percentage of missing measurements for Jason-1 and T/P over ocean and land. Jason-1 percentages are greater than the TOPEX ones due to the higher number of missing measurements for Jason-1 than for TOPEX over land. The 2 maps in figure 5 show the percentage of available measurements for Jason-1 and for TOPEX: it illustrates the high performance difference over land between both altimeters. Notice that if processing of elementary 20 Hz data may be improved for Jason-1 to retrieve some high rate data, the tracker capability between both instruments are not the same : Jason-1 is more "ocean" than T/P.

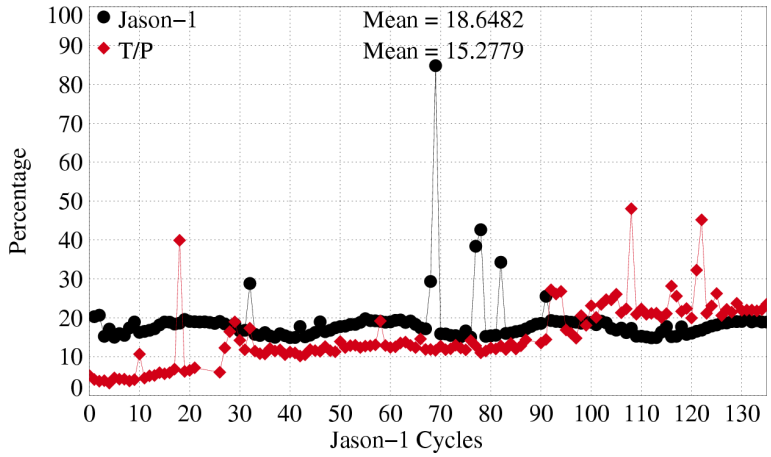

Figure 4: *Percentage of missing measurements over ocean and land for J1 and T/P*

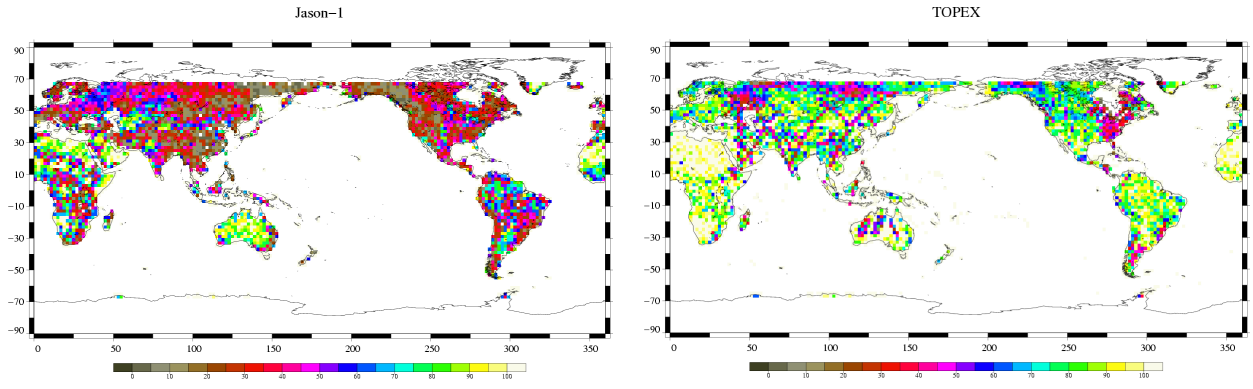

Figure 5: *Map of percentage of available measurements over land for Jason-1 on cycle 61 (left) and for TOPEX on cycle 404 (right)*

3.2 Edited measurements

3.2.1 Editing criteria definition

Editing criteria are used to select valid measurements over ocean. The editing criteria are divided into 3 parts. First, the quality criteria concern the flags which are described in section 3.2.2, 3.2.3 and 3.2.4. Then, threshold criteria are applied on altimeter, radiometer and geophysical parameters and are described in the table 6. Moreover, a spline criterion is applied to remove the remaining spurious data. These criteria defined for the GDR products "a" are also defined in AVISO and PODAAC User handbook. They will be modified for the GDR products "b" (see section 2.3). For each criterion, the cycle per cycle percentage of edited measurements has been monitored. This allows detection of anomalies in the number of removed data, which could come from instrumental, geophysical or algorithmic changes.

Parameter	Min thresholds	Max thresholds	mean removed
Sea surface height	$-130\ m$	$100\ m$	1.66%
Sea level anomaly	$-10\ m$	$10.0\ m$	2.25%
Number measurements of range	10	$Not\ applicable$	2.08%
Standard deviation of range	0	$0.2\ m$	2.13%
Square off-nadir angle	$-0.2\ deg^2$	$0.16\ deg^2$	1.75%
Dry troposphere correction	$-2.5\ m$	$-1.9\ m$	0.007%
Inverted barometer correction	$-2.0\ m$	$2.0\ m$	0.005%
JMR wet troposphere correction	$-0.5m$	$-0.001\ m$	0.20%
Ionosphere correction	$-0.4\ m$	$0.04\ m$	1.85%
Significant waveheight	$0.0\ m$	$11.0\ m$	1.32%
Sea State Bias	$-0.5\ m$	$0.0\ m$	1.35%
Ku-band Sigma0 [1]	$4.6\ dB$	$27.6\ dB$	1.13%
Ocean tide	$-5.0\ m$	$5.0\ m$	0.85%
Equilibrium tide	$-0.5\ m$	$0.5\ m$	0.00%
Earth tide	$-1.0\ m$	$1.0\ m$	0.00%
Pole tide	$-15.0\ m$	$15.0\ m$	0.00%
Altimeter wind speed	$0\ m.s^{-1}$	$30.0\ m.s^{-1}$	1.61%

Table 6: *E*diting criteria

[1] The thresholds used for the Ku-band Sigma0 are the same than for T/P, but the sigma0 bias between Jason-1

3.2.2 Flagging quality criteria: Land flag

In order to remove data over land, the altimeter land flag is used rather than radiometer land flag. Indeed, this allows us to keep more data near the coasts and then detecting potential anomalies in these areas. Furthermore, there is no impact on global performance estimations since the most significant results are derived from analyzes in deep ocean areas. Figure 6 shows the cycle per cycle percentage of missing measurements edited by this criterion.

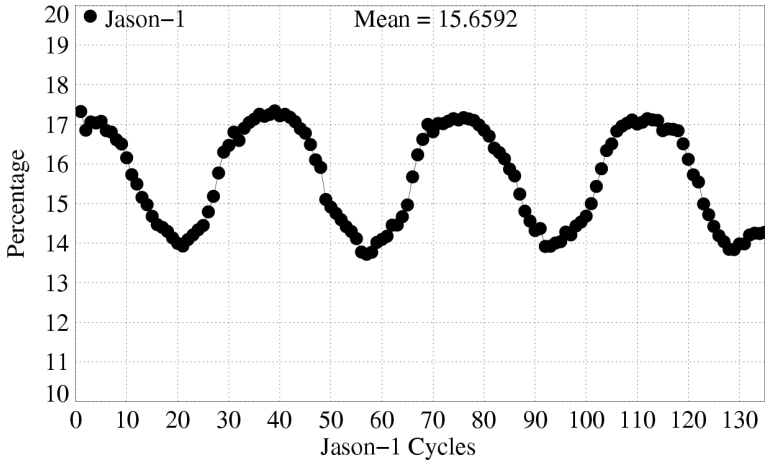

Figure 6: *Cycle per cycle percentage of edited measurements by land flag criterion*

and T/P (about 2.4 dB) is applied.

3.2.3 Flagging quality criteria: Ice flag

The ice flag is used to remove the sea ice data. Figure 7 shows the cycle per cycle percentage of missing measurements edited by this criterion. No anomalous trend is detected but an annual cycle is visible. Indeed, the maximum number of points over ice is reached during the northern fall. The ice flag edited measurements are plotted in Figure 8 for one cycle. It shows that the ice flag is not perfectly tuned especially in the northern hemisphere, for instance the Hudson Bay is divided into 2 parts.

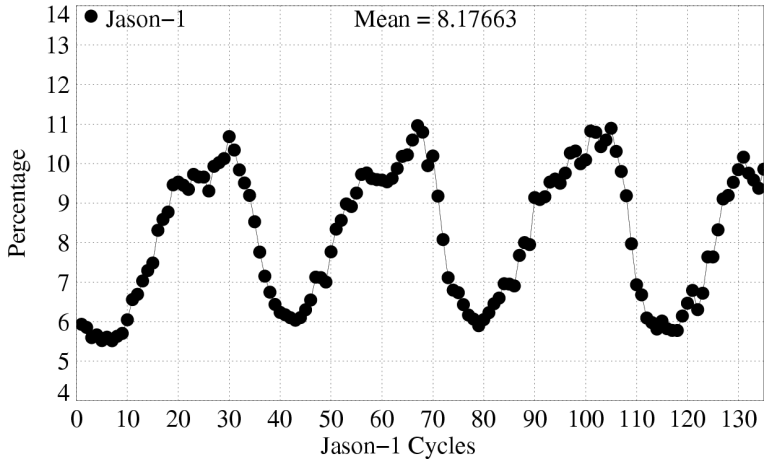

Figure 7: *Cycle per cycle percentage of edited measurements by ice flag criterion*

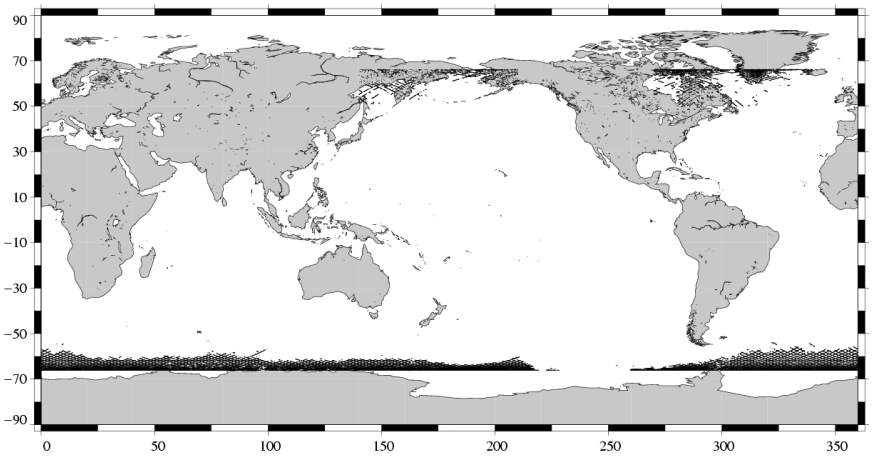

Figure 8: *Map of edited measurements by ice flag criterion on cycle 65*

3.2.4 Flagging quality criteria: Rain flag

The rain flag is not used for data selection since it is not yet tuned. It is thus recommended not to be used by users. The rain edited measurements are plotted in figure 9 for one cycle. It shows that too many measurements are edited by this flag. A new version of the rain flag will be available in the GDR product "b".

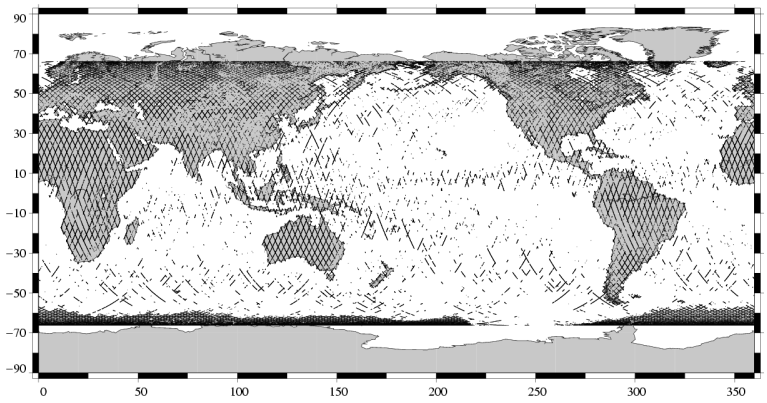

Figure 9: *Map of edited measurements by rain flag criterion*

3.2.5 Threshold criteria: Global

Instrumental parameters have also been analyzed from comparison with thresholds, after having applied flagging quality criteria (land and ice flag). Notice that no measurements are edited by the following corrections : dry troposphere correction, inverted barometer correction, equilibrium tide, earth and pole tide pole.

The percentage of measurements edited using each criterion has been monitored on a cycle per cycle basis (figure 10). The mean percentage of edited measurements is about 3.8%. An annual cycle is visible due to the seasonal sea ice coverage in the northern hemisphere. Indeed most of northern hemisphere coasts are without ice during northern hemisphere summer. Consequently some of these coastal measurements are edited by the thresholds criteria in summer instead of the ice flag in winter. This seasonal effect visible in the statistics is not balanced by the southern hemisphere coasts due to the shore distribution between both hemispheres.
Notice that for cycle 69 and 78, the percentage of edited measurements is higher than usual. This is due to the radiometer wet troposphere correction, see section 3.2.10. For last cycles, more measurements are edited due to mispointing values higher than usual as a result of star-tracker unavailability.

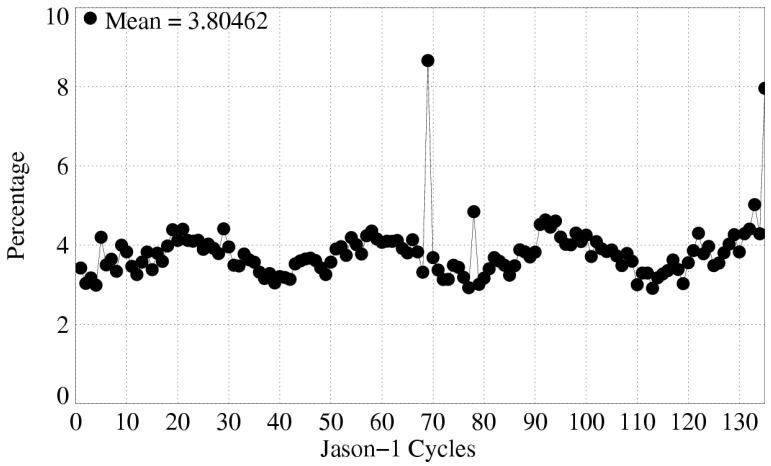

Figure 10: *Cycle per cycle percentage of edited measurements by threshold criteria*

3.2.6 Threshold criteria: 20-Hz measurements number

The percentage of edited measurements because of a too low number of 20-Hz measurements is represented in figure 11 and 12. No trend neither any anomaly has been detected.

The map of measurements edited by 20-Hz measurements number criterion is plotted in figure 12 for cycle 130.

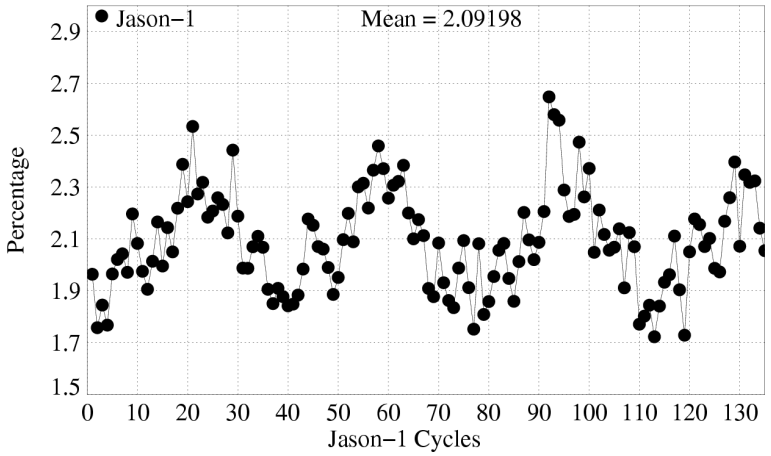

Figure 11: *Cycle per cycle percentage of edited measurements by 20-Hz measurements number criterion*

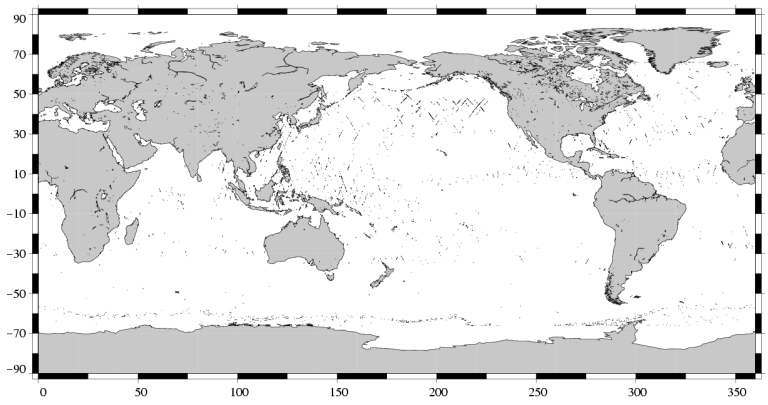

Figure 12: *Map of edited measurements by 20-Hz measurements number criterion for cycle 130*

3.2.7 Threshold criteria: 20-Hz measurements standard deviation

Same comment as in section 3.2.6 for the percentage of edited measurements due to the 20-Hz measurements standard deviation criterion (Figure 13 and 14).

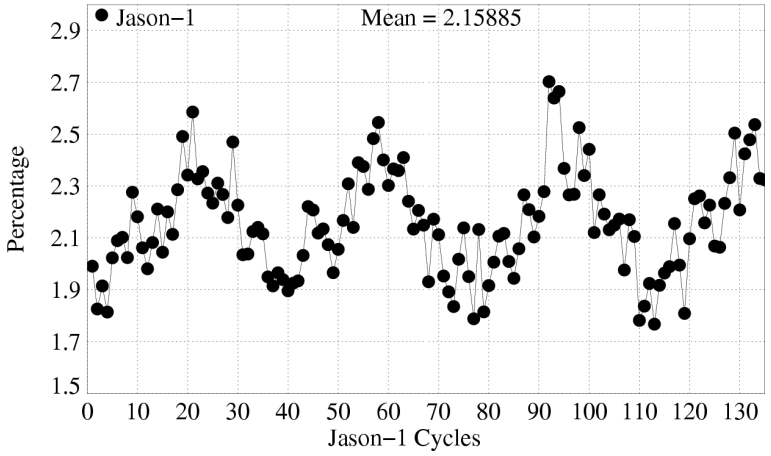

Figure 13: *Cycle per cycle percentage of edited measurements by 20-Hz measurements standard deviation criterion*

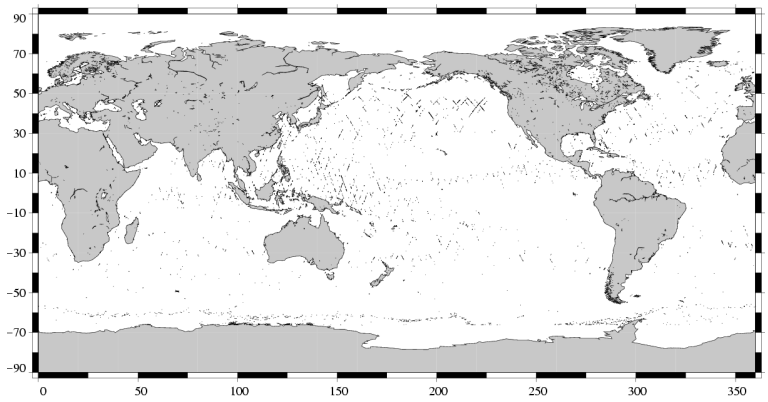

Figure 14: *Map of edited measurements by 20-Hz measurements standard deviation criterion for cycle 130*

3.2.8 Threshold criteria: Significant wave height

Same comment as in section 3.2.6 for the percentage of edited measurements due to the significant wave height criterion (Figure 15 and 16).

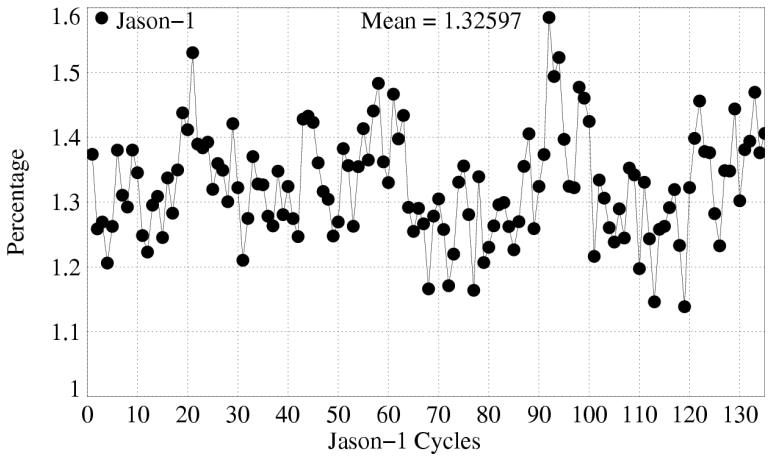

Figure 15: *Cycle per cycle percentage of edited measurements by SWH criterion*

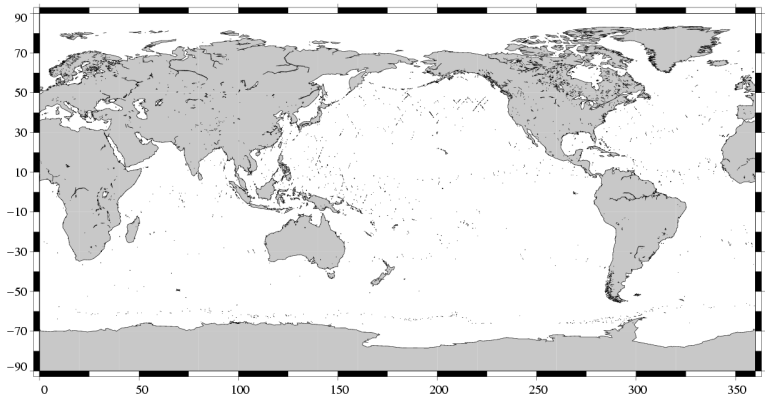

Figure 16: *Map of edited measurements by SWH criterion for cycle 130*

3.2.9 Backscatter coefficient

Same comment as in section 3.2.6 for the percentage of edited measurements due to the backscatter coefficient criterion (Figure 17 and 18).

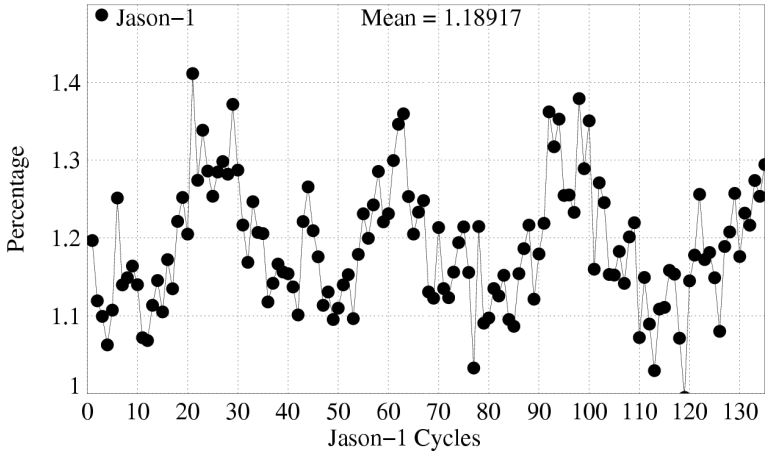

Figure 17: *Cycle per cycle percentage of edited measurements by Sigma0 criterion*

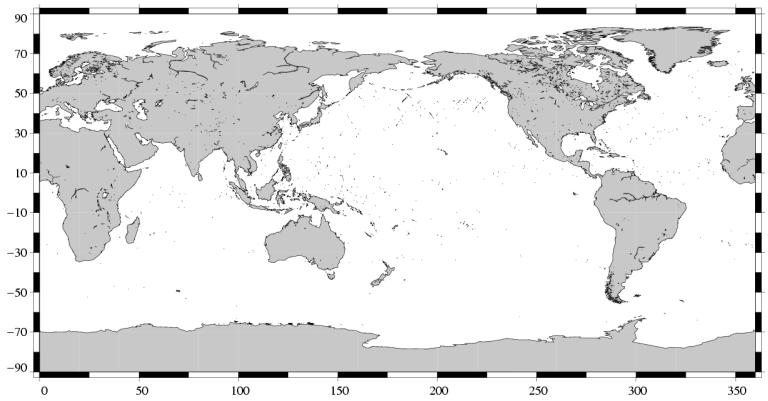

Figure 18: *Map of edited measurements by Sigma0 criterion for cycle 130*

3.2.10 Radiometer wet troposphere correction

Same comment as in section 3.2.6 for the percentage of edited measurements due to the radiometer wet troposphere criterion (Figure 19 and 20).
Notice that for cycle 69 and 78, the percentage of edited measurements is higher than usual. This is linked to the Jason hold safe mode on these cycles: the radiometer has been set 2 hours later than the altimeter. As a result, the radiometer wet troposphere correction has been set to default value during this period and these measurements have been edited.

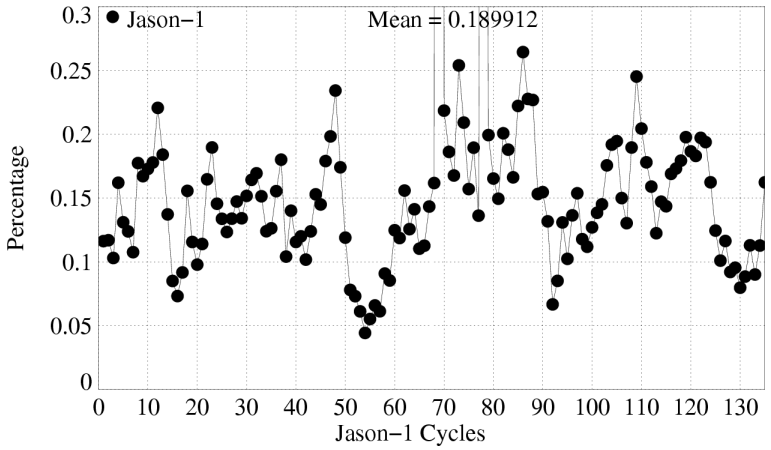

Figure 19: *Cycle per cycle percentage of edited measurements by radiometer wet troposphere criterion*

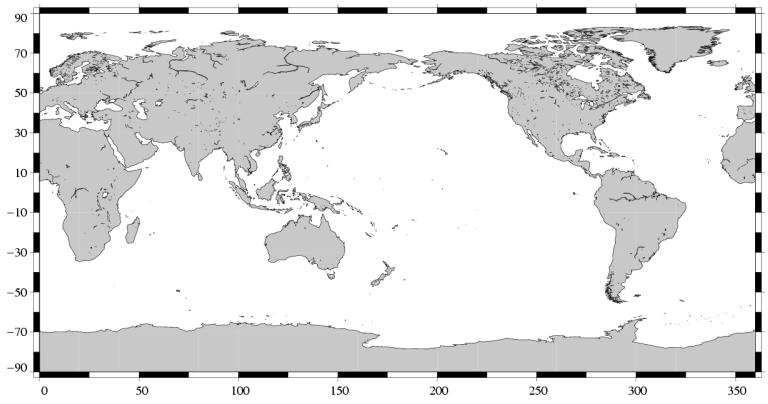

Figure 20: *Map of edited measurements by radiometer wet troposphere criterion for cycle 130*

3.2.11 Dual frequency ionosphere correction

Same comment as in section 3.2.6 for the percentage of edited measurements due to the dual frequency ionosphere criterion (Figure 21 and 22).

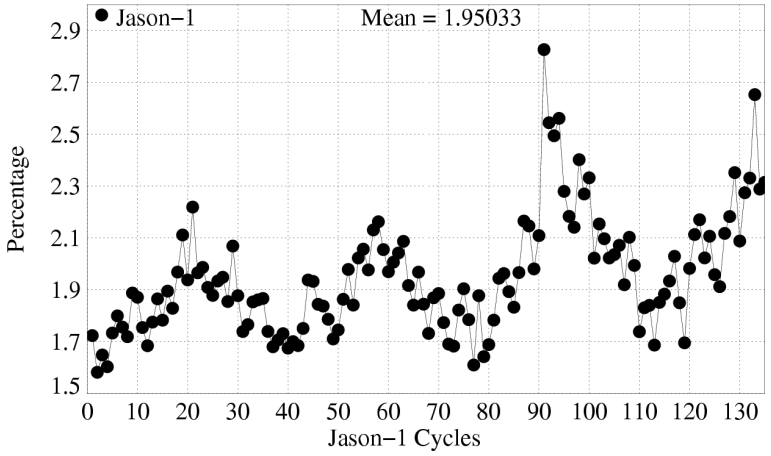

Figure 21: *Cycle per cycle percentage of edited measurements by dual frequency ionosphere criterion*

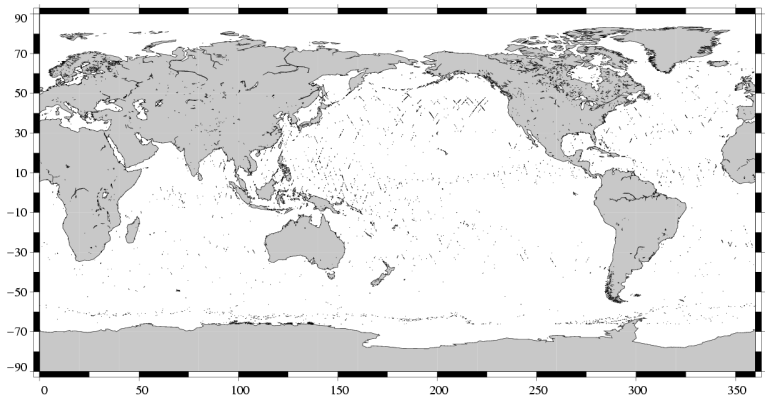

Figure 22: *Map of edited measurements by dual frequency ionosphere criterion for cycle 130*

3.2.12 Square off-nadir angle

Same comment as in section 3.2.6 for the percentage of edited measurements due to the square off-nadir angle criterion (Figure 23 and 24).

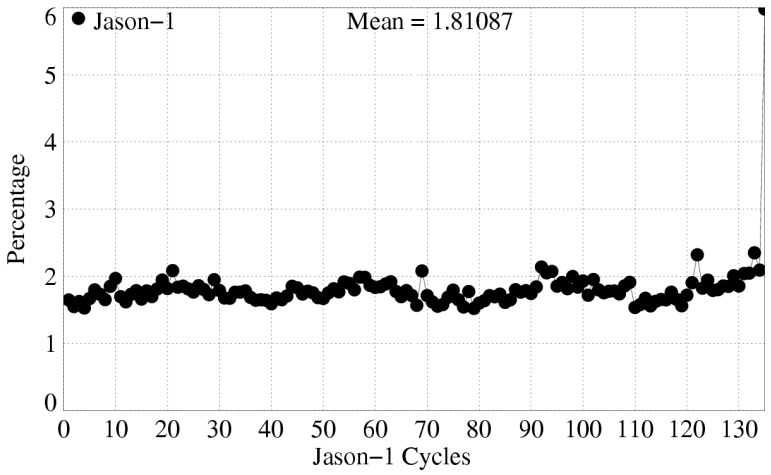

Figure 23: *Cycle per cycle percentage of edited measurements by square off-nadir angle criterion*

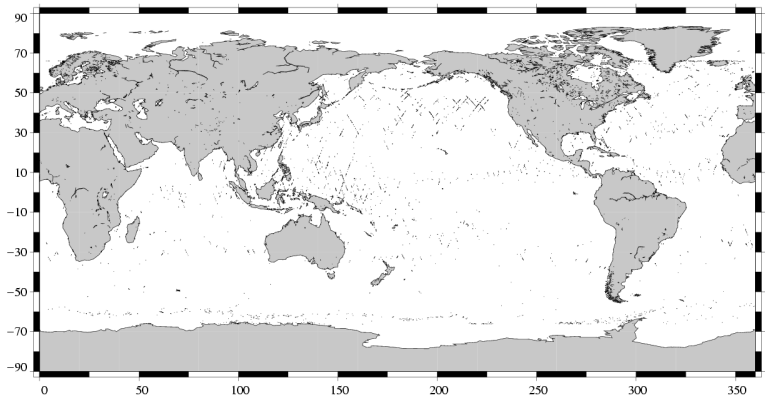

Figure 24: *Map of edited measurements by square off-nadir angle criterion for cycle 130*

3.2.13 Sea state bias correction

Same comment as in section 3.2.6 for the percentage of edited measurements due to the sea state bias criterion (Figure 25 and 26).

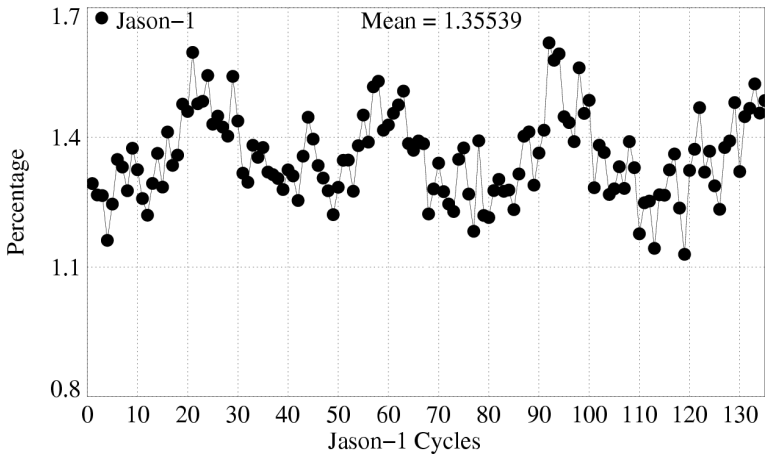

Figure 25: *Cycle per cycle percentage of edited measurements by sea state bias criterion*

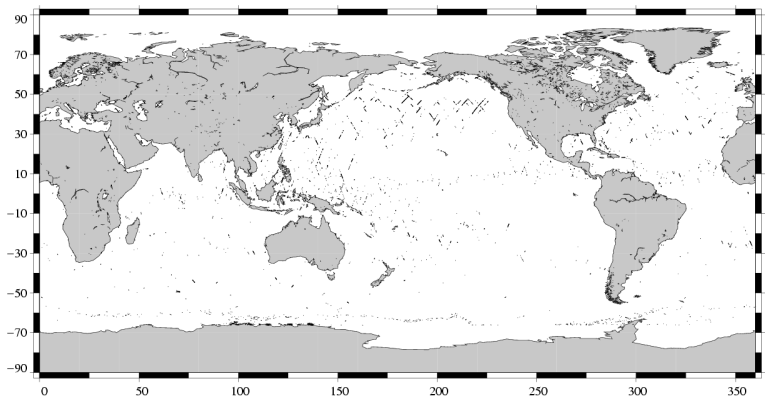

Figure 26: *Map of edited measurements by sea state bias criterion for cycle 130*

3.2.14 Altimeter wind speed

Same comment as in section 3.2.6 for the percentage of edited measurements due to the altimeter wind speed criterion (Figure 27 and 28).

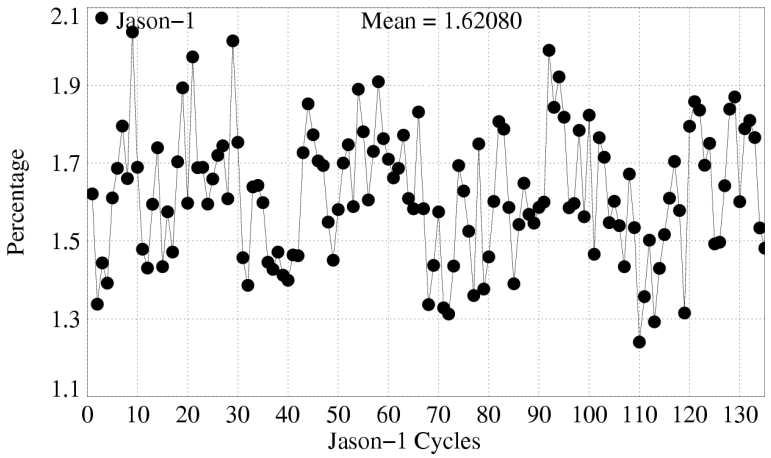

Figure 27: *Cycle per cycle percentage of edited measurements by altimeter wind speed criterion*

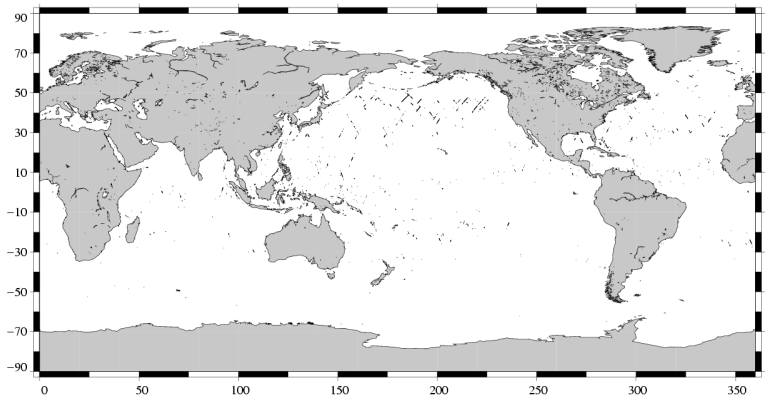

Figure 28: *Map of edited measurements by altimeter wind speed criterion for cycle 130*

3.2.15 Ocean tide correction

Same comment as in section 3.2.6 for the percentage of edited measurements due to the ocean tide criterion (Figure 29 and 30).

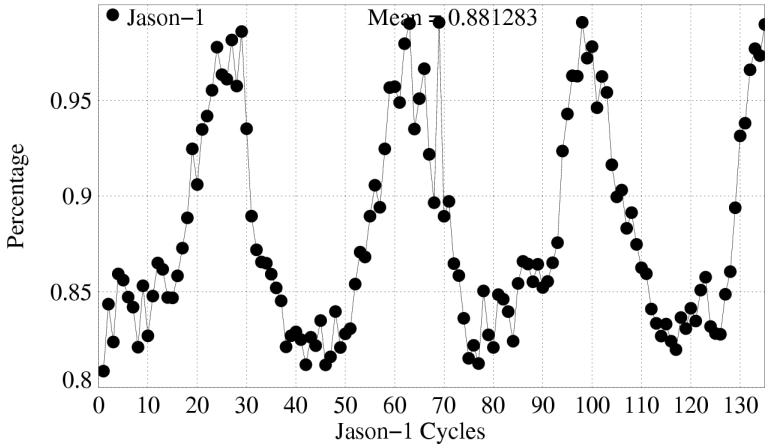

Figure 29: *Cycle per cycle percentage of edited measurements by ocean tide criterion*

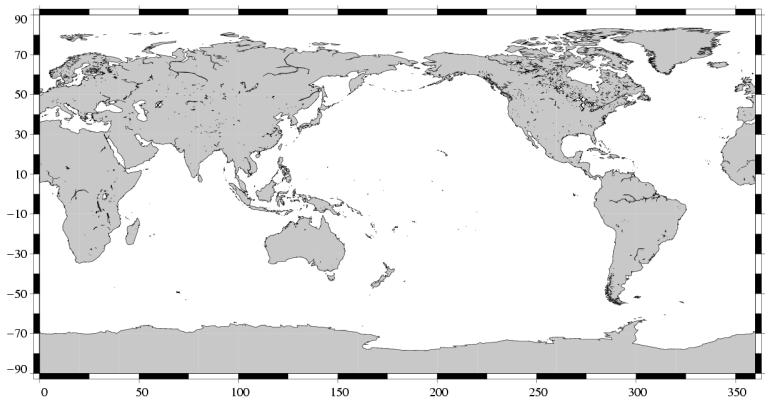

Figure 30: *Map of edited measurements by ocean tide criterion for cycle 130*

3.2.16 Sea surface height

Same comment as in section 3.2.6 for the percentage of edited measurements due to the sea surface height criterion (Figure 31 and 32).

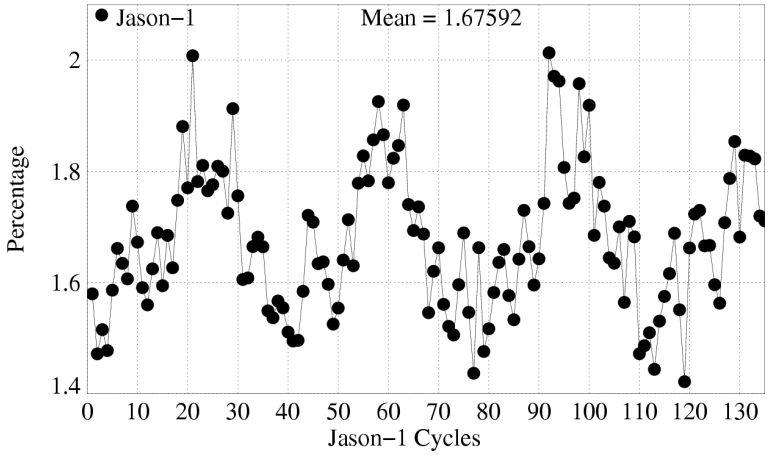

Figure 31: *Cycle per cycle percentage of edited measurements by sea surface height criterion*

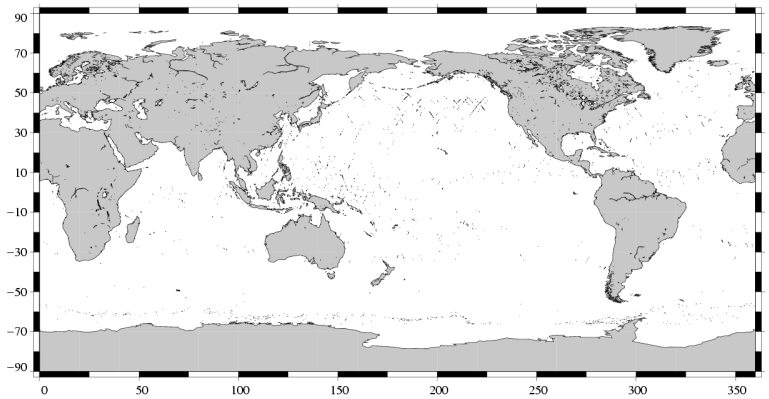

Figure 32: *Map of edited measurements by sea surface height criterion for cycle 130*

3.2.17 Sea level anomaly

Same comment as in section 3.2.6 for the percentage of edited measurements due to the sea level anomaly criterion (Figure 33). The map in figure 34 allows us to plot the measurements edited by the sea level anomaly criterion after applying all other threshold criteria.

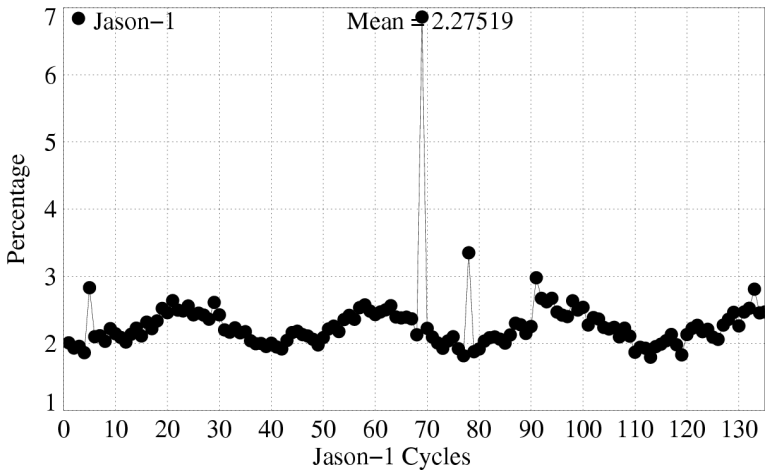

Figure 33: *Cycle per cycle percentage of edited measurements by sea level anomaly criterion*

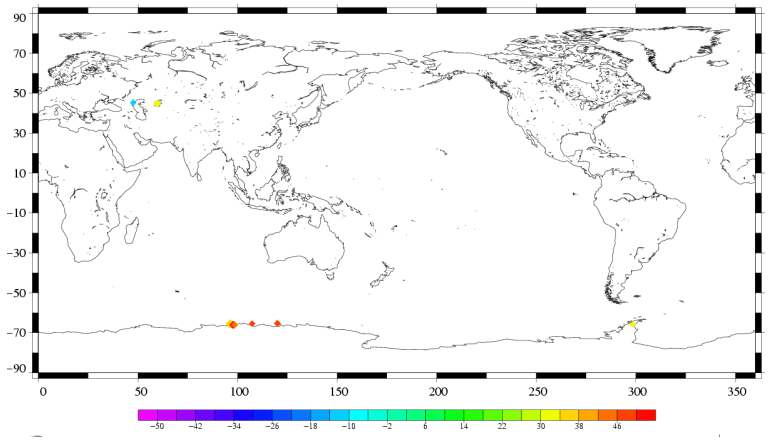

Figure 34: *Map of edited measurements by sea level anomaly criterion for cycle 130*

4 Monitoring of altimeter and radiometer parameters

4.1 Methodology

Both mean and standard deviation of the main parameters of Jason-1 have been monitored since the beginning of the mission. Moreover, a comparison with T/P parameters has been performed: it allows us to monitor the bias between the parameters of the 2 missions. Two different methods have been used to compute the bias:

- During the verification phase, Jason-1 and T/P ground tracks are on the same ground track and are spaced out about 1 minute apart. The mean of the T/P Jason-1 differences can be computed using a point by point repeat track analysis.
- From cycle Jason-1 22 (Cycle T/P 365), the 15th of August 2002, a maneuver sequence was conducted over 30 days to move T/P to the new Tandem Mission orbit : T/P is now located one half the TP/Jason-1 track spacing to the West of Jason-1.Geographical variations are then too strong to directly compare Jason-1 and T/P parameters on a point by point basis. Therefore cycle per cycle differences have been carried out to monitor Jason-1 and T/P differences, but data gaps on both satellites have been taken into account.

4.2 20 Hz Measurements

The monitoring of the number and the standard deviation of 20 Hz elementary range measurements used to derive 1 Hz data is presented here. These two parameters are computed during the altimeter ground processing. Before a regression is performed to derive the 1 Hz range from 20 Hz data, a MQE criterion is used to select valid 20 Hz measurements. This first step of selection thus consists in verifying that the 20 Hz waveforms can be effectively approximated by a Brown echo model (Brown, 1977 [7]) (Thibaut et al. 2002 [53]). Through an iterative regression process, elementary ranges too far from the regression line are discarded until convergence is reached. Thus, monitoring the number of 20 Hz range measurements and the standard deviation computed among them is likely to reveal changes at instrumental level.

4.2.1 20 Hz measurements number in Ku-Band and C-Band

Figure 35 shows the cycle per cycle mean of 20-Hz measurements number in Ku-Band (on the left) and C-Band (on the right). Apart from a weak seasonal signal, no trend neither any anomaly has been detected.

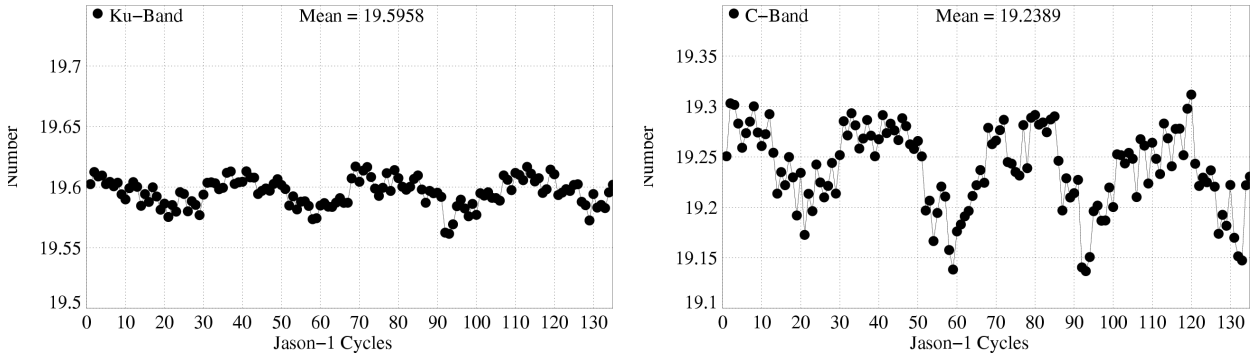

Figure 35: *Cycle per cycle mean of 20-Hz measurements number in Ku-Band (left) and C-Band (right)*

4.2.2 20 Hz measurements standard deviation in Ku-Band and C-Band

Same comment as in section 4.2.1 for the 20 Hz measurements standard deviation parameter (figure 36).

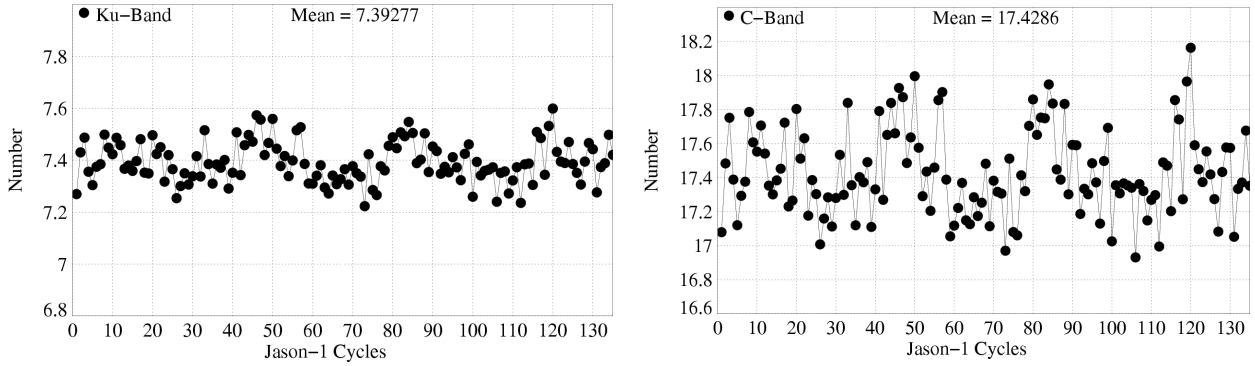

Figure 36: *Cycle per cycle mean of 20-Hz measurements standard deviation in Ku-Band (left) and C-Band (right)*

4.3 Off-Nadir Angle from waveforms

The off-nadir angle is estimated from the waveform shape during the altimeter processing. The square of the off-nadir angle, averaged in a one-cycle basis, has been plotted in figure 37. The mean value is very low, about -0.003 deg2. This mean value is not significant in terms of actual platform mispointing. The negative figure is only representative of a bias in the on-ground algorithm. In fact squared attitude is what is retrieved from waveforms, not attitude, and noise in the retrieval can cause this otherwise positive quantity to measure negative. A peak is evidenced for cycle 69: it is linked with the platform safe hold mode that occurred during this cycle. Mispointing seems to be larger between cycles 30 and 42: this correlated with short periods of unavailability of the Jason-1 star trackers. The same reason explains the strong mispointing values at the end of the period (from cycle 132 onward). As noticed by several investigators (Tournadre et al., 2002 [55]), there are some periods when the off-nadir angle is larger than the 0.2 degree specification, which can introduce errors in the altimeter parameters if not taken into account in the ground processing (Vincent et al., 2003). One improvement of the science processing with respect to the verification phase is that, in the present version of the IGDRs and for the whole GDR dataset, real time estimates of the mispointing angle are used in input of the ground retracking algorithm. This allows correcting re-tracked geophysical parameters for mispointing effects up to 0.3 deg. (Vincent et al. 2003c [59]). Further improvements available in the next GDR version (section 2.3) of the ground retracking algorithm would lead to correct estimations of altimeter parameters for mispointing angle errors up to 0.8 deg. (Amarouche et al. 2004 [5]).

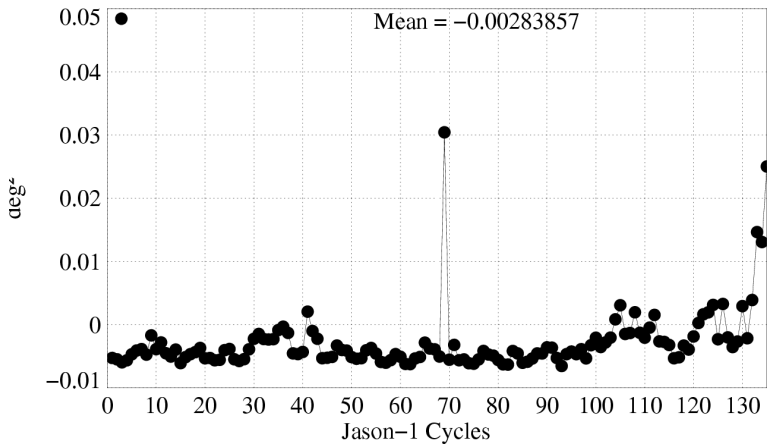

Figure 37: *Cycle mean of the square of the off-nadir angle deduced from waveforms (deg^2)*

4.4 Significant wave height

4.4.1 Ku-band SWH

Jason-1 and T/P Ku SWH are compared in terms of global statistics in figure 38: cycle means and standard deviations of both missions are presented in a cycle basis, as well as mean differences between T/P and Jason-1. Global variations of the SWH statistics are the same on the two missions. The (TOPEX - Jason-1) SWH bias is about 8.8 cm. This value remains steady at the 1 cm level throughout the Jason-1 mission, even if some variability is observed for particular cycles. It should be noticed that the global comparison method and the repeat-track analysis method agree very well, as shown in the first part of the mission (cycles 1 to 21). The estimation of the (Poseidon-1 - Poseidon-2) SWH difference is about 15.5 cm for Poseidon cycle 18 not plotted here. The same comparison with the C-band SWH 39 leads to a mean bias between TOPEX and Jason-1 of about 11 cm.
The coherence between the Jason-1 and T/P Ku SWH is good. However, it has been shown (Dorandeu et al. 2002b [18], Ray and Beckley 2003 [46]) that the Jason-1 (Poseidon-2 altimeter) SWH are slightly underestimated for high values of SWH, when compared to both TOPEX and Poseidon-1 altimeters. Studies about corrections tables to be applied to the altimeter parameters (Thibaut et al., 2004 [54]) have shown that updating these tables would cancel a large part of this difference between Jason-1 and T/P for high waves. This had be taken into account in the next GDR release (section 2.3).

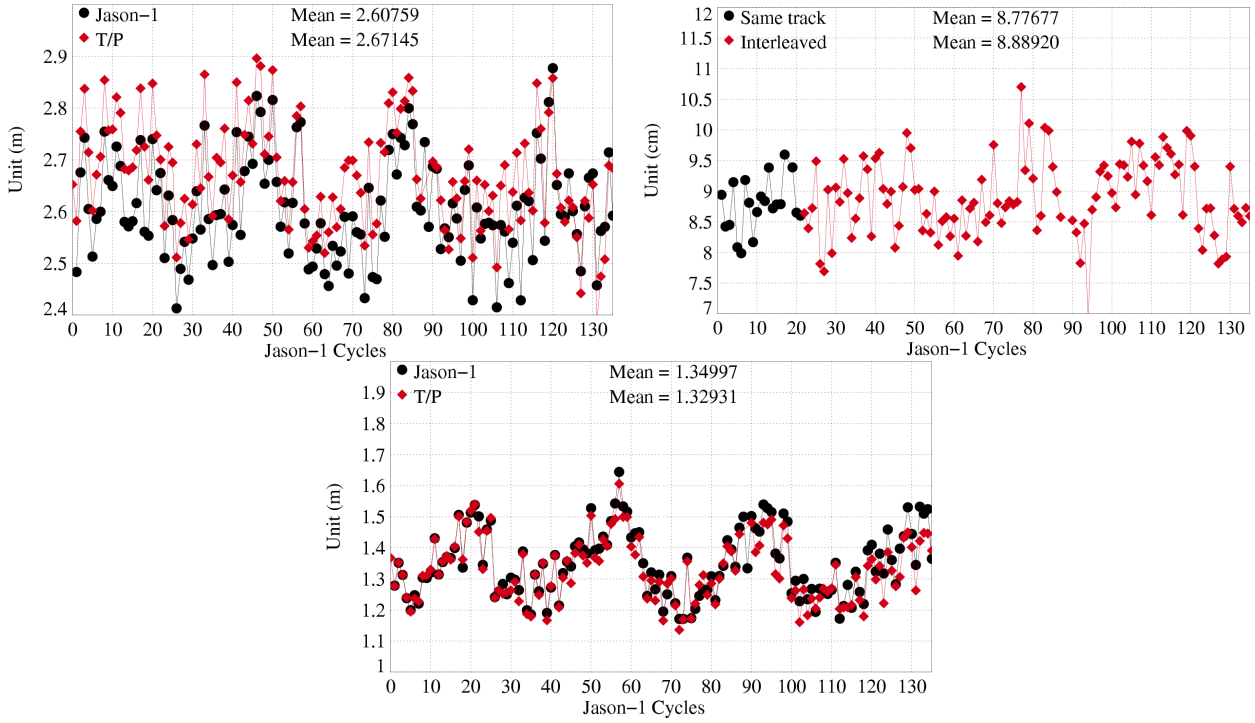

Figure 38: *Cycle per cycle mean (left), T/PJason mean differences (right), and standard deviation (bottom) of Ku-band SWH*

4.4.2 C-band SWH

Same comment as in section 4.4.1 for the C-band SWH parameter (figure 39).

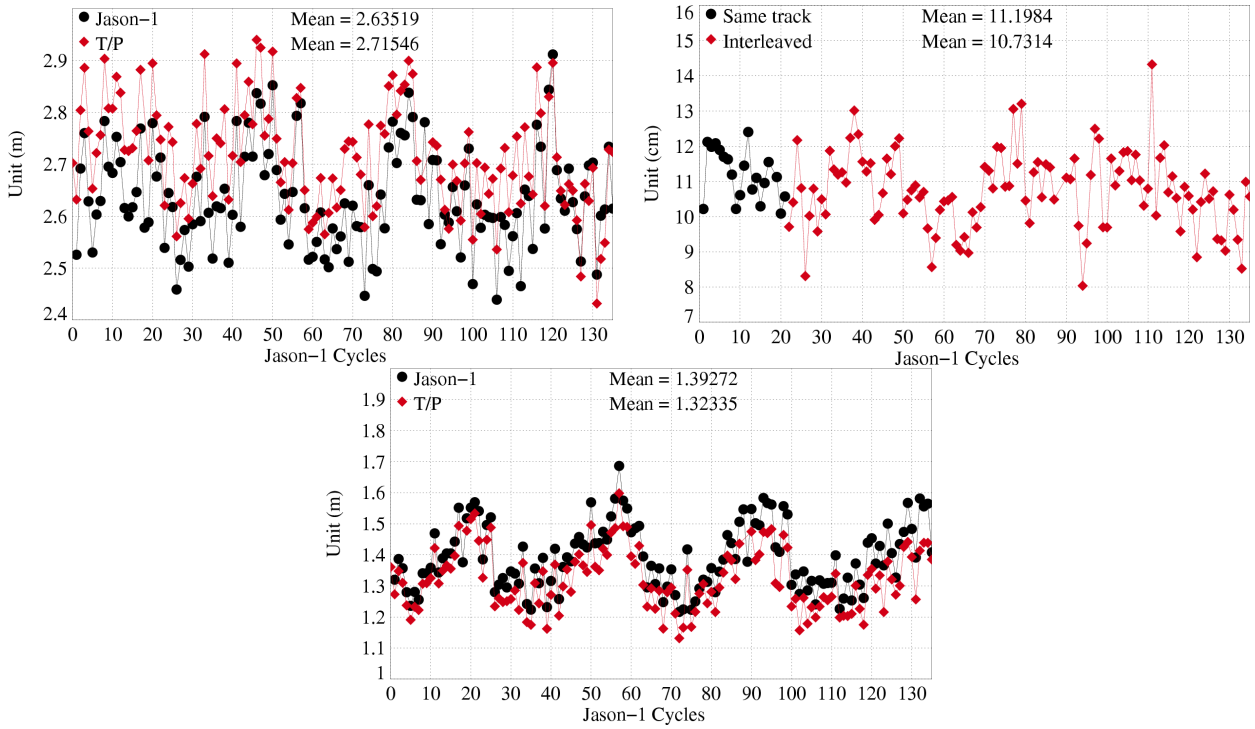

Figure 39: *Cycle per cycle mean (left), T/PJason mean differences (right), and standard deviation (bottom) of C-band SWH*

4.5 Backscatter coefficient

4.5.1 Ku-band Sigma0

The cycle per cycle mean (figure 40: top panel on the left) for Jason-1 (black curve) is coherent with the TOPEX mean (red curve). In order to compare both parameters and keep a significant dynamic scale, TOPEX Ku-Sigma0 is biased by a 2.26 dB value to align TOPEX with the Jason-1 uncalibrated Sigma0. The bias between the two corrections (figure 40: top panel on the right) is quite stable about -2.4 dB: this value is near from the -2.26 dB bias which is applied in the ground processing and that was anticipated to represent the TOPEX to Jason-1 bias when computed on a small volume of data.
Notice that the absolute bias is higher than usual from T/P cycle 433 to 437 by 0.1 dB : this is due to the TOPEX Sigma0. Indeed, the satellite attitude was impacted by a pitch wheel event linked to the T/P safe-hold mode occurred on cycle T/P 430 (see electronic communication : T/P Daily Status (26/07/2004). This anomaly has probably biased the TOPEX sigma0 during this period.
The strong Jason-1 mispointing values from cycle 132 to 135 have a very weak impact on the Sigma0 bias by 0.05 dB.
Jason-1 and T/P curves on bottom panel, showing the standard deviation differences, are very similar .

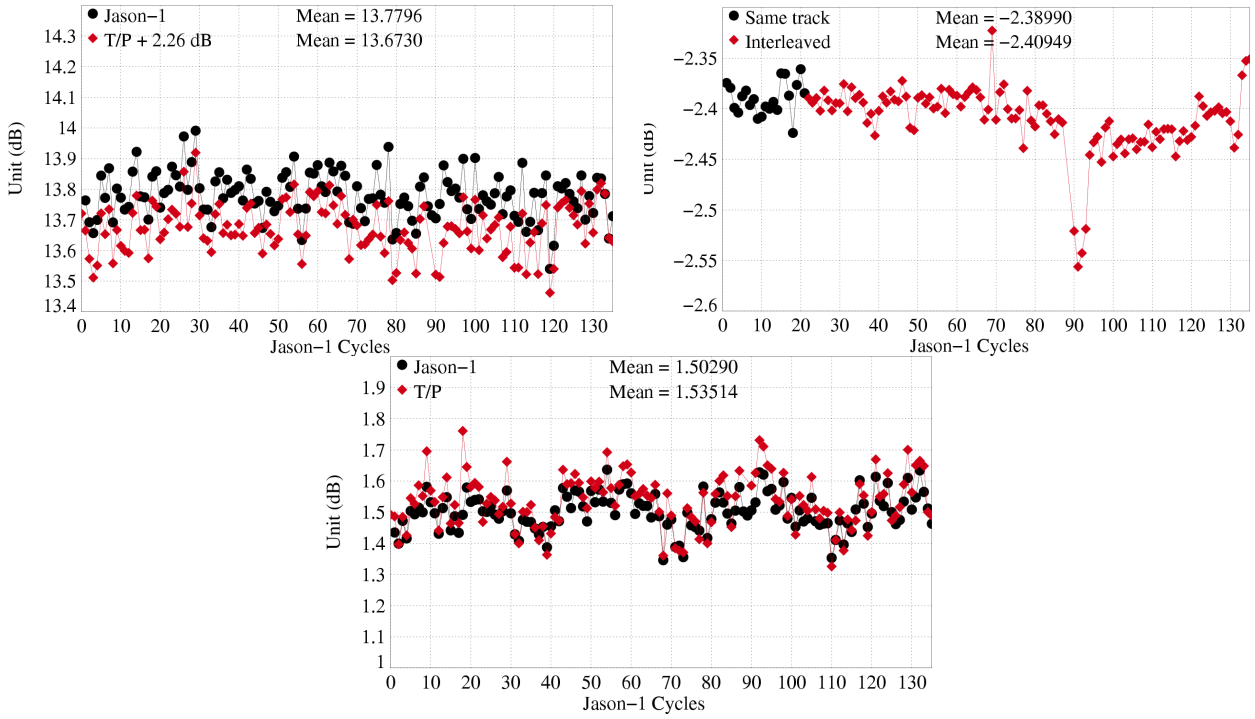

Figure 40: *Cycle per cycle mean (left), T/PJason mean differences (right), and standard deviation (bottom) of Ku-band SIGMA0*

4.5.2 C-band Sigma0

Same comment as in section 4.5.1 for the C-band Sigma0 parameter (figure 41). The bias between TOPEX and Jason-1 decreases from -0.6 dB to -0.7 dB. This is due to the T/P C-band Sigma0 (Ablain et al. 2004 [3]).
Notice that, the Jason C-Sigma0 is biased by a -0.26 dB value to align it on TOPEX in the science processing software.

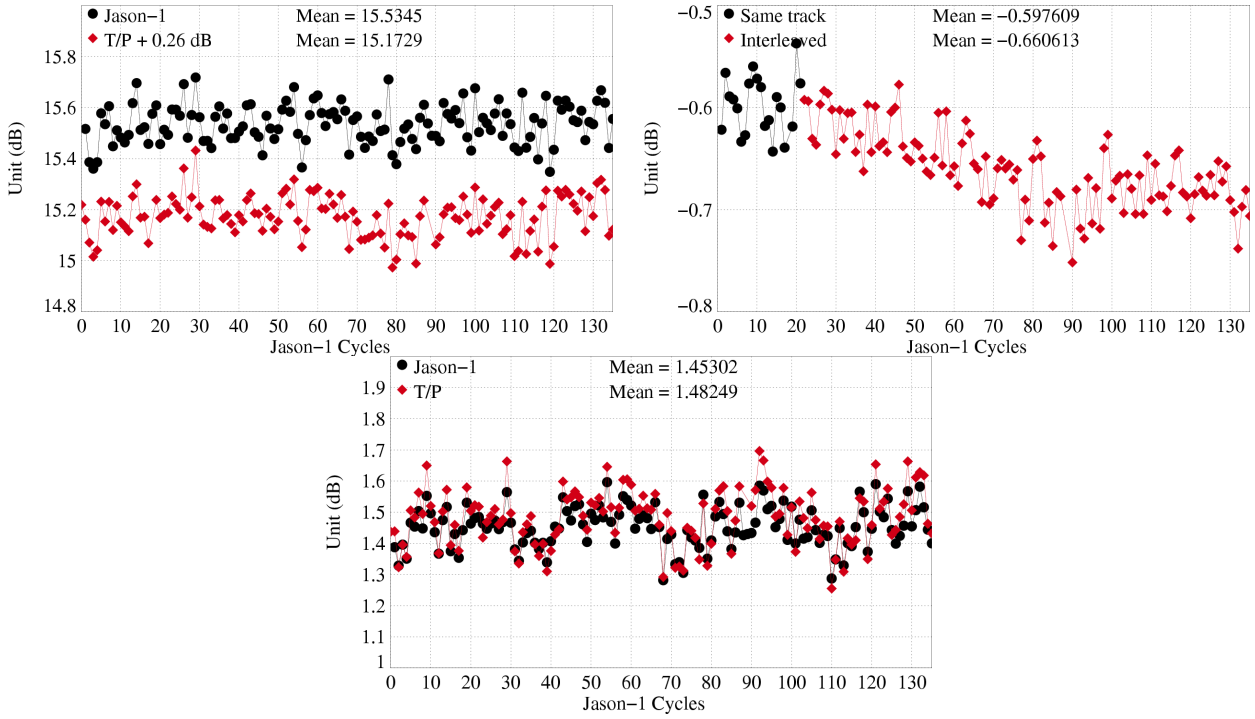

Figure 41: *Cycle per cycle mean (left), T/P Jason mean differences (right), and standard deviation (bottom) of C-band SIGMA0*

4.6 Dual-frequency ionosphere correction

The dual frequency ionosphere corrections derived from the TOPEX and Jason-1 altimeters have been monitored and compared in the same way (figure 42). The mean difference between TOPEX and Jason-1 estimates is about -2.7 mm, with cycle to cycle variations lower than 2 mm. This slight difference shows that the C-band calibration is thus not exactly the same for the two altimeters. Differences in the ionosphere correction may depend on the Sea State Bias (SSB) model used to correct the Ku-band and C-Band ranges. Apart from this bias, the two corrections are very similar and vary according to the solar activity. Notice that, as for TOPEX (Le Traon et al. 1994 [33]), it is recommended to filter the Jason-1 dual frequency ionosphere correction before using it as a SSH geophysical correction (Chambers et al. 2002 [11]). A low-pass filter has thus been used to remove the noise of the correction in all SSH results presented in the following sections.

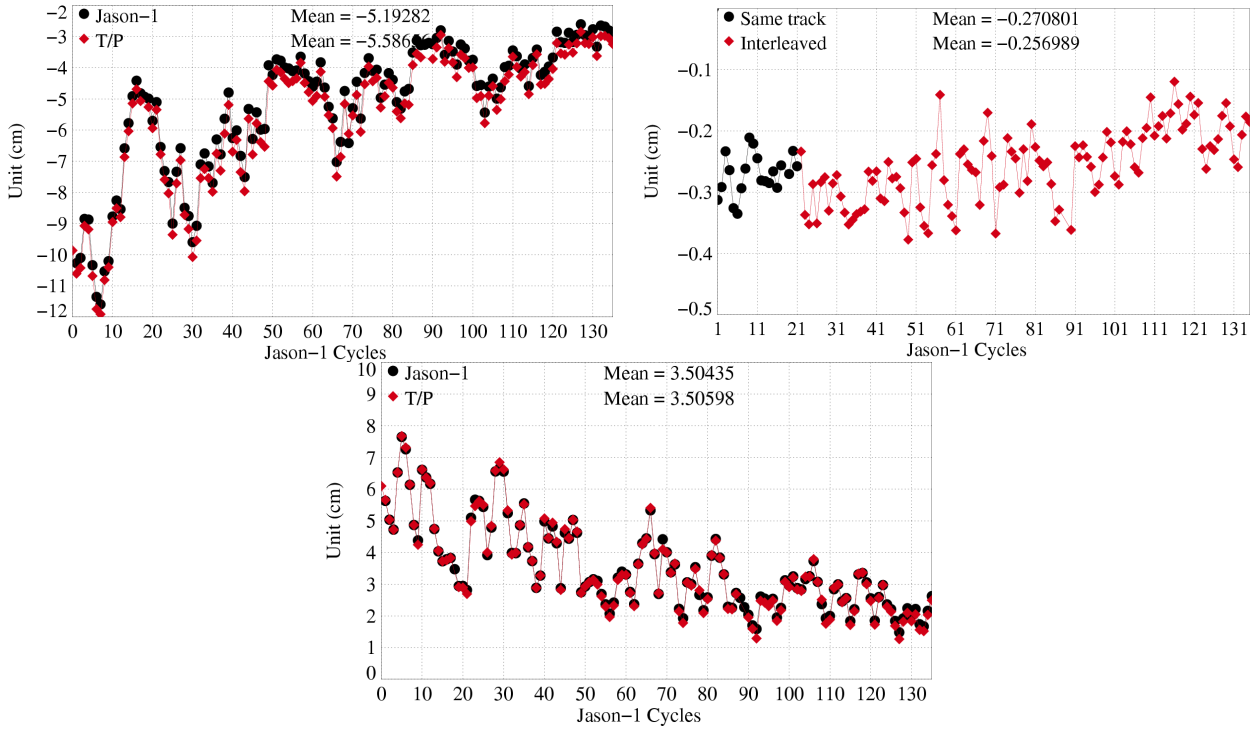

Figure 42: *Cycle per cycle mean (left), T/P Jason mean differences (right), and standard deviation (bottom) of dual frequency ionosphere correction*

4.7 Wet troposphere correction

4.7.1 Radiometer wet troposphere correction

Extensive studies have been performed during the Jason-1 verification phase to compare the JMR and the TOPEX Microwave Radiometer (TMR) corrections. These analyzes (D. Chambers, personal communication) allowed detecting systematic offsets in both Jason-1 and TOPEX corrections related to transitions between fixed yaw and sinusoidal yaw regimes of both platforms (Vincent et al. 2003a [57]). Ruf et al. (2002a) [49] explained that these effects were induced by different thermal environments in each yaw mode. The JMR calibration coefficients were updated twice during the calibration and validation phase (Ruf et al. 2002a [49] , Ruf et al. personal communication 2003). JMR calibration coefficients are applied to the whole GDR dataset (version "a") . They are also intended to correct for the yaw-dependent effects in the JMR troposphere corrections. Global statistics of the JMR wet troposphere correction are plotted in figure 44, together with comparisons relative to the TMR correction - after applying a drift as identified by Keihm et al. (2000) [29]. Large differences are observed in the comparison between the two corrections. Dependence on the T/P yaw regimes has been corrected (see T/P annual report [3]) on the plot (figure 44:top on the right). Moreover TMR drift estimation has been applied according to Scharroo et al. (2004) [51]. Two major steps in the (TMR - JMR) differences are observed. First, a decreasing trend occurred from cycle 27 to cycle 32. It resulted in a bias between the two corrections of about 0.5 cm from cycle 32 onward. Second, a large jump at cycle 69 added a -1 cm bias in the (TMR - JMR) difference after the platform safe hold. These two JMR events have been taken into account in the next GDR release (section 2.3).

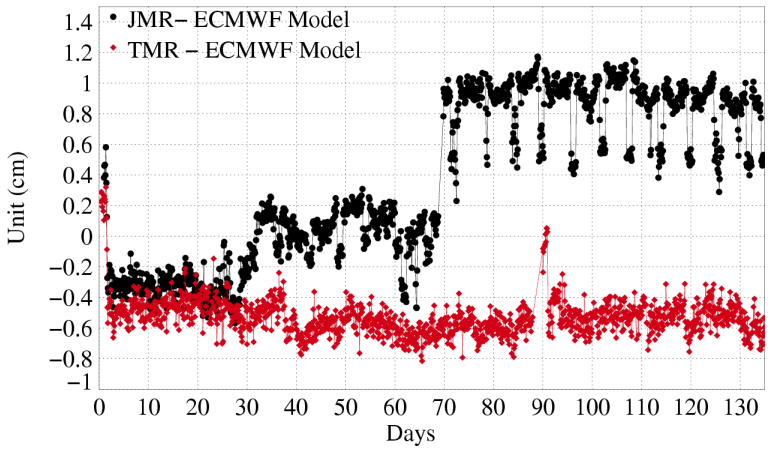

Figure 43: *Daily mean of radiometer and ECMWF model wet troposphere correction differences for Jason-1 and T/P*

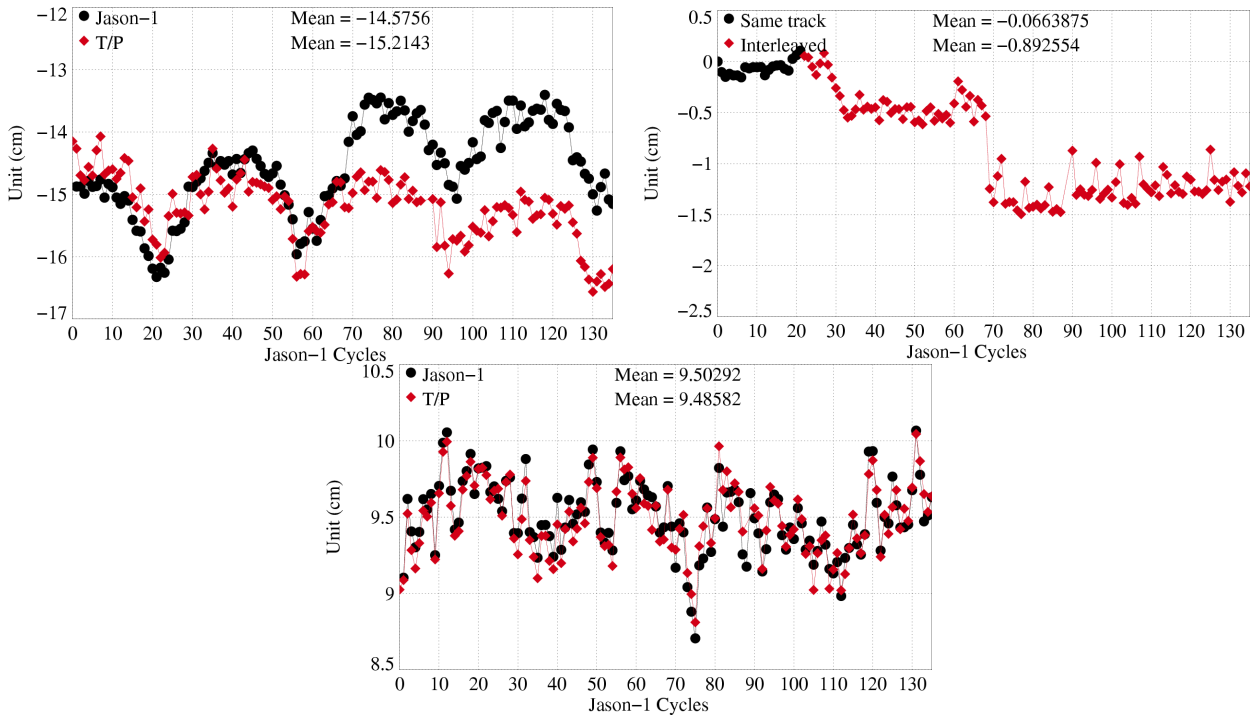

Figure 44: *Cycle per cycle mean (left), T/P Jason mean differences (right), and standard deviation (bottom) of radiometer wet troposphere correction*

4.7.2 ECMWF model wet troposphere correction

The ECWMF wet troposphere correction has been used to check the two radiometer corrections (figure 43). Indeed, in terms of comparisons between the two radiometers, the model correction can be used as an independent reference point. Through the Jason-1 mission, no significant change in the ECMWF model occurred impacting the wet troposphere correction computation (see http://www.ecmwf.int/products/data/operational_system/evolution/evolution_2003.html) except during cycle 1 (January 2002). Thus, it is worth comparing the correction from the model and both Jason-1 and TOPEX radiometers. Then, the trend observed in figure 44 through cycles 27-32 in the (TMR - JMR) differences is also detected, with the same order of magnitude, between the JMR and the ECMWF corrections. That shows that instrumental changes occurred during that period. These changes are investigated in details in Obligis et al. (2004) [39] using 3 different methods for analyzing the respective contribution of each of the three JMR channels. The second strong step observed in the (TMR - JMR) differences is also clearly captured in the (JMR - ECMWF) differences. It occurs just after the safe hold mode of the Jason-1 platform on cycle 69. Finally, the comparison with the model correction also shows that in the last cycles, the JMR correction is more impacted by yaw modes than at the beginning of the mission, with differences around 0.5 cm between different regimes.

5 Crossover analysis

Crossover differences are systematically analyzed to estimate data quality and the Sea Surface Height (SSH) performances. Furthermore, T/P crossover performances have been monitored in order to compare both performances. SSH crossover differences are computed on a one cycle basis, with a maximum time lag of 10 days, in order to reduce the impact of ocean variability which is a source of error in the performance estimation. The main SSH calculation for Jason-1 and T/P are defined below. For Jason-1 and TOPEX, new standards have been used for the tidal and atmospheric corrections. These corrections will be present in the next GDR release (see section 2.3).

$$SSH = Orbit - Altimeter\ Range - \sum_{i=1}^{n} Correction_i$$

with $Jason-1\ Orbit = POE\ CNES\ orbit$ and

$$\begin{aligned}
\sum_{i=1}^{n} Correction_i \;=\; & Dry\ troposphere\ correction : new\ S1\ and S2\ atmospheric\ tides\ applied \\
+\; & Combined\ atmospheric\ correction :\ MOG2D\ and\ inverse\ barometer \\
+\; & Radiometer\ wet\ troposphere\ correction \\
+\; & Filtered\ dual\ frequency\ ionospheric\ correction \\
+\; & Non\ parametric\ sea\ state\ bias\ correction \\
+\; & Geocentric\ ocean\ tide\ height,\ GOT\ 2000 :\ S1\ atmospheric\ tide\ is\ applied \\
+\; & Solid\ earth\ tide\ height \\
+\; & Geocentric\ pole\ tide\ height
\end{aligned}$$

Note that for TOPEX data, a non-parametric sea state bias has been updated over TOPEX B period according to the collinear method (Gaspard et al., October 2002, [24]). For Poseidon-1 data, non-parametric SSB is not yet available.

5.1 Mean crossover differences

The mean of crossover differences represents the average of SSH differences between ascending and descending passes. It should not be significantly different from zero. The cycle mean of Jason-1 and T/P SSH crossover differences is plotted for the whole Jason-1 period in figure 45 (bottom). Slightly larger variations are observed for Jason-1 than for TOPEX in the first cycles. However, some correlation between the two curves can be deduced from this figure. That shows that consistent signals impact the two systems. The map of the Jason-1 crossover differences averaged over the whole mission has been plotted in figure 45 (on the left). Systematic differences between ascending and descending passes, as large as 4 cm, are observed depending on geographical areas. The same map produced for T/P on the same time period leads to comparable results, with similar geographical patterns not necessarily in the same area, but nearly the same order of magnitude in the systematic crossover differences (figure 45 on the right). This kind of signals is due to geographically correlated orbit errors, in particular gravity model errors (e.g. Luthcke et al. 2003 [35]). Notice that the JGM3 gravity model is presently used for both Jason-1 and T/P precise orbit calculations. Substantial improvements in orbit calculation are expected from the use of new gravity models, see section 7.4.

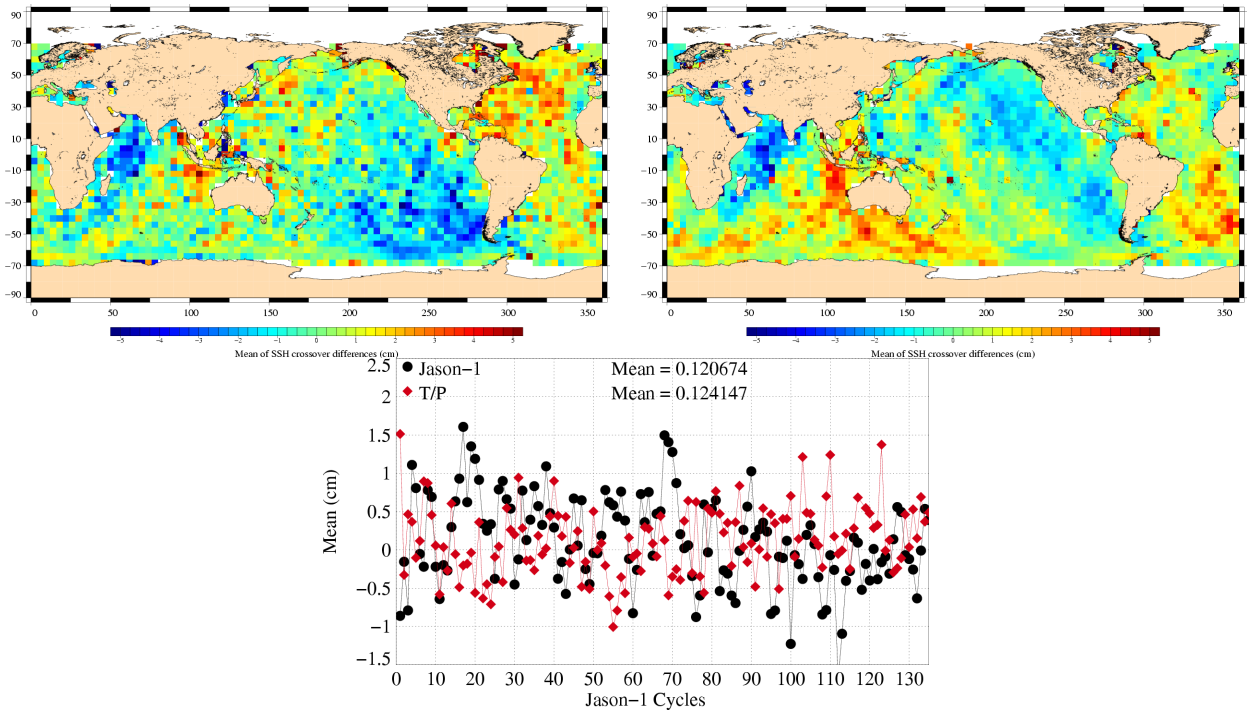

Figure 45: *Map of mean crossovers for Jason (right) and T/P (left) from Jason-1 cycle 1 to 135, and cycle per cycle mean crossovers (bottom)*

5.2 Standard deviation of crossover differences

The cycle per cycle standard deviation of crossover differences are plotted in figure 46 (on the left) according to different crossover selection. 3 selections are applied:

- Black curve: no selection is applied. The mean value is 7.74 cm. It shows an annual signal linked to the sea ice variations in the Northern Hemisphere.
- Red curve: shallow waters have been removed (bathy<-1000m). The previous annual signal has been removed by this selection even though it remains a signal probably due to seasonal ocean variations.
- Blue curve: the last selection allows monitoring the Jason-1 system performance. Indeed, areas with shallow waters (1000 m), of high ocean variability (> 20 cm) and of high latitudes (> |50| degrees) have been removed. The standard deviation then provides reliable estimate of the altimeter system performances. In that case, no trend is observed in the standard deviation of Jason-1 SSH crossovers: good performances are obtained, with a standard deviation value of about 6.1 cm all along the mission.

The map of standard deviation of crossover differences over cycle 1 to 135, in figure 46 (on the right) shows usual results with high variability areas linked to ocean variability.

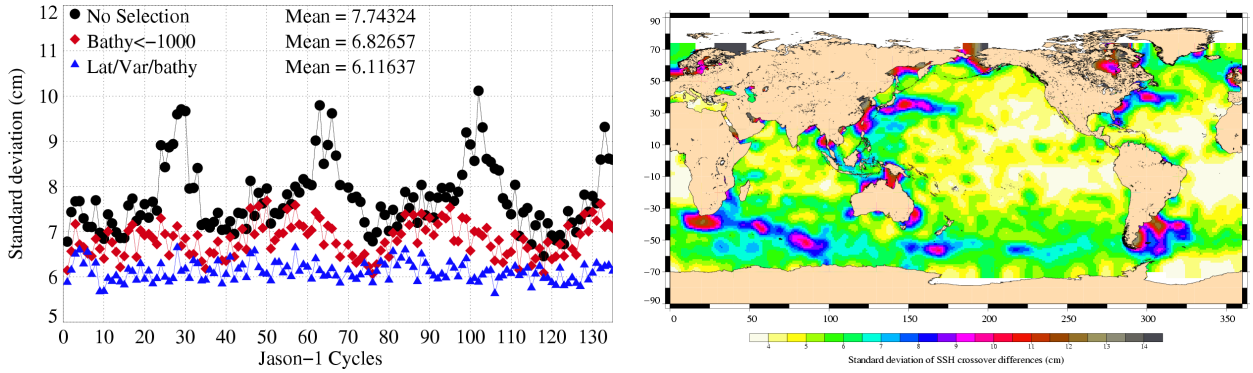

Figure 46: *Cycle per cycle standard deviation crossovers with different selections and map of Jason-1 standard deviation crossovers*

5.3 Compare Jason-1 and T/P at crossovers

When comparing performances relative to another mission, much care has to be taken in order to cancel out the contributions of ocean variability and geophysical corrections. Such a comparison between Jason-1 and T/P results has been performed. Apart from homogeneity in geophysical corrections for the two missions, additional processing care has been taken in order to get the most meaningful comparison figures as possible: only open ocean data are selected, away from areas with large ocean variability or with seasonal coverage by sea ice. Furthermore, to account for missing measurements on both missions - in particular due to tape recorder problems on T/P - data are only considered from common datasets. Finally, the SSH computation at crossovers is performed with exactly the same interpolation procedure using cubic spline functions. In order to keep the full 1 Hz high frequency content of the two missions, the spline functions are forced to go through the exact values of the points used in the interpolation, without any smoothing.

In order to distinguish between the effects of long wavelength signals such as orbit errors and the effects of short wavelengths such as instrumental noise, an along-track filtering procedure is used before crossovers are computed. A low-pass filter (Hamming, 1977 [26]) with a cut-off wavelength of 50 km is applied to both Jason-1 and T/P (SSH - MSS) differences. In this case, the CLS01 MSS global model is used. The low frequency signal is directly the output of the filtering routine, while the high frequency signal is derived from the difference between the original signal and the low frequency signal. Then the standard deviation of crossover differences is computed for both satellites on three different datasets: for all wavelengths, for wavelengths larger than 50 km and for wavelengths shorter than 50 km.

The results are presented in figure 47 (bottom). The overall standard deviation is higher for Jason-1 than for TOPEX. However, the 1 Hz high frequency content is not the same, due to different altimeter ground processing. At the opposite of TOPEX, Jason-1 data are processed by a ground retracking algorithm which makes altimeter measurements more decorrelated (Zanife et al. 2003 [60]). Therefore, TOPEX data are then smoother than Jason-1 data: the 1 Hz high frequency content is lower for TOPEX. The respective contribution of low and high frequencies in Jason-1 and TOPEX crossover residuals is displayed in figure 47.

Figure 47 on the top right shows that short wavelengths contribute a lot in the difference between Jason-1 and TOPEX. While a value of 3 cm is obtained for Jason-1, less than 2.5 cm is observed on TOPEX when wavelengths shorter than 50 km are only considered. Note that for T/P cycle 361 (Jason-1 cycle 18), the Poseidon-1 altimeter was switched on and leads to comparable results relative to Jason-1. Still in figure 47 on the right, another interesting feature is observed from T/P cycles 366 to 369 (Jason-1 cycles 22 to 25): the T/P standard deviation increases and then remains higher than at the beginning of the series. During this period, the T/P satellite was moved away from its original ground track (presently the Jason-1 ground track). Since the along-track filtering is performed on (SSH - MSS) differences, (SSH - MSS) differences between ascending and descending passes are computed instead of SSH differences. Thus errors of the global MSS model away from the initial nominal T/P ground track impact the T/P results after the orbit is moved. Since the crossover location is the same on the two passes - ascending and descending -, higher variance reveals the signature of MSS slope errors in the crossing directions, away from the nominal track used to compute the MSS.

The contribution of wavelengths higher than 50 km is analyzed in figure 47 on the left. Larger differences between Jason-1 and TOPEX are observed before Jason-1 cycle 8. Then Jason-1 and T/P curves are very similar, even if TOPEX figures are slightly lower than Jason ones. Orbit errors are probably responsible for Jason-1 degraded results on early cycles. It is worth recalling that when producing the GDR dataset,

improvements have been brought to the Jason-1 POE orbit calculation, in particular to manage maneuvers. Because these orbits were recomputed from cycle 9 only, higher variance is obtained for the 8 first Jason-1 cycles.

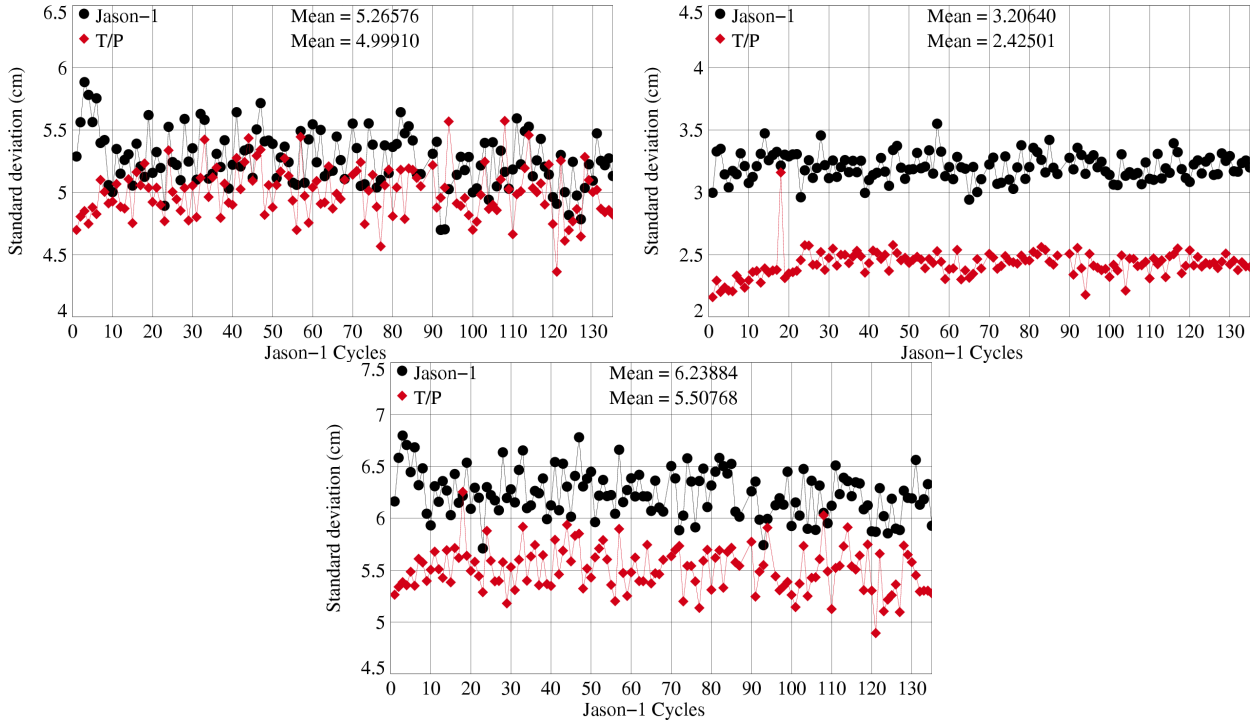

Figure 47: *Cycle per cycle standard deviation crossovers for long wave length content (left), short wave length content (right) and total content (bottom)*

6 Along-track analysis

This analysis is used to compute Sea Level Anomalies (SLA) variability and thus to estimate data quality; it is used to determine the SSH bias between Jason-1 and T/P and the trend in the Mean Sea Level (MSL).

6.1 Along-track performances

6.1.1 Along-track performances before along-track filtering

Along track analyzes are also used to assess the altimeter system performances, by computing Sea Level Anomalies (SLA). The SLA variance gives an estimate of the errors of the system, even though the ocean variability fully contributes in this case. As in the crossover analysis (see in section 5.3), the same type of comparison between Jason-1 and T/P has been performed computing the variance of SLA relative to the CLS01 MSS. This allows global and direct calculations.
The SLA standard deviation is plotted in figure 48 for Jason-1 and T/P. It exhibits similar and good performances for both satellites. However, during the verification phase, the variability is slightly higher for Jason-1 but from cycle 26 onward the performances are very similar. A significant signal is observed from cycle 25 to 35. It is due to the 2002-2003 "El Niño" (McPhaden, 2003, [40]).

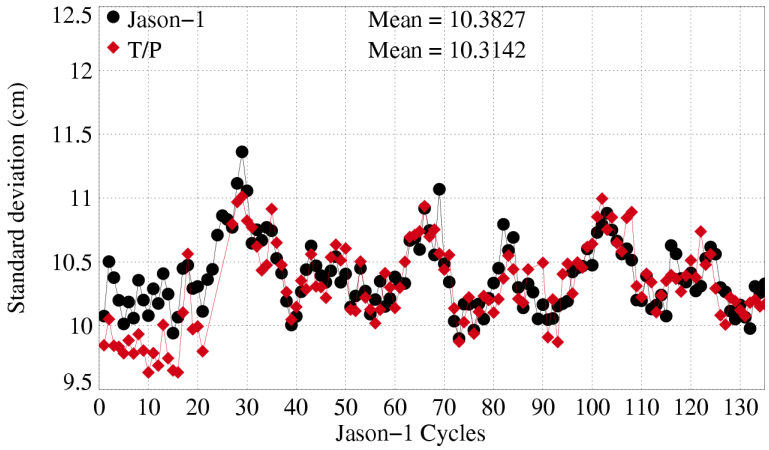

Figure 48: *Cycle per cycle SLA standard deviation*

6.1.2 Along-track performances after along-track filtering

Prior filtering of (SSH - MSS) differences has been applied to produce estimations of the variance (standard deviation) of Jason-1 and T/P SLA according to the selected wavelengths. SLA are computed relative to a global MSS model because the data can be processed in the same way before and after the T/P ground track moves. Moreover, like in the crossover analysis case, measurements are carefully extracted from common datasets and identical processing is applied to both missions.

Figure 49 shows the standard deviation of Jason-1 and T/P SLA differences after along-track filtering, in order to investigate different ranges of wavelengths: less than 50 km, between 50 and 500 km, and more than 500 km. Since geophysical corrections are the same for the two satellites, the first wavelength interval is expected to mostly represent differences in high frequency content, while the last should mainly evidence orbit error differences. Like in the crossover analysis, the Jason-1 high frequency content is higher than the TOPEX one. As already explained, the difference mainly comes from different altimeter ground processing. Poseidon cycle 361 (Jason-1 cycle 18) is evidenced on the curve, with a standard deviation estimation very close to those of Jason-1. For Wavelengths between 50 and 500 km (figure 49 on the right), the standard deviation curves obtained for Jason-1 and T/P are indistinguishable when the two satellites are flying on the same ground track. The signature of MSS errors appears in both figures 49 on the right and bottom after the T/P ground track changes. The long wavelength content showed in figure 49 on the left principally differs between the two satellites in the beginning of the Jason-1 mission. Until Jason-1 cycle 8, larger orbit errors are present on Jason-1 data because these cycles have not been reprocessed, as explained previously. However the difference seems to continue to around cycle 15, contrary to what was observed in the crossover analysis. Higher orbit errors on these Jason-1 particular cycles might be one explanation of this higher variability relative to the MSS. After the first cycles, even slightly larger, the Jason-1 results are much closer to the T/P ones.

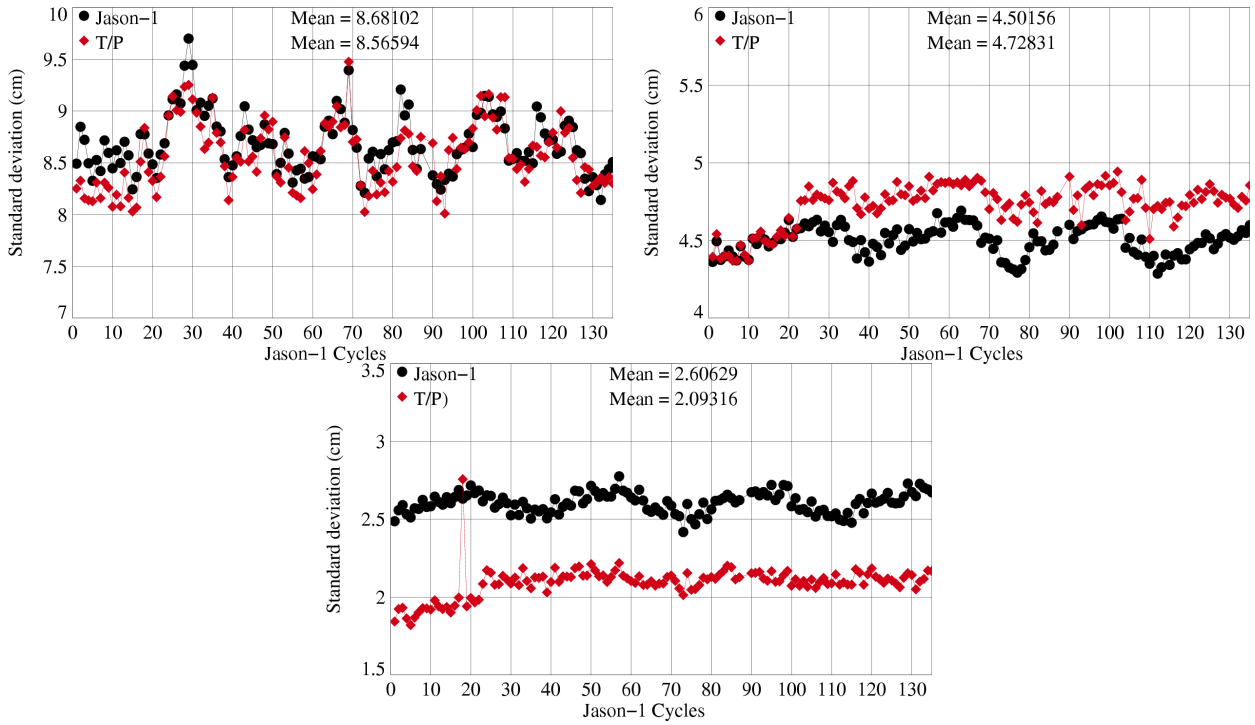

Figure 49: *Cycle per cycle SLA standard deviation for long wavelength content (left), medium wave length content (right) and short wavelength content (bottom)*

6.2 Mean sea level

6.2.1 Sea surface height estimation

The JMR wet troposphere correction experienced two major changes from the beginning of the Jason-1 mission. These changes significantly impact Jason-1 SSH estimations at the 1 cm level. Therefore, before instrumental and algorithmic investigations performed at JPL and applied in the next GDRs release, the Jason-1 radiometer wet troposphere correction is not suitable for Mean Sea Level (MSL) estimations. In order to assess the Jason-1 altimeter performances in terms of MSL estimations, the ECMWF wet troposphere correction is used, as no change in the model has impacted the data since Jason-1 cycle 1.
MSL estimations from Jason-1 and T/P are plotted in figure 50 (on the left), after reduction of the relative bias between the two measurements. The results are obtained after area weighting (Dorandeu and Le Traon 1999 [16]). The figure shows good agreement between the two missions and demonstrates that the Jason-1 mission will ensure continuous precise MSL monitoring as it was done for more than a decade by the T/P mission. On both missions, seasonal signals are observed, because the inverse barometer correction has been applied in the SSH computation (Dorandeu and Le Traon 1999 [16]). Moreover, 60-day signals are also detected on Jason-1 and T/P series, with nearly the same amplitude. This signal might be due to residual orbit errors since variations of the so-called Beta-prime angle are present at this period for both satellites. Another source of error could be from the largest tidal constituents at twice-daily periods which alias at periods near 60 days for Jason-1 and T/P (Marshall et al. 1995 [36]). Orbit errors in T/P altimeter series used to compute the tide solutions could also have contaminated these models (Luthcke et al. 2003 [35]).
On the right figure 50, annual, semi-annual, and 60-days signals have been adjusted. This allows to decrease the adjustement formal error for both satellites. The global MSL slope is very similar.

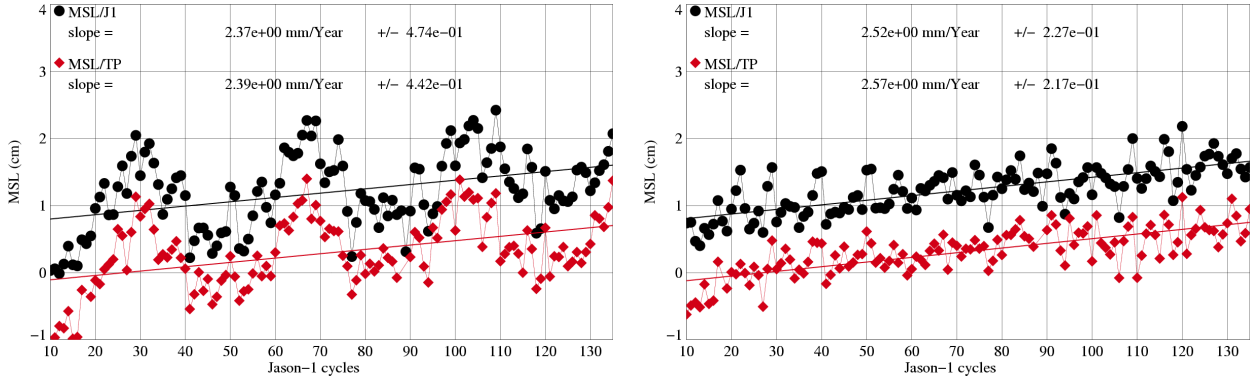

Figure 50: *Jason-1 and T/P mean sea level (on the left) with annual and semi-annual adjustment (on the right)*

6.2.2 SSH bias between Jason-1 and T/P

The ECWMF wet troposphere correction is also used in figure 51 which represents the SSH bias between T/P and Jason-1. This prevents from errors due to radiometer biases, as the model correction is the same for the two missions. The impact of all geophysical corrections and the particular effect of the SSB correction are also investigated in the figure. Among all geophysical corrections, the greater impact on the T/P to Jason-1 SSH bias estimation is produced by the SSB correction, since results differ by more than 6 cm when applying or not this correction. Notice that present results have been obtained using a dedicated TOPEX Side B SSB estimation (S. Labroue et al. 2002), since TOPEX side A and side B SSB models are different (e.g. Chambers et al. 2003). Apart from some higher variability in the first Jason-1 cycles, probably because of orbit calculation, the T/P to Jason-1 SSH bias nearly remains constant through the Jason-1 mission period.

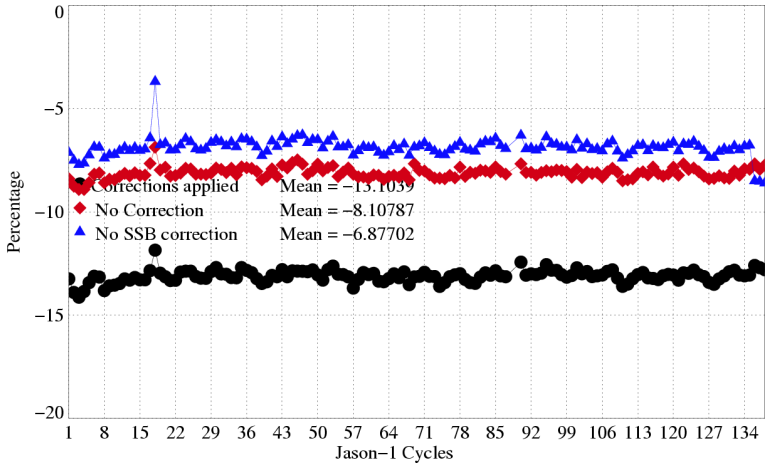

Figure 51: *Cycle per cycle mean of (T/P Jason-1) SSH differences*

6.2.3 Hemispheric SSH bias between Jason-1 and T/P

In order to further investigate (T/P−Jason-1) SSH biases, the same calculation has been performed at global and hemispheric scales. The results are presented in figure 52. Contrary to the global estimation, large hemispheric differences appear between T/P and Jason-1. From the northern hemisphere to the southern hemisphere the (T/P−Jason-1) SSH bias estimates can thus differ by up to 2 cm. These hemispheric differences seem consistent from one cycle to another, following a long period signal: three periods can be identified on the curves, with large, low and again large hemispheric differences. These differences are mainly due to the orbit :see section 7.4 dedicated to the impact of orbit calculation.

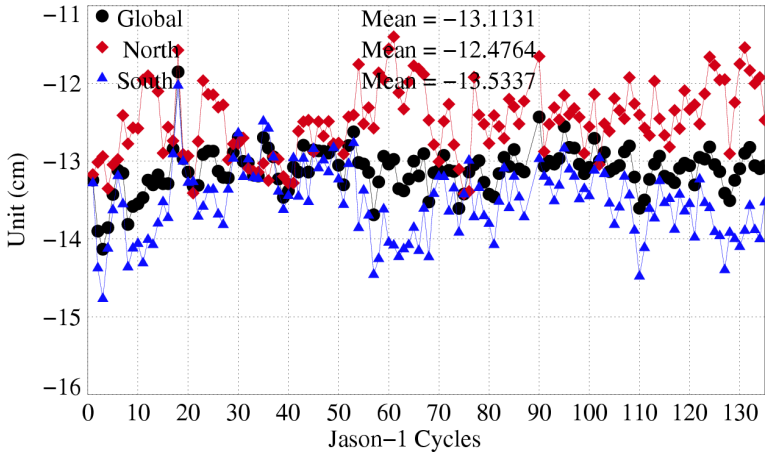

Figure 52: *Cycle per cycle mean of (T/PJason-1) SSH differences by hemisphere*

6.2.4 Map of SSH bias between Jason-1 and T/P

Jason-1 and T/P have not been on the same track from cycle 21 onward. Consequently, the SSH differences can not be obtained directly as a result of the ocean variability. Thus, the map of the SSH differences between Jason-1 and T/P is obtained at the Jason-T/P crossovers in figure 53. As in previous figure 52, an hemispheric signal is visible. Residual orbit errors on both missions could be one candidate to explain such differences. The impact of the orbit calculation is described in section 7.4.

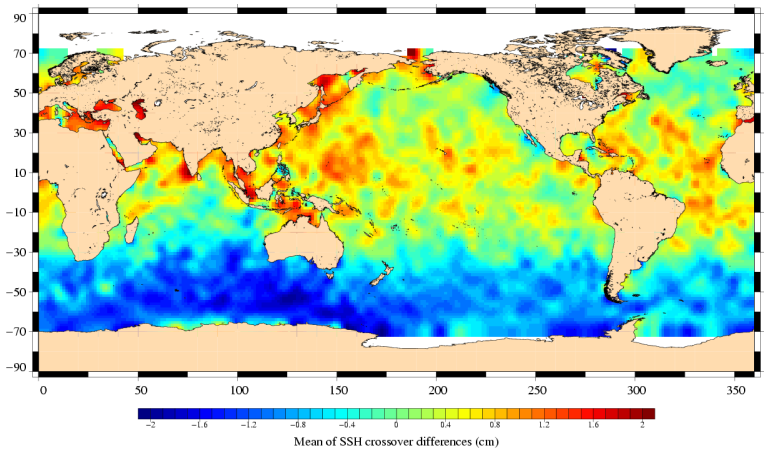

Figure 53: *Map of (T/PJason-1) SSH differences*

6.3 Sea level seasonal variations

From Sea Level Anomalies computed relative to the Mean Sea Surface CLS 2001 (Hernandez et al, 2001), the surface topography seasonal variations have been mapped in figure 54 for the overall Jason-1 data set. Major oceanic signals are showed clearly by these maps: it allow us to assess the data quality for oceanographic applications. The most important changes are observed in the equatorial band with the development of an El Niño in 2002-2003. The event peaked in the fourth quarter of 2002, and declined early in 2003. Conditions indicate an event of moderate intensity that is significantly weaker than the strong 1997-1998 El Niño (McPhaden,2003, [40]).

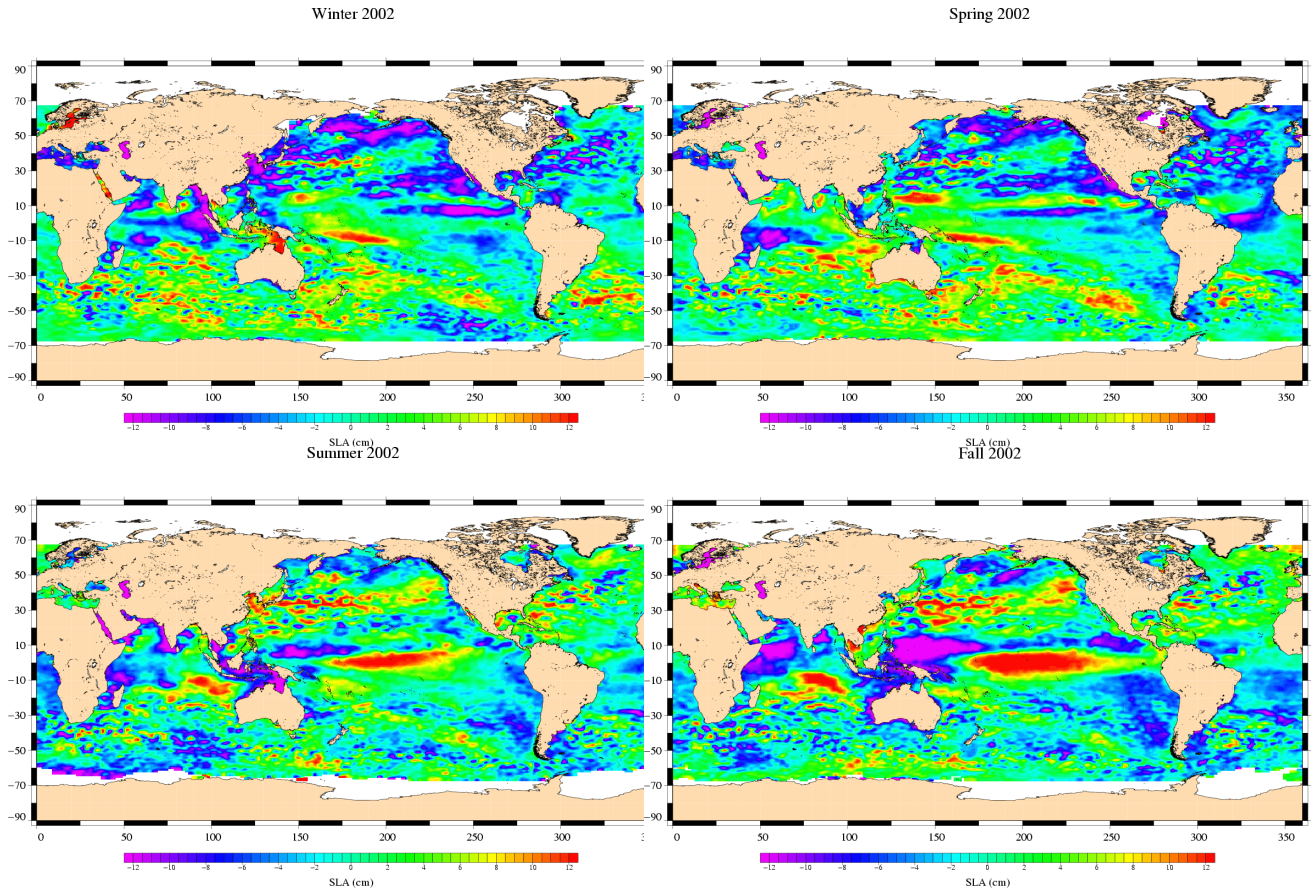

Figure 54: *Seasonal variations of Jason SLA (cm) for year 2002 relative to a MSS CLS 2001*

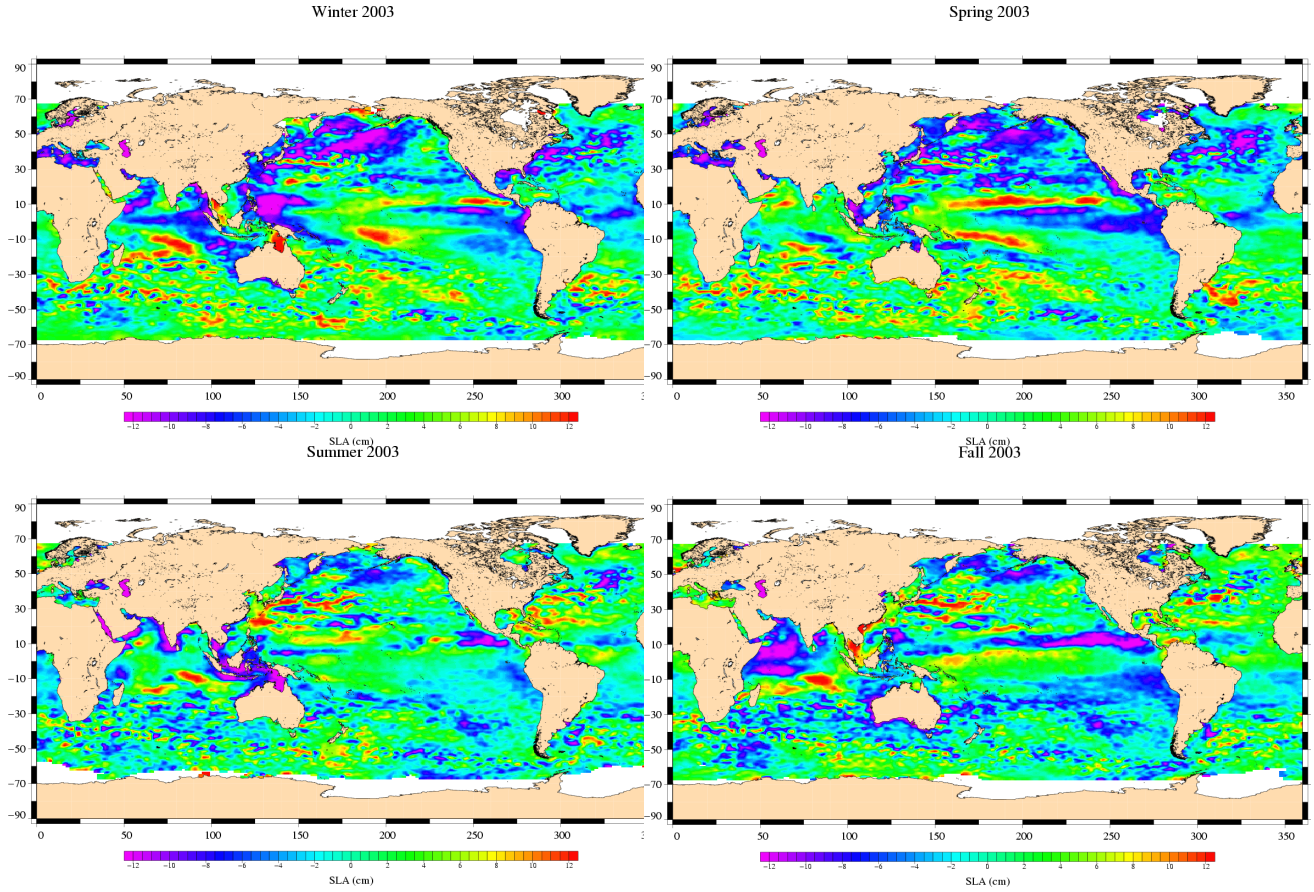

Figure 55: *Seasonal variations of Jason SLA (cm) for year 2003 relative to a MSS CLS 2001*

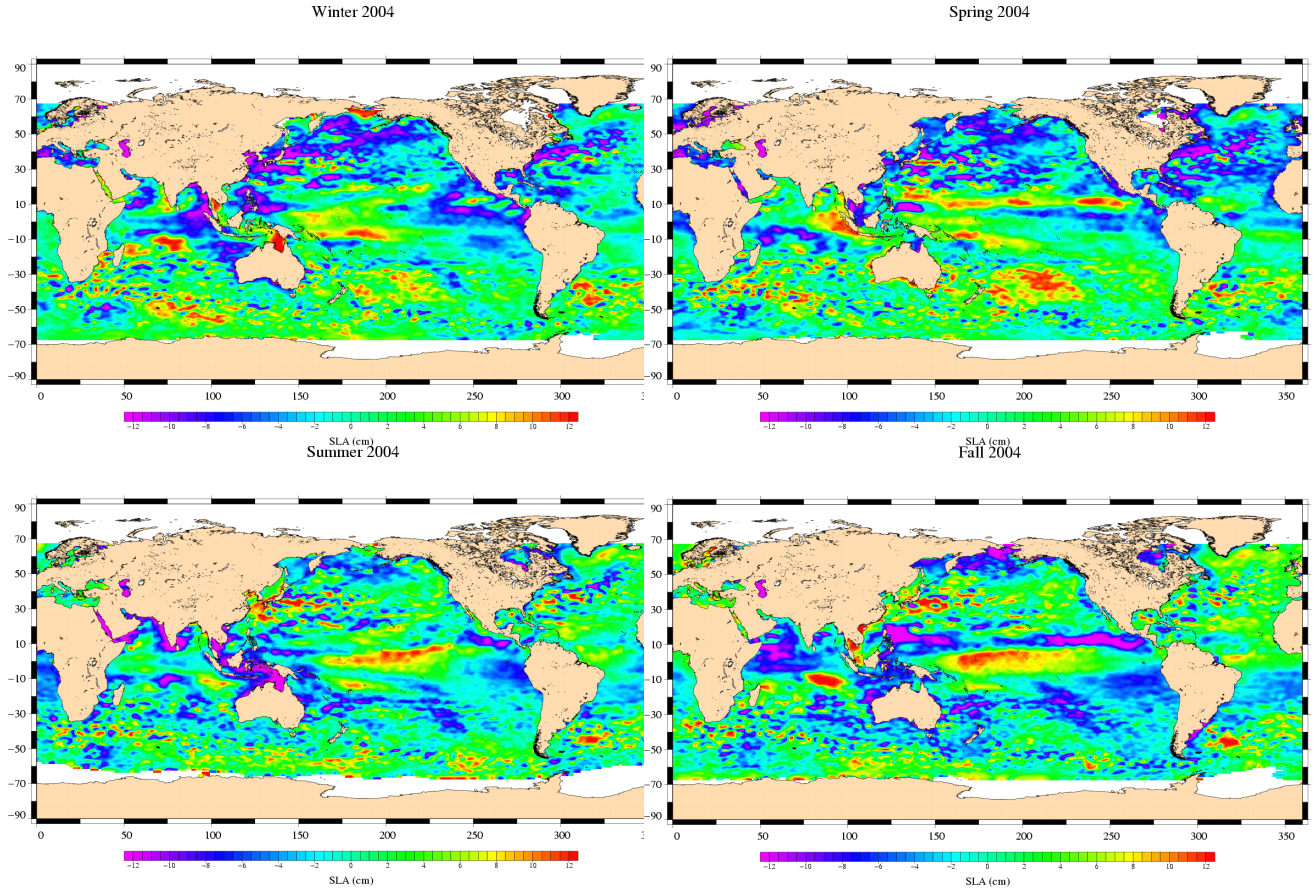

Figure 56: *Seasonal variations of Jason SLA (cm) for year 2004 relative to a MSS CLS 2001*

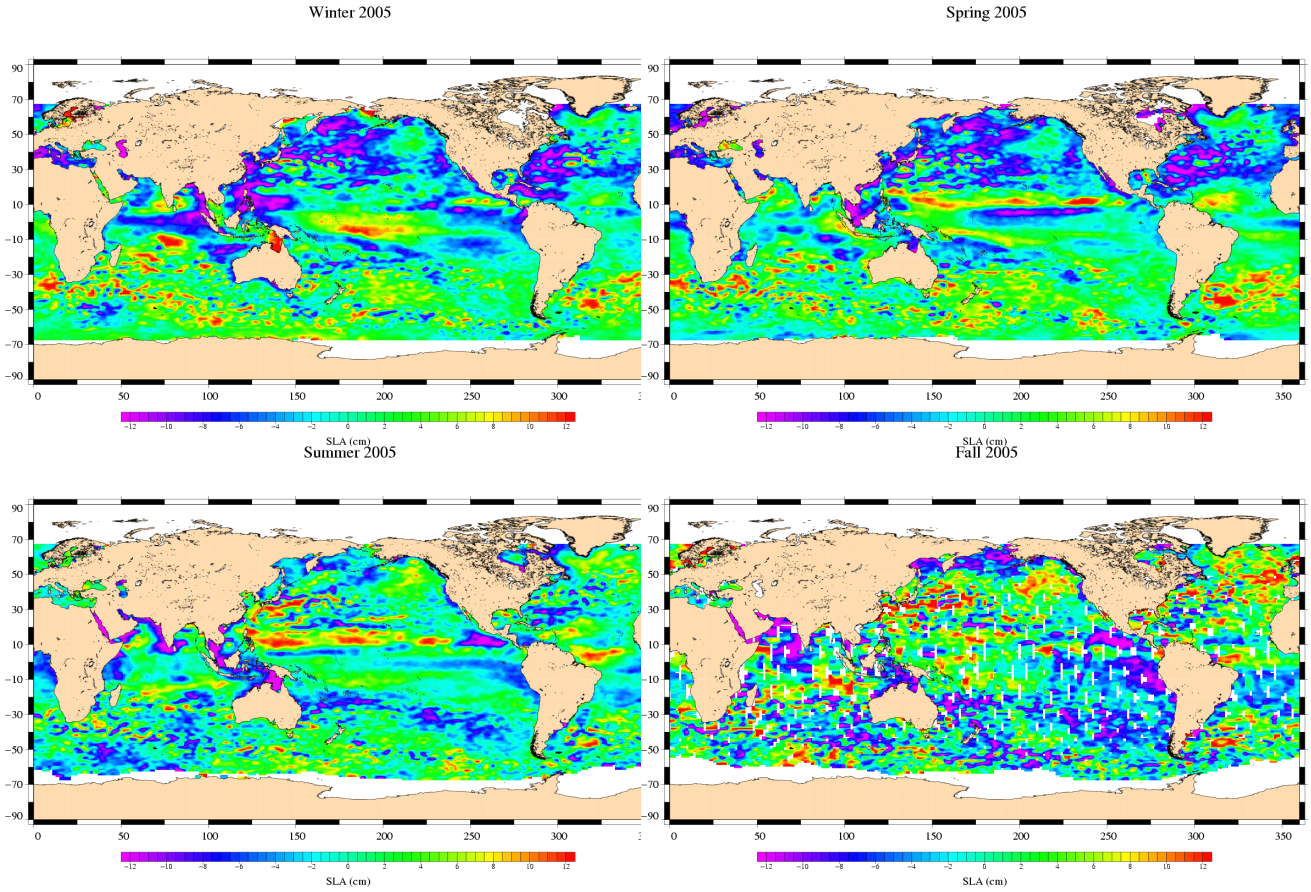

Figure 57: *Seasonal variations of Jason SLA (cm) for year 2005 relative to a MSS CLS 2001*

7 New Standards

The objective of this section is to show the performance impact of new geophysical corrections such new tidal models and MOG2D correction in the GDRs 'b' described in section 2.3. The impact of the orbit using new gravity field is also described.

7.1 Statistical evaluation of Fes2004 tide model

7.1.1 Introduction

First, the FES04 model is compared to GOT00 model. Then, it is compared to older models, GOT99 and Fes99. Finally the impact of the new dynamic long period tide component is analyzed.
The performance criteria are the variance of SSH differences at crossovers and the variance of along track Sea Level anomalies. The analysis has been done on Jason-1, Envisat and GFO. The results for Jason-1 satellite are similar to those which would have been obtained for TOPEX/Poseidon satellite, as both satellites are on the same ground track.

7.1.2 Comparison Between FES2004 and GOT00V2

In this part, the FES04 model is compared to GOT00 model on a two-year period on Jason-1 (31-104), Envisat (11-31) and GFO (98-140).

7.1.2.1 SSH formulae

The parameters used to compute the sea surface height (SSH) for Jason-1 and Envisat are:

- radiometer wet troposphere correction
- ECMWF dry troposphere correction (rectangular grids)
- dual frequency ionospheric correction
- non parametric SSB
- MOG2D
- pole tide correction
- earth tide correction
- oceanic tide correction

The FES04 tide correction contains:

- the S1 and S2 atmospheric tide
- the dynamic long period tide

The original GOT00 tide correction contains:

- the S2 atmospheric tide
- the static long period tide

to be consistent, GOT00 has been computed as following:

$$\begin{aligned} GOT00_{used} &= original\ GOT00\ tide \\ &+ the\ S1\ atmospheric\ tide \\ &- static\ long\ period\ tide \\ &+ dynamic\ long\ period\ tide \end{aligned}$$

7.1.2.2 Along track differences

Figure 58 shows the mean differences between FES04 and GOT00 on the 3 satellites. The differences are around 0 for Jason-1. On Envisat, the differences can locally overtake 1 cm. The strongest differences are in Indonesia and at high latitude. On GFO, the differences are weak at mid and low latitude, but have strong values above 60°. This behavior is not explained so far.

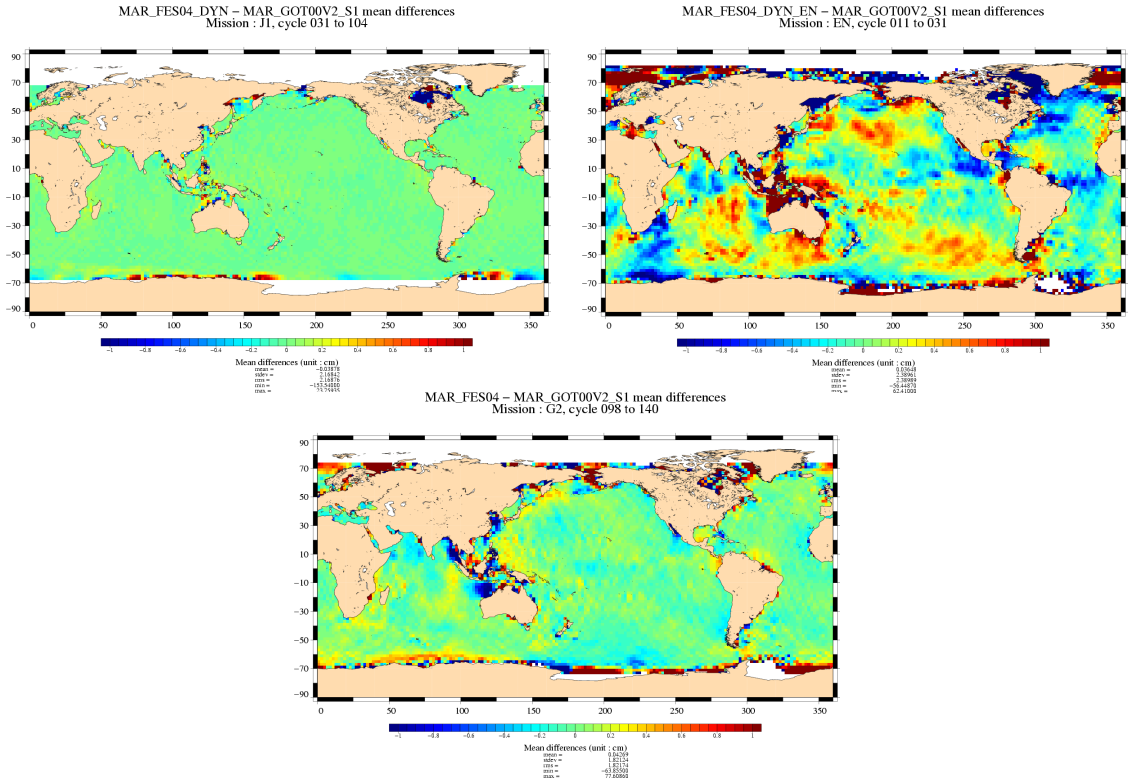

Figure 58: *Mean differences*

Figure 59 shows the variance of the difference between FES04 and GOT00 on the 3 satellites. The 3 maps are similar. High differences are found on low bathymetry areas and at high latitudes.

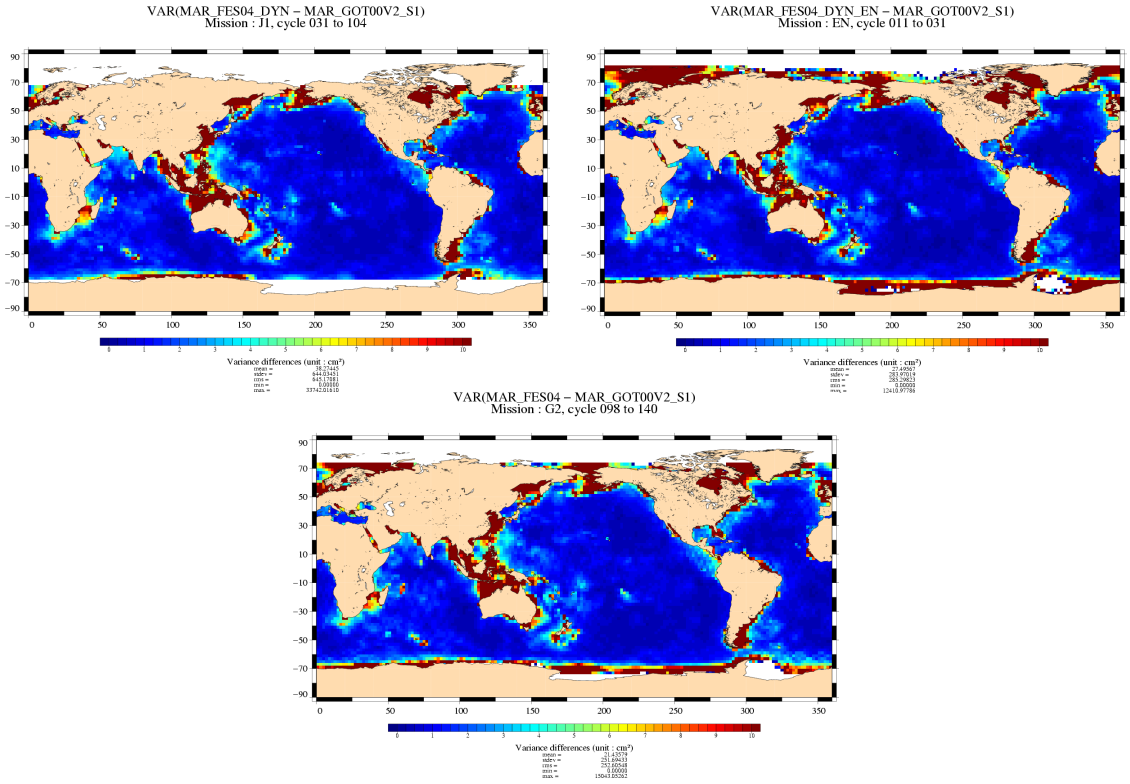

Figure 59: *Variance differences*

7.1.2.3 Performance at crossovers

Figures 60 and 61 show respectively the gain and the normalized gain at crossovers between FES04 and GOT00 on the 3 satellites. The blue color means that FES04 has a lower variance of SSH differences at crossover than GOT00. The red color means that FES04 has a larger variance of SSH differences at crossover than GOT00. For the 3 satellites, in open ocean at mid and low latitude, FES04 and GOT00 have approximately the same performances. In coastal regions and semi enclosed seas, at mid and low latitude, GOT00 better performs than FES04. It is especially true for Indonesia, China sea, Okhotsk Sea, Bering Sea or Hudson bay. This is due to the use of regional models in GOT00. At high latitude FES04 better performs than GOT00. This is particularly visible on Envisat because of its inclination.
The average variance differences over the period are summarized on tables 7, 8 and 9. These values confirm the pattern observed on the figures.

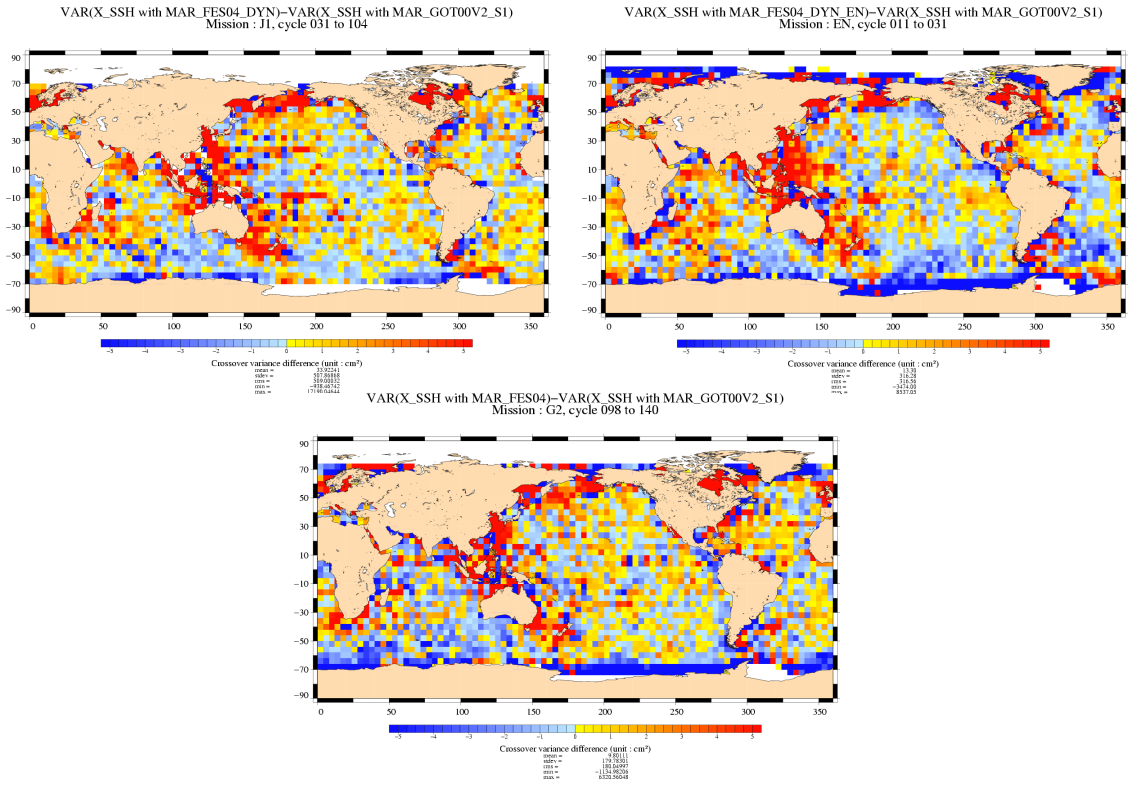

Figure 60: *Gain at crossovers*

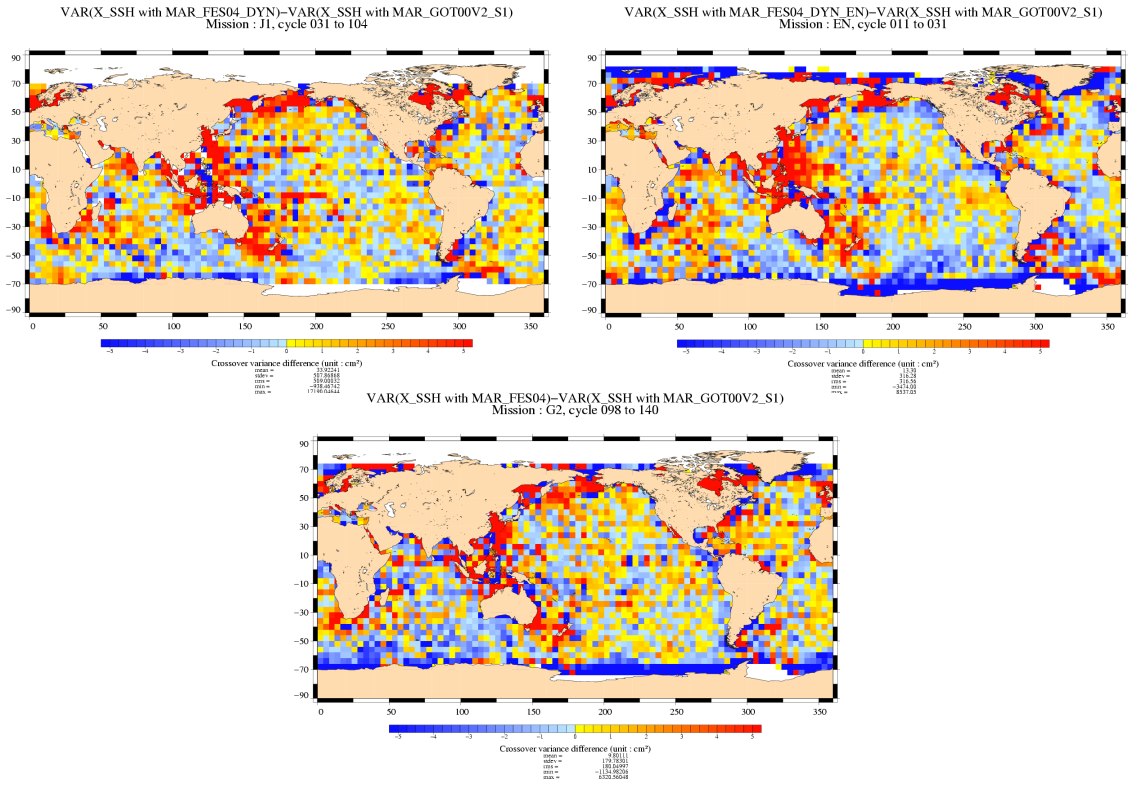

Figure 61: *Normalized gain at crossovers*

Bathy \ Lat	No selection	$\|Lat\| < 50$	$\|Lat\| > 50$
No selection	13.25	–	–
Bathy < -1000 (m)	0.15	0.41	-0.05
Bathy > -1000 (m)	110.4	167.6	83.22

Table 7: *J*ASON var(X_SSH_FES04)-var(X_SSH_GOT00V2)

Bathy \ Lat	No selection	$\|Lat\| < 50$	$\|Lat\| > 50$
No selection	-1.64	–	–
Bathy < -1000 (m)	-1.80	0.008	-4.50
Bathy > -1000 (m)	4.83	55.50	-12.15

Table 8: *E*NVISAT var(X_SSH_FES04)-var(X_SSH_GOT00V2)

Bathy \ Lat	No selection	$\|Lat\| < 50$	$\|Lat\| > 50$
No selection	1.09	–	–
Bathy < -1000 (m)	-0.01	0.31	-2.34
Bathy > -1000 (m)	13.79	36	5.82

Table 9: *G*FO var(X_SSH_FES04)-var(X_SSH_GOT00V2)

7.1.2.4 Along track performances

Figures 62 and 63 show respectively the gain and the normalized gain along track between FES04 and GOT00 on the 3 satellites. The blue color means that FES04 has a lower variance of SLA than GOT00. The red color means that FES04 has a larger variance.
The results obtained along track are similar to those obtained at crossovers. Some oceanic signals are however observed on Envisat and GFO notably around the equator.

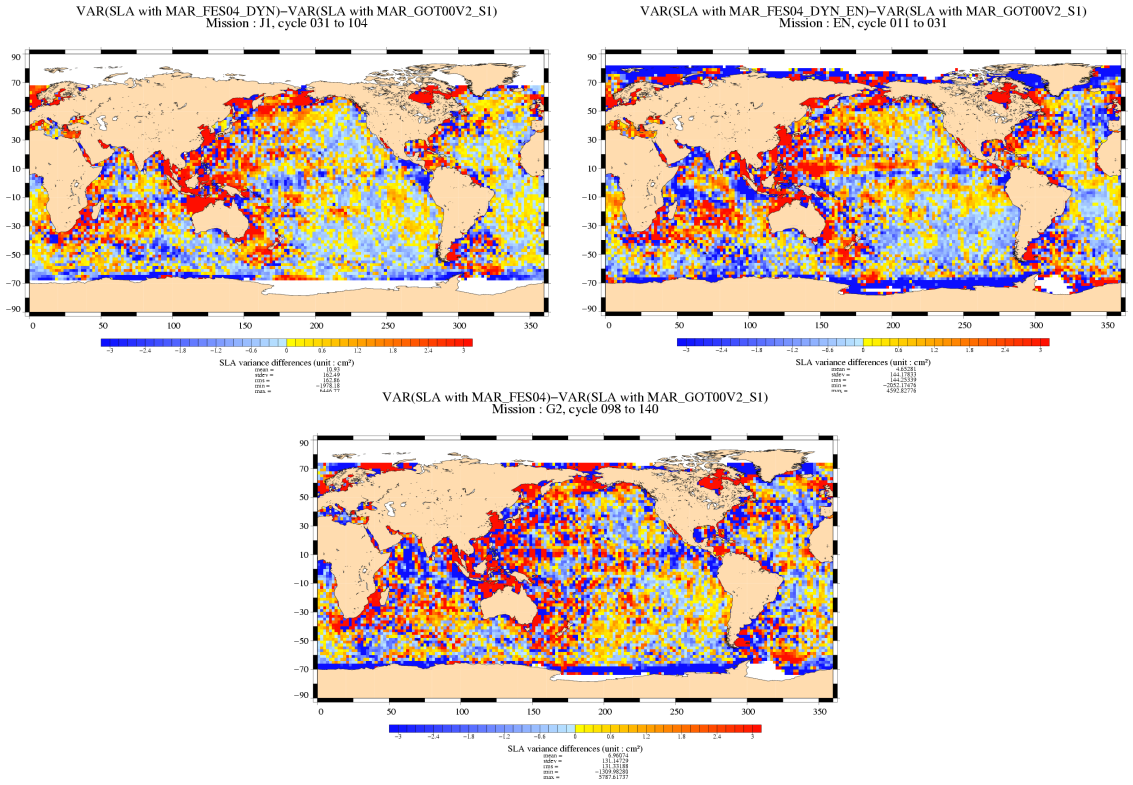

Figure 62: *Along track gain*

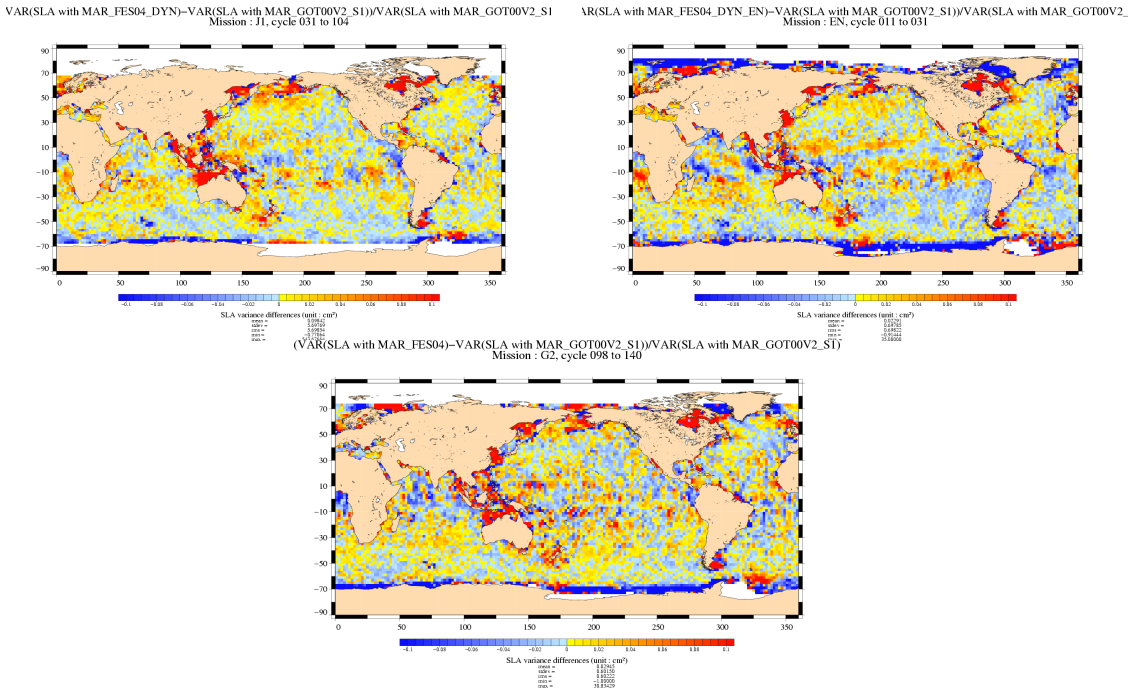

Figure 63: *Normalized gain at crossovers*

7.1.3 Comparison between FES2004, GOT99 and FES99

In this part, the FES04 model is compared to older models, GOT99 and FES99.
Note that FES04 and GOT00 include S1 and S2 atmospheric tide and dynamic long period tide.
FES04 is compared to GOT00 on Envisat (11-30) (a two-year period of data)

7.1.3.1 SSH formulae

The parameters used to compute the sea surface height (SSH) for Envisat are:

- radiometer wet troposphere correction
- ECMWF dry troposphere correction (rectangular grids)
- dual frequency ionospheric correction
- non parametric SSB
- MOG2D
- pole tide correction
- earth tide correction
- oceanic tide correction

The FES04 tide correction contains:

- the S1 and S2 atmospheric tide
- the dynamic long period tide

The original FES02 tide correction contains:

- neither contains S1 nor S2 atmospheric tide
- contains the static long period tide

The original GOT99 tide correction contains:

- the S2 atmospheric tide
- the static long period tide

For this analysis, FES04 has been computed as following:

$$\begin{aligned} FES04 &= original\ FES04\ tide \\ &+ static\ long\ period\ tide \\ &- dynamic\ long\ period\ tide \end{aligned}$$

So FES04 is not fully consistent with FES02 and GOT99.

7.1.3.2 Along track differences

Figure 64 shows the mean differences FES04-FES02 and FES04-GOT99 on Envisat. The S2 signal is clearly visible on the first map. The FES04-GOT99 differences are very similar to the FES04-GOT00 differences.

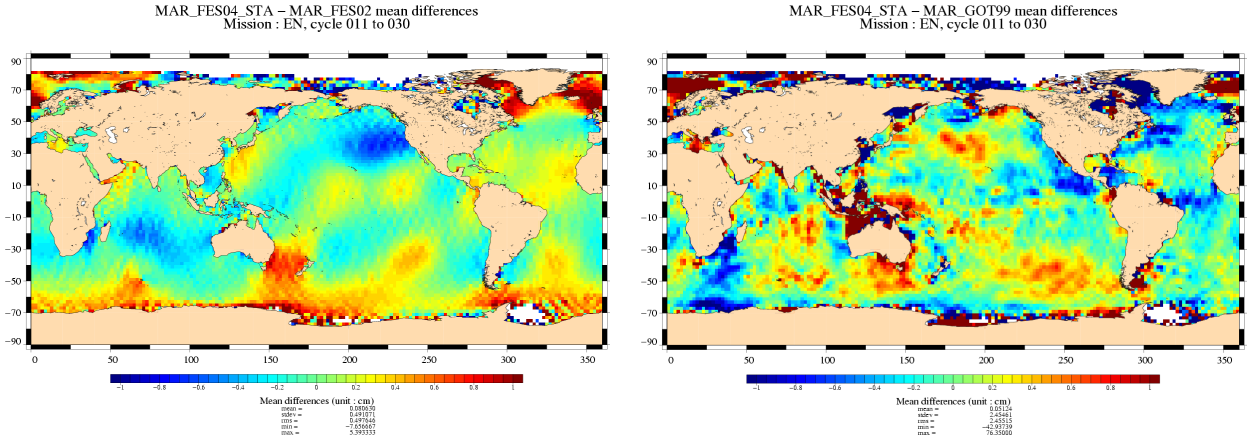

Figure 64: *Mean differences*

Figure 65 shows the variance of the differences FES04-FES02 and FES04-GOT99 on Envisat. As expected, the differences FES04 and FES02 are consistent. High differences are found on FES04-GOT99 in low bathymetry areas and at high latitudes.

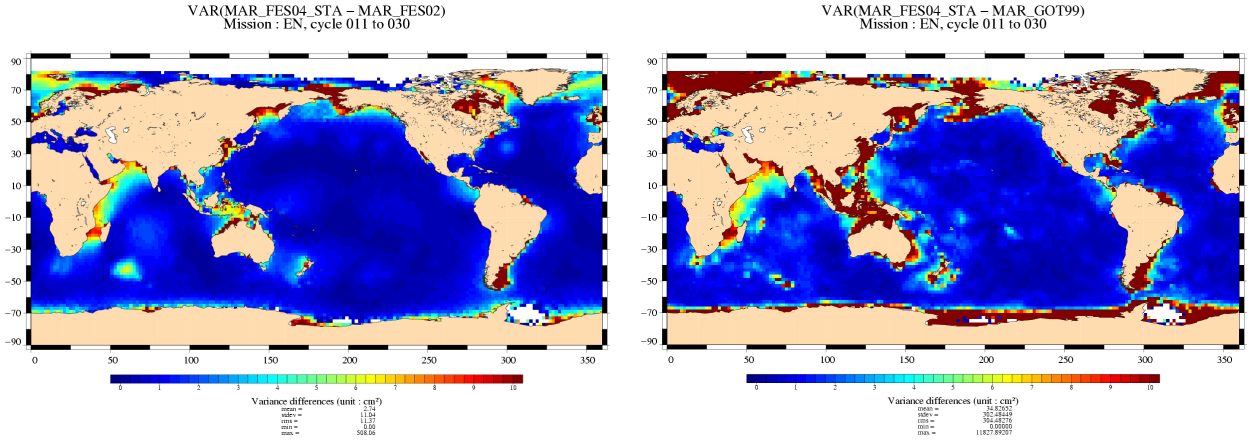

Figure 65: *Variance differences*

7.1.3.3 Performance at crossovers

Figure 66 shows the gain at crossovers between FES04/FES99 FES04/GOT99 on Envisat. The blue color means that FES04 has a lower variance of SSH differences at crossover than FES99 or GOT99. FES04 has, in average, lower variance than FES99 and GOT99, especially in high latitude and low bathymetry areas. However, GOT99 has, locally, a lower variance: over Indonesia and in the Indian ocean for example.

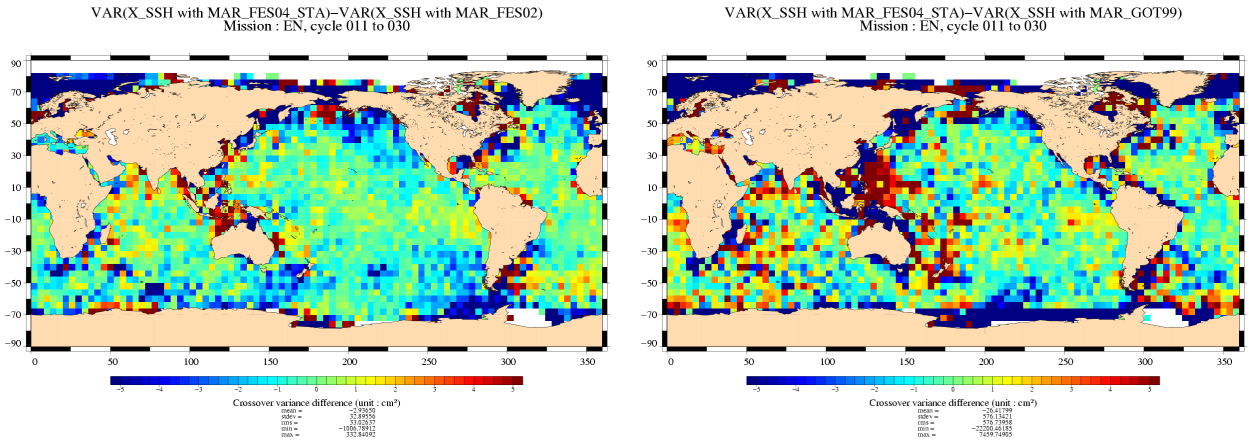

Figure 66: *Gain at crossovers*

7.1.3.4 Along track performances

Figure 67 shows the gain along track between FES04 and GOT00 on the 3 satellites. The results obtained along track are similar to those obtained at crossovers. Some oceanic signals are however observed.

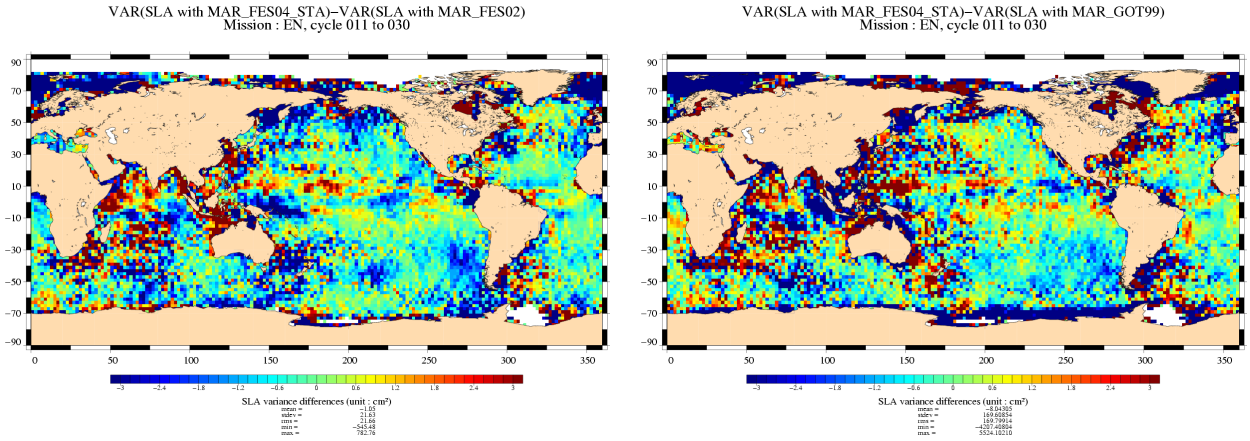

Figure 67: *Along track gain*

7.1.4 Impact of the dynamic long period tides

In this part, the impact of the new dynamic long period tide is analyzed on Envisat.
FES04 (dynamic) is compared to FES04 (static) on Jason-1 (1-101) (a three-year period of data)

7.1.4.1 SSH formulae

The parameters used to compute the sea surface height (SSH) for Jason-1 are:

- radiometer wet troposphere correction
- ECMWF dry troposphere correction (rectangular grids)
- dual frequency ionospheric correction
- non parametric SSB
- MOG2D
- pole tide correction
- earth tide correction
- oceanic tide correction

7.1.4.2 Along track differences

Figure 68 shows the mean difference Dynamic-Static long period tide. The differences are not very important, lower than 1cm.

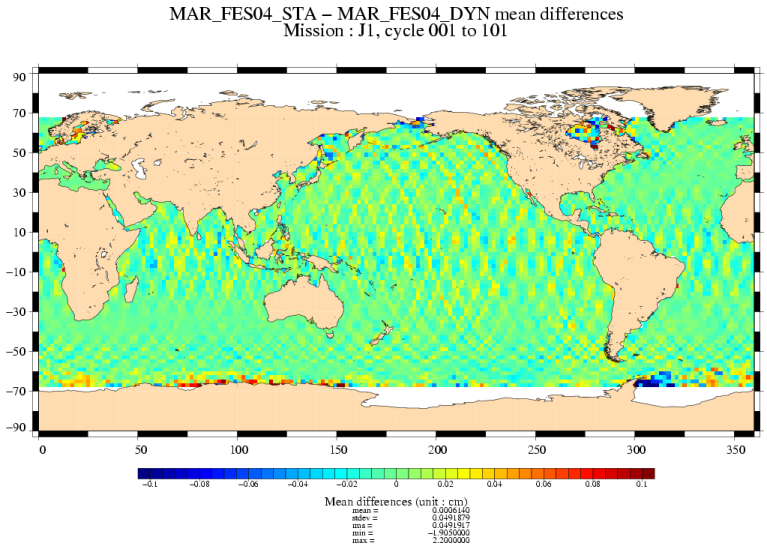

Figure 68: *Mean differences*

Figure 69 shows the variance of the difference Dynamic-Static long period tide.

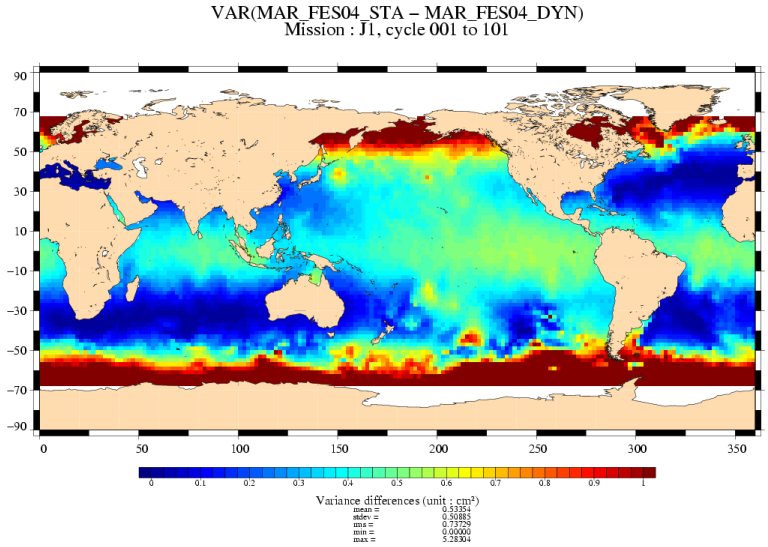

Figure 69: *Variance differences*

7.1.4.3 Performance at crossovers

Figure 70 shows the gain at crossovers between Static and dynamic. The red color means that the dynamic long period tide correction has a lower variance of SSH differences at crossover than the static long period tide correction. The differences are around 0 (-0.066 cm2). However, in the Pacific Ocean at mid latitude the dynamic long period tide has lower variance, and at latitude lower than 50˚S the static long period tide has lower variance.

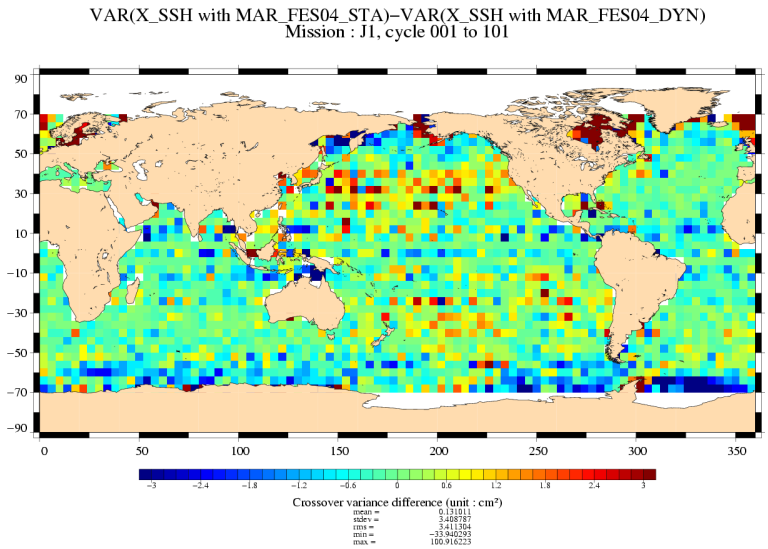

Figure 70: *Gain at crossovers*

7.1.4.4 Along track performances

Figure 71 shows the gain along track between Static and dynamics. The results obtained along track are similar to those obtained at crossovers.

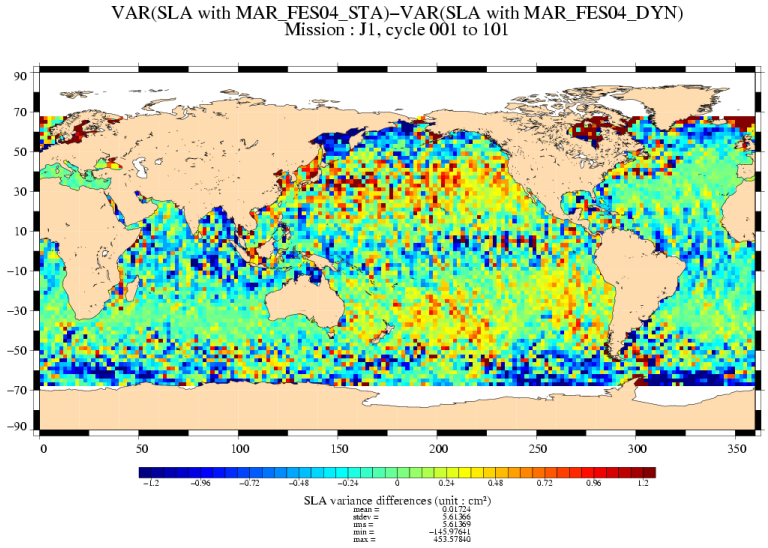

Figure 71: *Along track gain*

7.1.5 Conclusion

These 3 analyzes allow us to choose a tide model for our products between FES04 and GOT00. In open ocean at mid and low latitudes the performances of the 2 models are very close. FES04 better performed at high latitudes which is strongly visible on Envisat and GFO, but less obvious on Jason-1. GOT00 is better in coastal areas thanks to the use of regional model.

FES04 assimilation technique is more physical than GOT00. GOT00 is strongly adjusted on altimetric data. So with equivalent performance, the best choice would be FES04. Moreover the dynamic long periods have been computed for FES04. However the fact that FES04 has, locally, lower performances than GOT00 is an argument leading to the choice of GOT00.

7.2 Impact of the MOG2D correction

As a first approximation, the so-called Inverse Barometer correction is conventionally used to correct altimeter data. This simple correction assumes a static ocean response to atmospheric pressure forcing. Neither dynamical effects at high frequency nor wind effects are taken into account in this correction.
In order to take account of dynamical effects and wind forcing, a new correction is computed from the MOG2D (Carrere and Lyard, 2003 [9]) barotropic model forced by pressure (without S1 and S2 constituents) and wind. Only the high frequency part of these model outputs are retained and combined to the low frequency inverse barometer.
A comparison between the 2 types of corrections was made for the Envisat period. The Figure 72 displays comparisons between the two types of correction. It shows that in comparison to the inverse barometer correction, the MOG2D correction reduces greatly the crossover variance and SLA variance in regions of high frequency variability (high latitudes and shallow water).

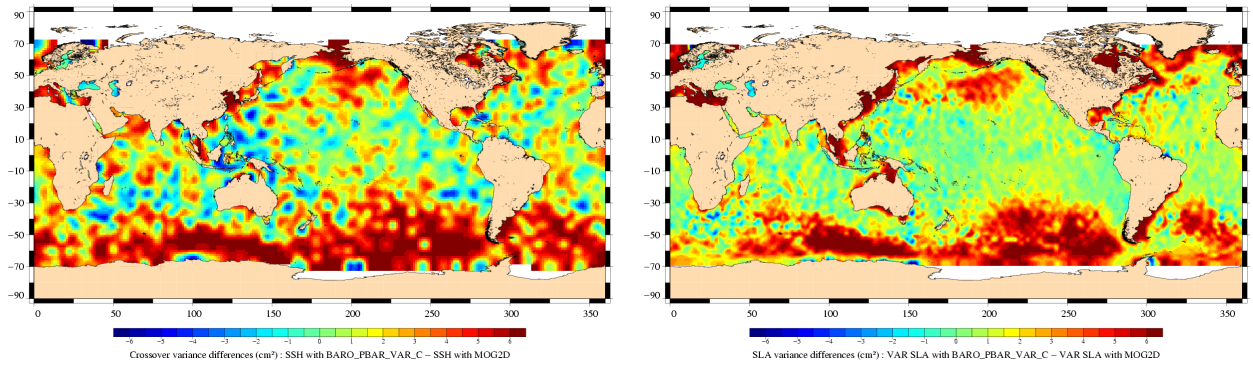

Figure 72: *Crossover variance difference (left) and SLA variance difference (right) when using correction MOG2D rather than inverse barometer correction*

7.3 Impact of new S1S2 wave model in dry troposphere

The S1 and S2 radiational tides are not well retrieved by ECMWF atmospheric fields (in particular because of poor temporal sampling). Following the QWG recommendation, the original S1 and S2 components are now filtered out from atmospheric and re-estimated using an S1/S2 model (Ponte and Ray, 2003 [48]) before computing the dry troposphere correction.
The figure 73 displays comparisons between the two dry tropospheric corrections for Jason-1 period. The two corrections are very close.

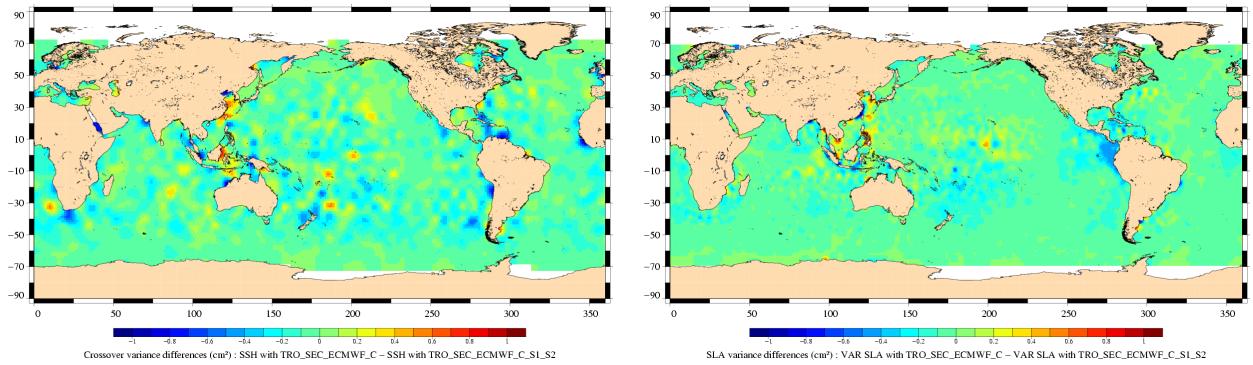

Figure 73: *Crossover variance difference (left) and SLA variance difference (right) when using dynamic S1S2 or only static S1S2 contributions for dry troposphere correction*

7.4 Impact of orbit calculation

7.4.1 Introduction

A new solution has been developed at CNES for the computation of the Jason POE orbit in September 2005. A new processing software and preliminary standards have been used. Cycle 110 to 132 have been reprocessed. The objective of this study is to assess and compare the reprocessed POE orbit to the GDR POE orbit. The new 3-technic orbit (further on called POE_J1_3T) has a configuration which will be close to the one furnished with the new GDR (CMA version 7.1).

7.4.2 Data

7.4.2.1 Processing

Cycle 110 to 132 have been computed and delivered, excluding cycles 121, 126 and 130 due to processing problems.
The reprocessed POE orbit has been updated in our database for cycles 120 to 129 allowing us to compare them to the GDR orbit.

After a first analysis, poor performances have been noticed for the following days:
- 2005-04-09 (cycle 120)
- 2005-04-19 (cycle 120)
- 2005-04-29 (cycle 122)
- 2005-06-07 (cycle 125)
- 2005-06-17 (cycle 127)
- 2005-07-10 (cycle 129)
- 2005-07-11 (cycle 129)
- 2005-07-17 (cycle 129)

These additional days have therefore been removed.

7.4.2.2 Orbit configurations

The main details of the processing of the POE are:

- Gravity: EIGEN3
- Eccentricity correction on Laser data
- Weighting Laser according to the quality of the site
- Oceanic load correction on laser station

7.4.3 Comparison POE_3T/GDR POE

7.4.3.1 Orbit differences

Figure 74 shows the mean differences over the period 120-129. On the two figures on the top, the ascending and descending passes have been plotted separately. On the bottom figure all the passes have been taken into account. There are local biases that can reach +4 and -3 cm in some areas. In South-West Pacific for example, between longitude 225 and 275, the reprocessed orbit has higher values than the GDR orbit, whereas in equatorial West Atlantic it has lesser values than the GDR orbit. The mean difference is very different on ascending and descending passes. In North Atlantic for example, the difference is negative on descending passes, slightly positive on ascending passes and consequently around zero using both.

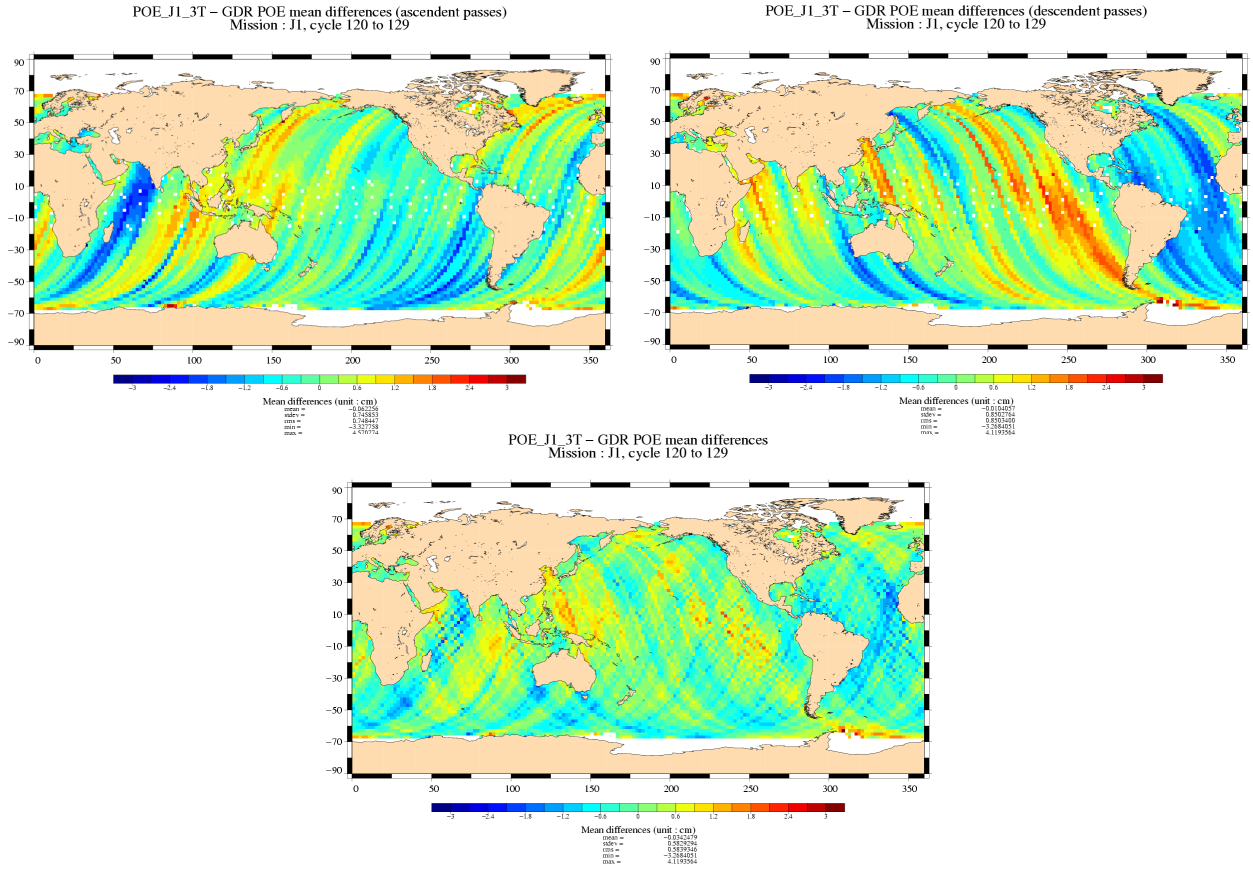

Figure 74: *POE_J1_3T 2005 - GDR POE mean differences. Ascending passes (left), descending passes (right) and total (bottom).*

Figure 75 shows the variance of the differences. The variance is quite low (generally less than 1cm2) in the Pacific for ascending passes and in the Indian ocean for descending passes. Elsewhere it can reach till 8cm2. This means that in these areas, the differences of the 2 orbits have a high temporally variability. On the total data set, the differences are quite big, especially in the North and South Atlantic, in the eastern South Pacific and in the western part of the Indian Ocean, where the differences exceed 3cm2.

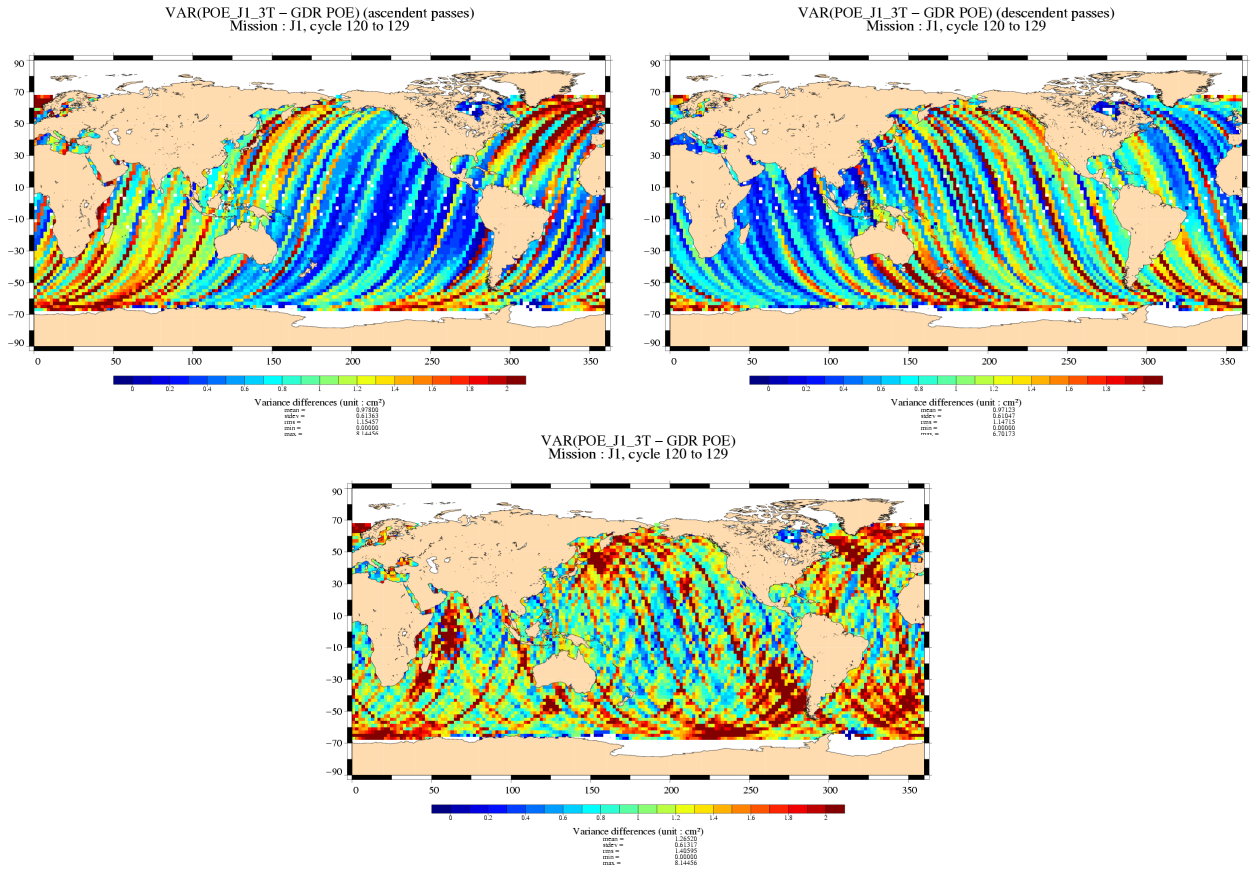

Figure 75: *Var(POE_J1_3T 2005 - GDR POE). Ascending passes (left), descending passes (right) and total (bottom).*

Figure 76 shows the cycle by cycle mean and variance of differences. The global bias between the two orbits is less than 2 mm. It is for the cycles 120-122 positive, for the other cycles (cycle 123-129) negative. The variance is about 1.6 cm2.

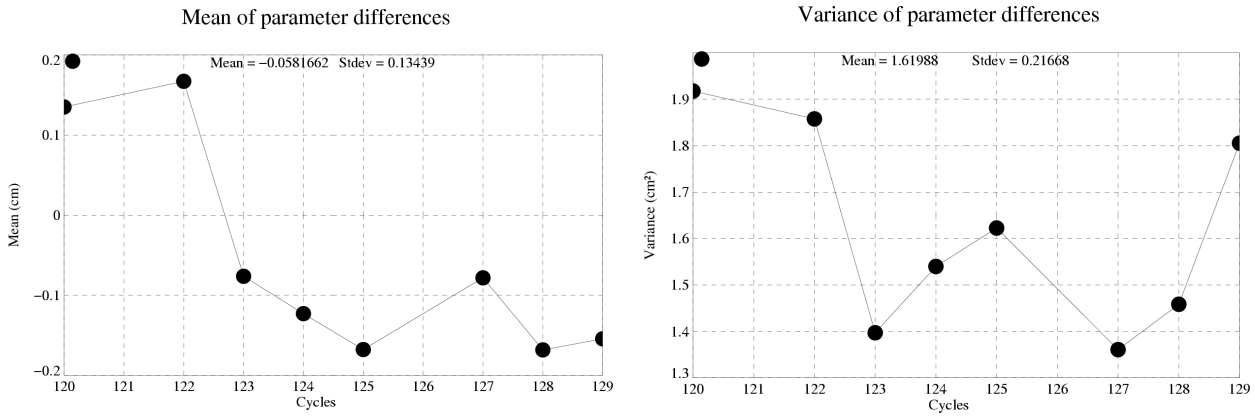

Figure 76: *Statistics per cycle of differences: mean (left) and variance (right).*

7.4.3.2 Crossovers performances

Figure 77 shows the mean SSH differences at crossovers using the POE_J1_3T orbit and the GDR orbit. With the GDR orbit, there are strong geographically correlated signals. On these areas (in red) the difference is positive which means that SSH on descending tracks > SSH on ascending tracks.

The geographically correlated signals are largely reduced with the new orbit. That is due to the use of the EIGEN3 gravity model in the new configuration.

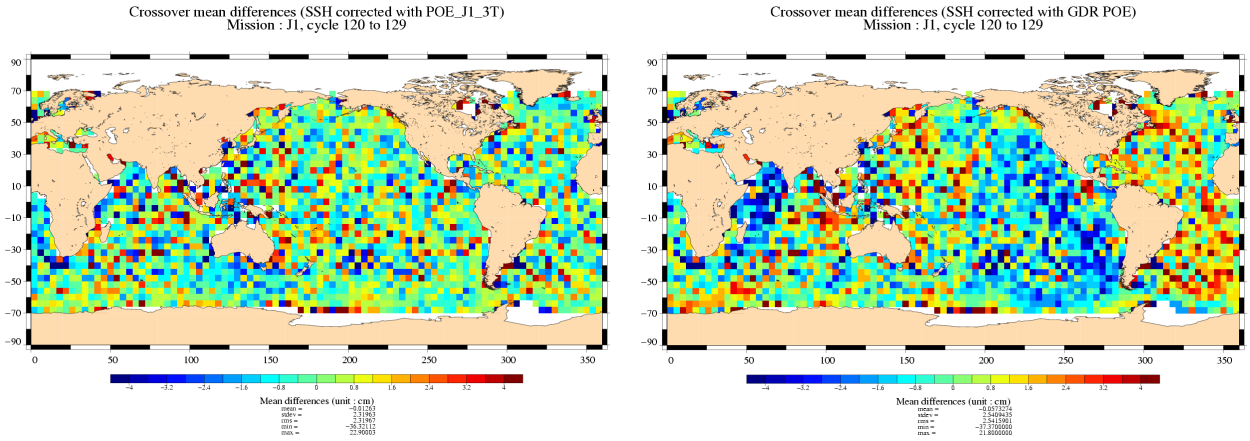

Figure 77: *Crossover mean differences. SSH corrected with POE_J1_3T 2005 (left) and GDR POE (right).*

Figure 78 shows the gain in variance of SSH differences at crossovers using the POE_J1_3T GDR orbit. The blue color means that the POE_J1_3T orbit has a lower variance of SSH differences at crossover than the GDR. The gain is very inhomogeneous. The POE_J1_3T orbit improves the performances in some regions of the south Pacific, the south Atlantic and Indian Ocean, whereas it deteriorates the performances in other regions.

Figure 79 shows the cycle by cycle mean and standard deviation of differences. The signal of mean differences at crossovers is centered on zero and has an amplitude of 1-2 cm. From cycles 120 to 123 the 2 lines are quite close. The standard deviation of the SSH difference at crossovers using the POE_J1_3T orbit is lower by about 1mm in average (7.18cm to 7.11cm). The gain in variance is plotted on Figure 80. Using the POE_J1_3T orbit allows us to improve the performance by 0.5 to 1.5 cm2, depending on the cycle.

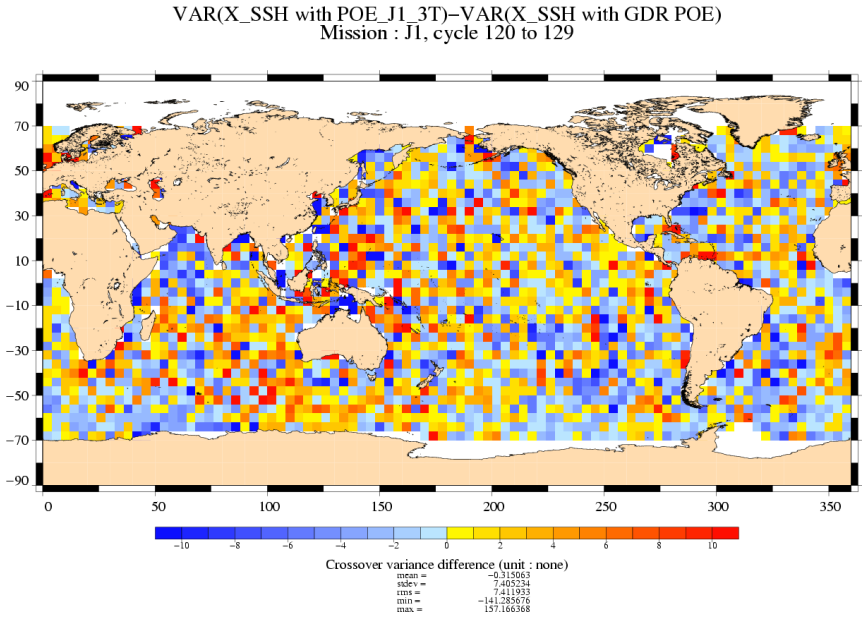

Figure 78: *VAR(X_SSH with POE_J1_3T 2005) - VAR(X_SSH with GDR POE).*

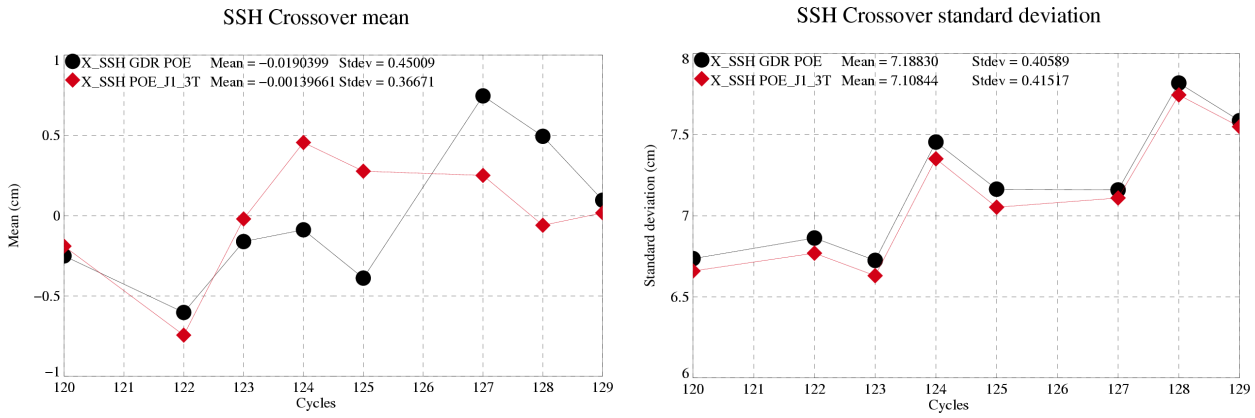

Figure 79: *Statistics per cycle of SSH: crossover mean (left) and crossover standard deviation (right).*

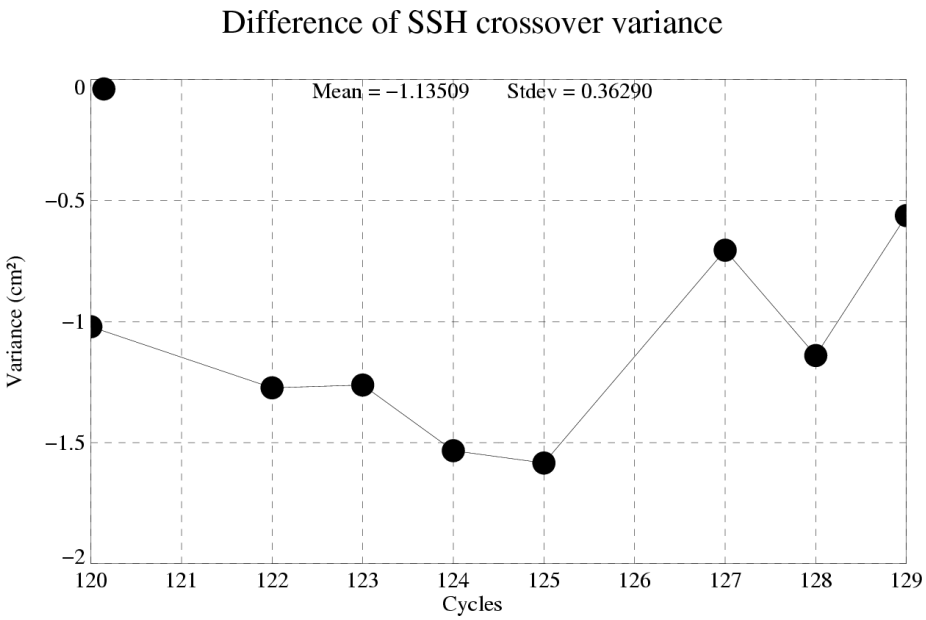

Figure 80: *Var(SSH differences at Xovers with POE_J1_3T 2005) - Var(SSH differences at Xovers with GDR POE).*

7.4.3.3 Along track performances

Figure 81 shows the gain in variance of SSH differences at crossovers using the POE_J1_3T /GDR orbit. The blue color means that the POE_J1_3T orbit has a lower variance of SSH differences at crossover than the GDR. The gain is not very clear. Regions of improvement and regions of deterioration are just side by side.

Figure 82 shows the cycle by cycle mean and standard deviation of SLA with the two orbits. As previously seen, there is almost no impact on the Mean Sea level. The SLA standard deviations are quite close from cycle 123 on. The gain in variance is plotted on Figure 83. Using the POE_J1_3T orbit allows only from cycle 123 on to improve the performance by 0 to 2 cm2, for cycle 120 to 122 it deteriorates the performances.

Figure 84 shows the cycle by cycle mean SLA with the two orbits decomposing ascending and descending passes. As already seen on figure 79 the sea level has not the same mean value on ascending and descending passes.

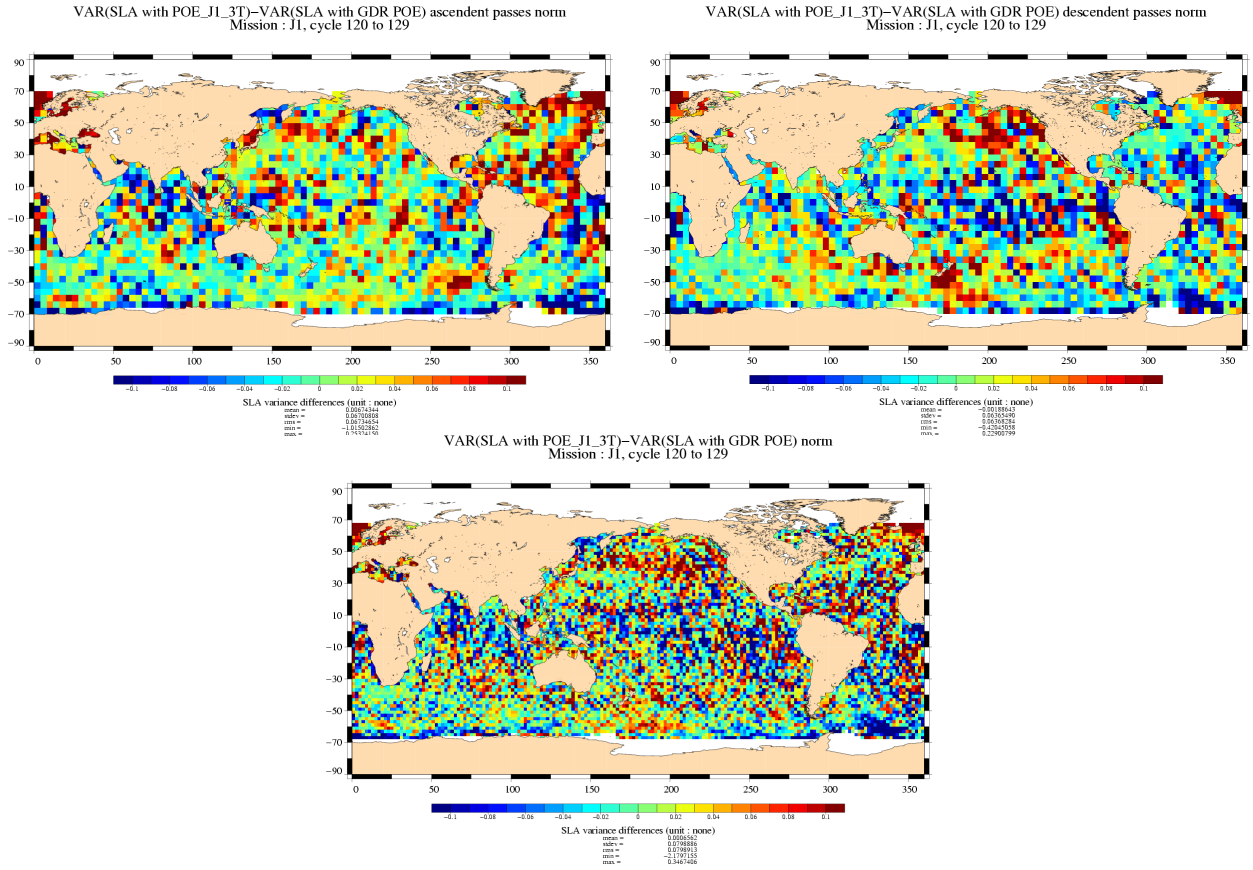

Figure 81: *[Var(SLA with POE_J1_3T 2005) - Var(SLA with GDR POE)]/Var(SLA with POE_J1_3T 2005). Ascending passes (left), descending passes (right) and total (bottom).*

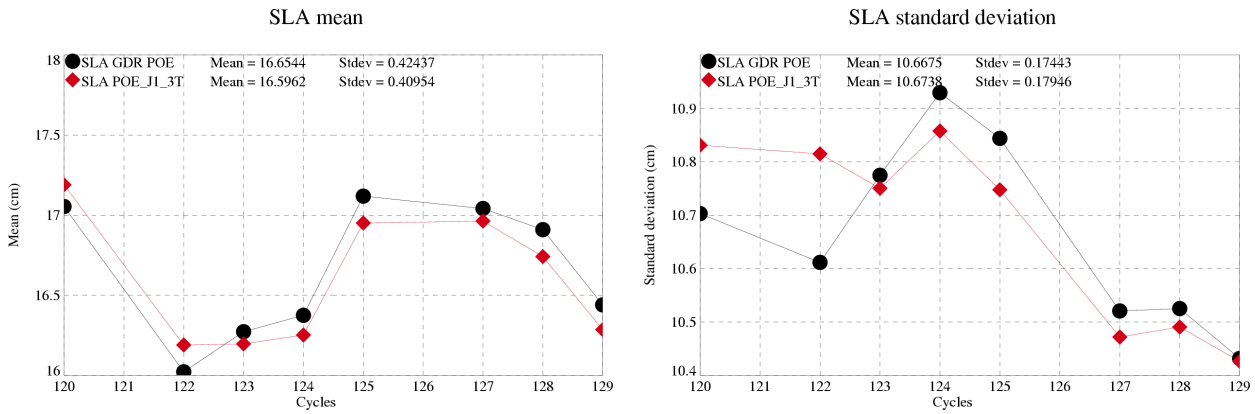

Figure 82: *SLA mean (left) and standard deviation (right) per cycle.*

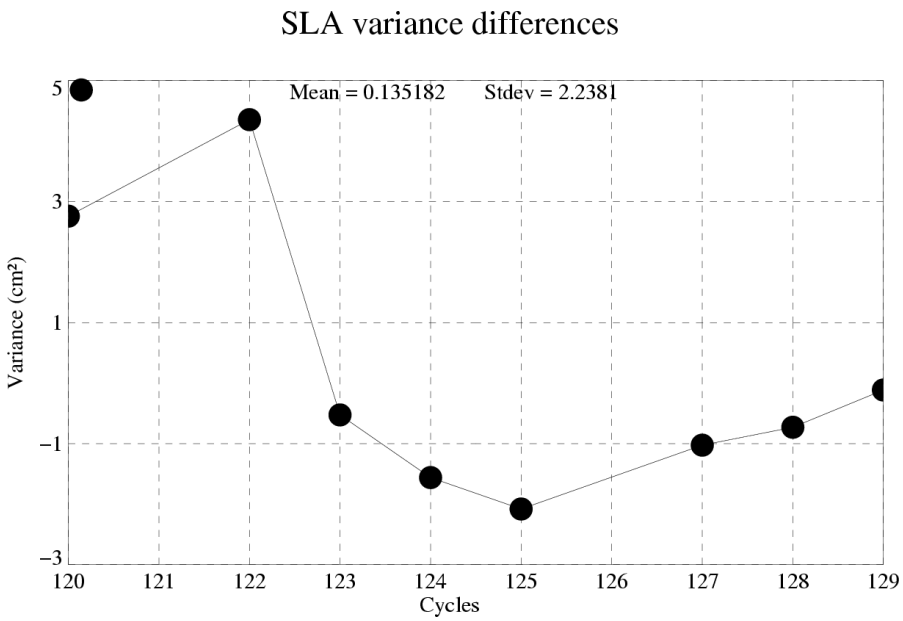

Figure 83: *Var(SLA with POE_J1_3T 2005) - Var(SLA with GDR POE).*

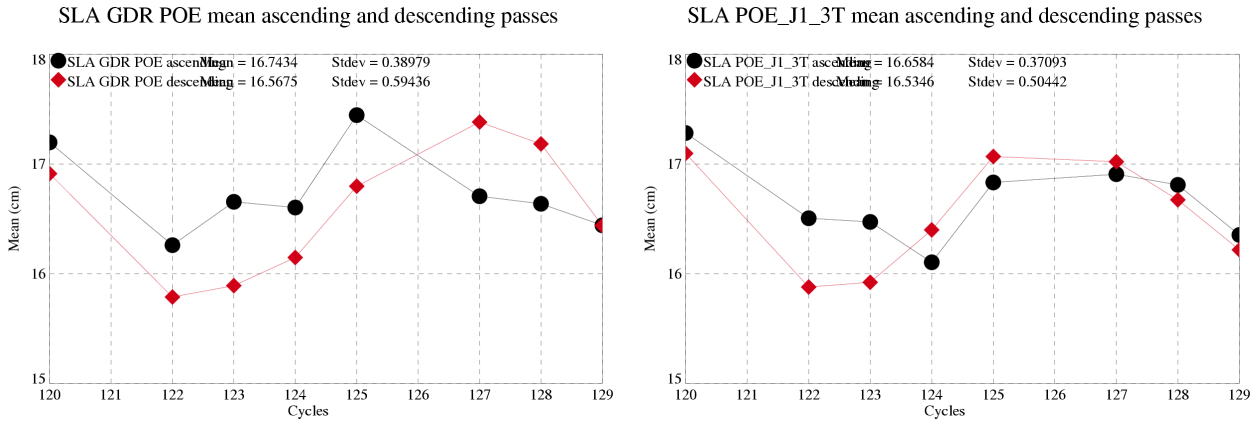

Figure 84: *SLA mean with GDR POE (left) and POE_J1_3T 2005 (right) per cycle.*

7.4.4 Conclusion

An analysis between the new CNES POE orbit and the GDR orbit has been performed. The variance of difference between the 2 orbits is 1.6 cm2. The use of the EIGEN3 gravity model has allowed reducing the geographical disparities of the crossover mean differences. The gain at crossovers, using the reprocessed POE orbit instead of the GDR orbit, is approximately 1.1 cm2. It is slightly less than expected. It is planned to continue this study with the final orbits used in the Jason GDR provided with the CMA version 7.1.

8 Mean Sea Level (MSL) and Sea Surface Temperature (SST) comparisons

This study has been carried out in order to monitor the MSL seen by all the operational altimeter missions. Long-term MSL change is a variable of considerable interest in the studies of global climate change. Then the objective here is on the one hand to survey the mean sea level trends and on the other hand to assess the consistency between all the MSL. Besides, the Reynolds SST is used to compare the MSL with an external data source. The mean SST is calculated the same way as the MSL.
The following missions have been used : TOPEX/Poseïdon (T/P), Jason-1 (J1), Geosat Follow-On (GFO) and Envisat. The MSL and SST time series have been plotted over global ocean. This allows us to correlate the MSL trends seen by each mission and to compare them with the SST.
In addition to these analysis, the maps of regional MSL change and SST change have been plotted for each mission over the Jason-1 period and the Envisat period. The differences of these maps have been performed; this is a way to display eventual local drifts.

8.1 SSH definition for each mission

The SSH formula is defined for all the satellites as below :

$$SSH = Orbit - Altimeter\ Range - \sum_{i=1}^{n} Correction_i$$

with :

$$\begin{aligned}
\sum_{i=1}^{n} Correction_i \;=\; & Dry\ troposhere\ correction : new\ S1\ and S2\ atmospheric\ tides\ applied \\
+\; & Combined\ atmospheric\ correction :\ MOG2D\ and\ inverse\ barometer \\
+\; & Radiometer\ wet\ troposhere\ correction \\
+\; & Filtered\ dual\ frequency\ ionospheric\ correction \\
+\; & Non\ parametric\ sea\ state\ bias\ correction \\
+\; & Geocentric\ ocean\ tide\ height,\ GOT\ 2000 :\ S1\ atmospheric\ tide\ is\ applied \\
+\; & Solid\ earth\ tide\ height \\
+\; & Geocentric\ pole\ tide\ height
\end{aligned}$$

Some additional corrections have been applied :

- For Jason-1 and Envisat the wet troposhere correction has been changed by the ECMWF model in order to remove the effects of abnormal changes or trends observed on the radiometer wet troposhere correction.
- For Envisat, the USO correction (Martini, 2003 [37]) has been applied.
- For T/P, the radiometer wet troposhere correction has been corrected from correction (Scharroo R., 2004 [51])

- For T/P, the relative bias between TOPEX and Poseidon and between TOPEX A and TOPEX B has been taken into account
- For T/P, the drift between the TOPEX and DORIS ionosphere corrections has been corrected for on Poseidon cycles.
- For Geosat Follow-On, the GIM model has been used for the ionospheric correction.

8.2 MSL and SST time series

8.2.1 MSL over global ocean

The MSL has been monitored for each satellite altimeter over global ocean in figure 85 over T/P period and Jason-1 period. The trends are similar for each satellite except for Envisat. The estimation of the Envisat MSL slope seems impacted by a strange behaviour on the first year as explained in Faugere et al. (2005, [22]). However, on the last two years, the Envisat slope is fully consistent with Jason-1 and T/P. The unexplained behavior of the first year of Envisat data is currently under investigation.

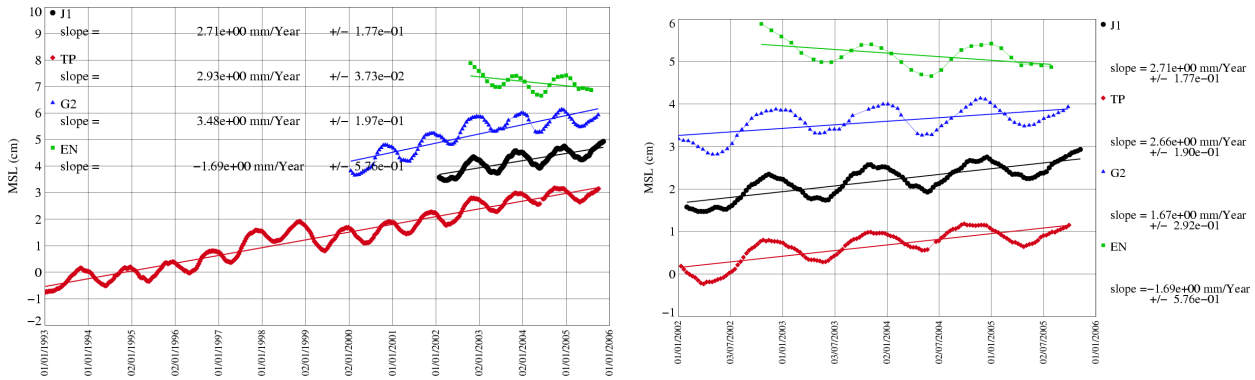

Figure 85: *MSL over global ocean for the T/P period on the left and the Jason-1 period on the right.*

In the following figure 86, MSL have been plotted after removing annual signal, semi-annual signal, and signals lower than 60 days. The T/P, Jason-1 and GFO MSL slopes over the Jason-1 period are still similar, respectively 2.75 mm/year, 2.3 mm/year and 1.8 mm/year with an adjustement formal error arround 0.2 mm/year. Notice that, for GFO, the slope computed over the global period is stronger, 3.2 mm/year. Beside, the orbit quality of Jason-1 early cycles is lower than usual. When those cycles are not taken into account, the Jason-1 slope increases by 0.3 mm/year to reach 2.6 mm/year. The conclusion is that the slope estimation is very sensitive. The formal error adjustement is only a mathematical error, not linked with the physical errors such as the orbit errors for instance.

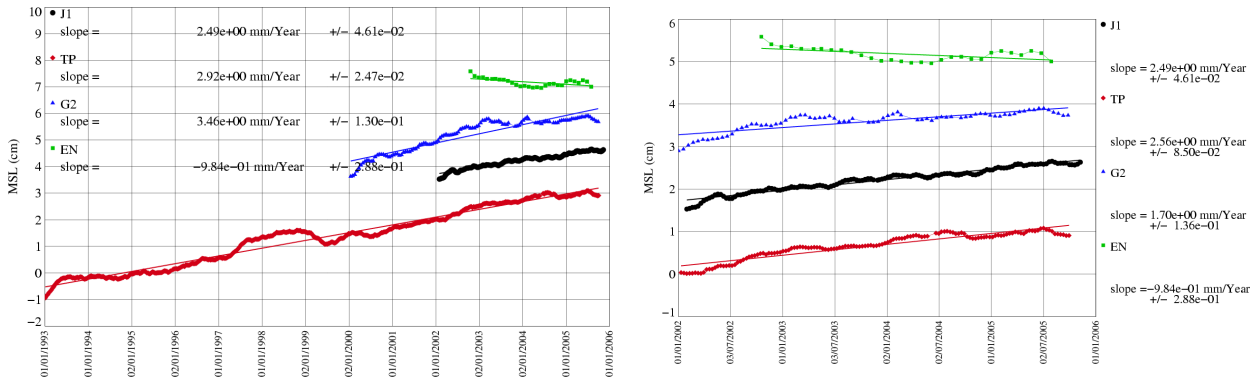

Figure 86: *MSL over global ocean for the T/P period on the left and the Jason-1 period on the right after removing annual, semi-annual and 60-day signals.*

8.2.2 SST over global ocean

In figure 87 on the left, the SST mean is compared to the T/P MSL. In the same figure on the right, annual signal, semi-annual signal, and signals lower than 60 days have been removed. Notice that the SST has been computed exactly over the T/P tracks. The SST increases by about 0.015 degree/year over the T/P period with a formal error close to 0.001 degree/year. The MSL and the SST don't have the same unit ("cm" and "degree"), thus to compare the 2 quantities, the SST scale is adjusted on the MSL scale so that the SST trend and the MSL trend are visually the same. This allows us to highlight that the SST dynamic is stronger than the MSL one. Inter-annual signal or climatic phenomena have a greater impact on the SST than on the MSL. Thus the SST trend estimation over a short period is not significant.

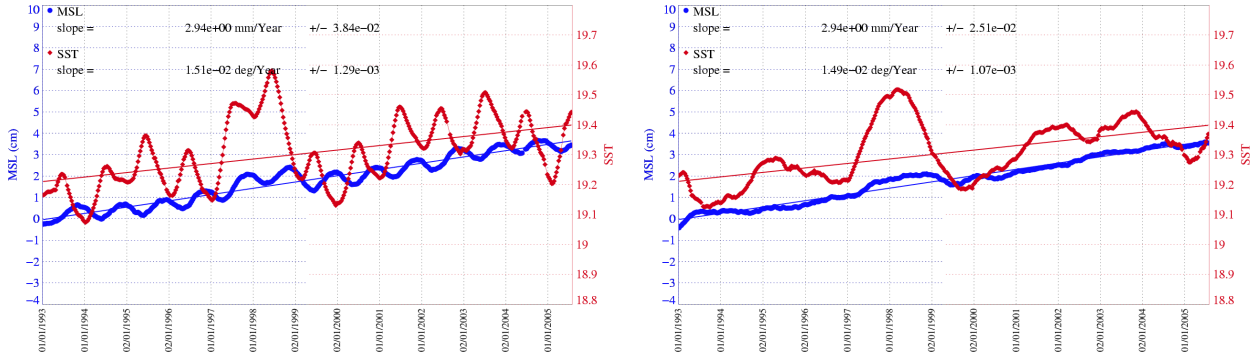

Figure 87: *MSL and SST over global ocean for the T/P period on the left, and after removing annual, semi-annual and 60-day signals on the left.*

8.3 Spatial MSL and SST slopes

8.3.1 Methodology

In order to monitor the MSL, the spatial MSL slopes have been calculated. The SLA grids (2x2 degree bins) have been computed cycle per cycle, and the slope has been computed on each grid point. As for time analysis, 60 day, semi-annual and annual signals have been removed before estimating the slopes. Then, the MSL slopes have been mapped for each mission. These maps are used to compare the MSL slopes between each altimeter mission. This allows us to detect potential local drifts.
Besides, the SST slopes have been computed the same way in order to correlate them with the MSL slopes.

8.3.2 Spatial MSL slopes over Jason-1 period

The MSL slopes have been plotted for Jason-1 (on the right) and T/P (on the left) over Jason-1 period in figure 88. The MSL trends seen by the two satellites are similar. However, differences greater than 4mm/year can be observed on the T/P-Jason-1 map (at the bottom).

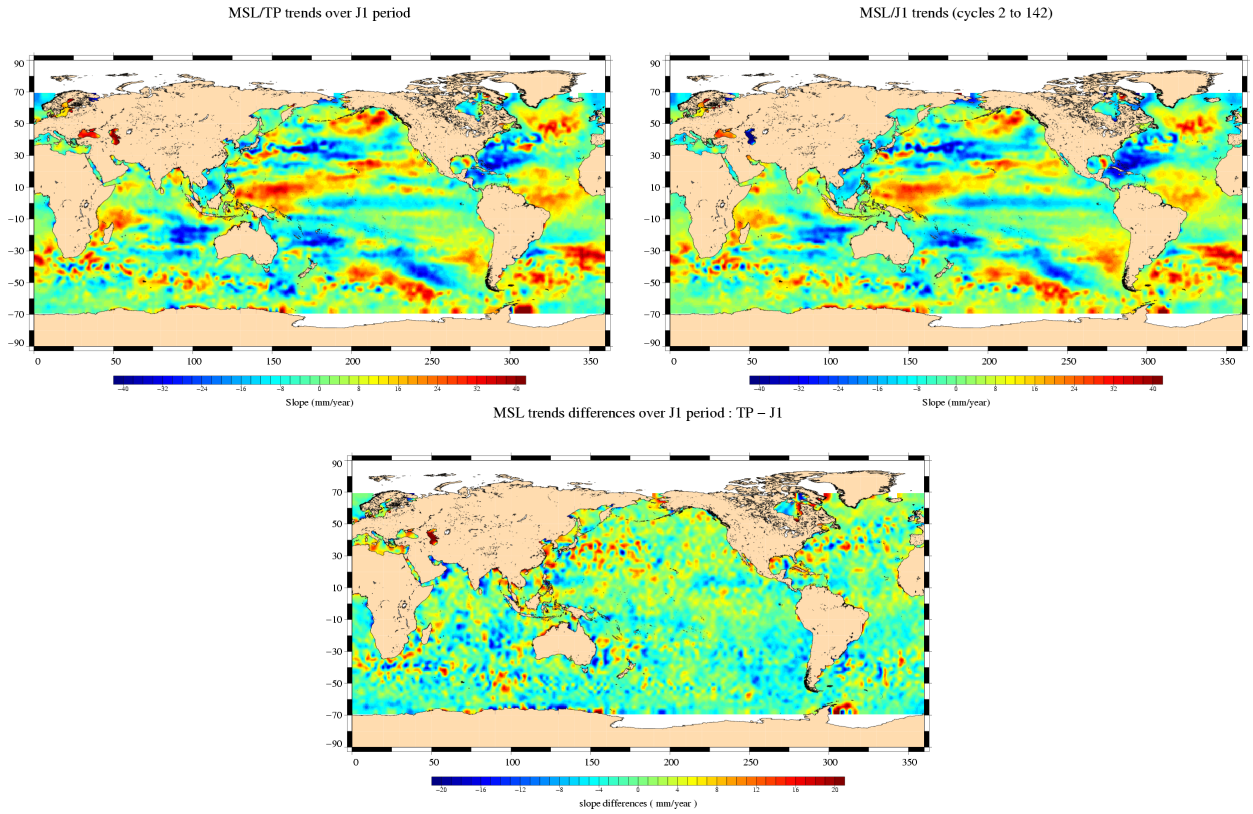

Figure 88: *MSL slopes over Jason-1 period for T/P (left) and Jason-1 (right), MSL slope differences between Jason-1 and T/P (bottom)*

8.3.3 Spatial MSL slopes over Envisat period

The same work has been performed over Envisat period using Envisat data in figure 89. The 3 maps are very similar.
In figure 90, the slope differences between each mission have been plotted. They allow us to observe differences in equatorial areas between Jason-1 and Envisat, and between T/P and Jason-1. Between Envisat and T/P, the difference has not the same geographical pattern. Investigations are on-going to understand the reasons of this observation.

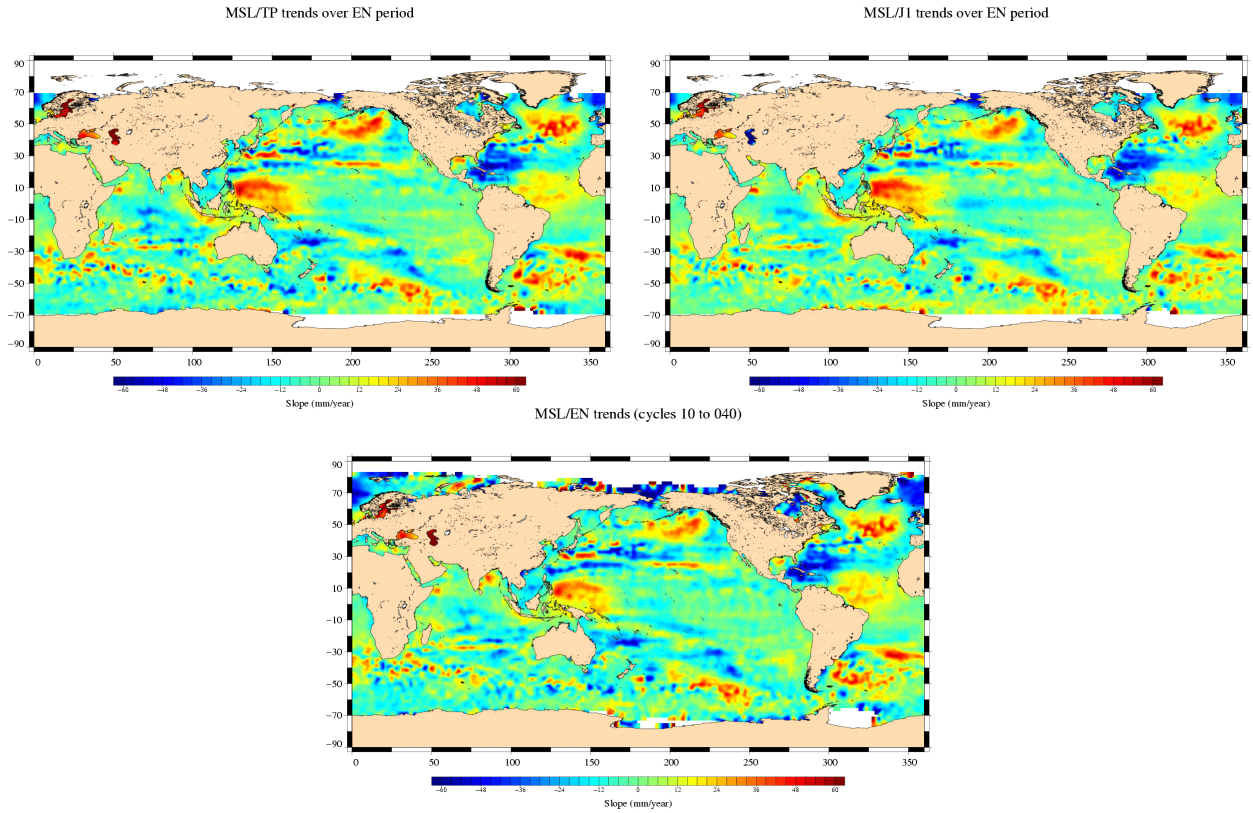

Figure 89: *MSL slopes over Envisat period for T/P (left), Jason-1 (right) and Envisat (bottom)*

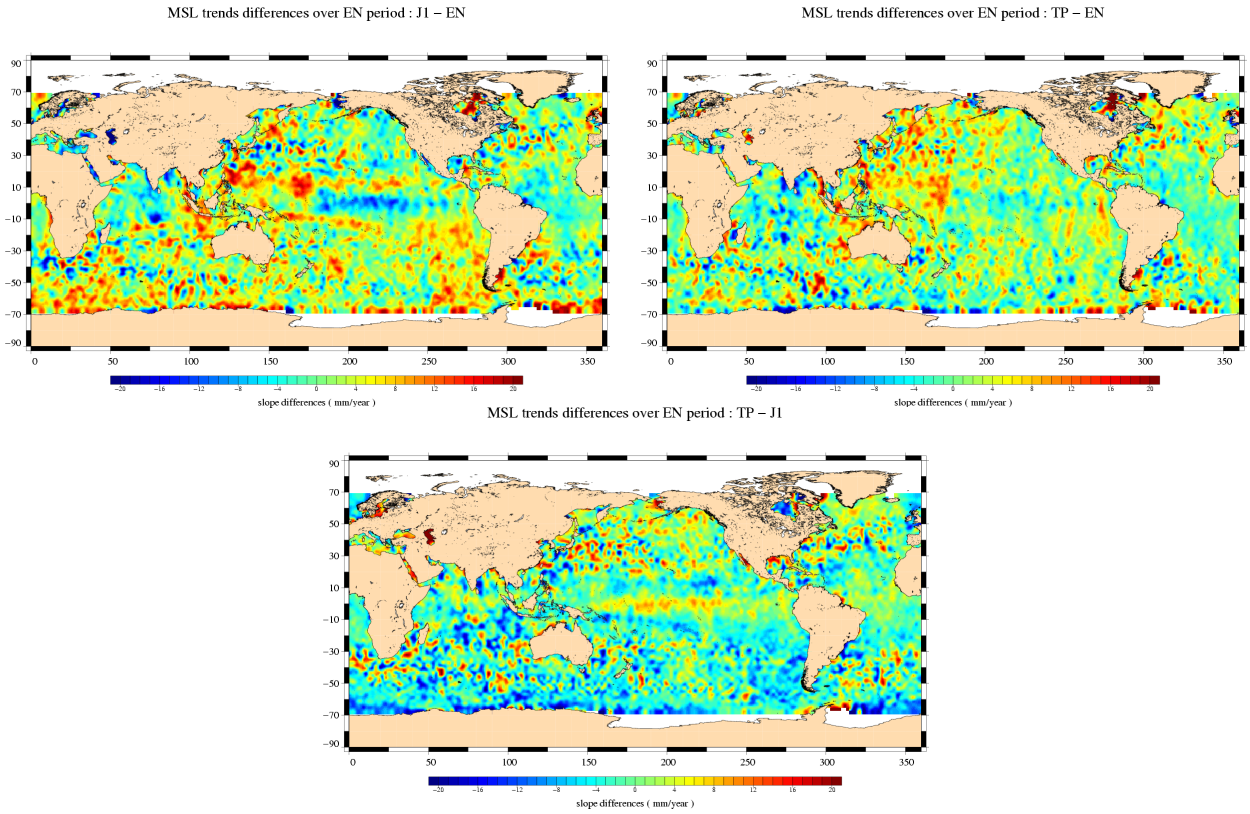

Figure 90: *MSL slopes differences over Envisat period between Jason-1 and Envisat (left), T/P and Envisat (right) and T/P and Jason-1 (bottom)*

8.3.4 Spatial SST and MSL slopes for T/P

The T/P MSL slopes are mapped in figure 91 on the left. In order to correlate the MSL and the SST, the SST slopes have been plotted in the same figure on the right.
13 years of T/P data have been used to estimate the slopes; this allows us to have a good estimation of the local MSL trends. The adjustment errors of the MSL and the SST slopes are mapped in figure 92.

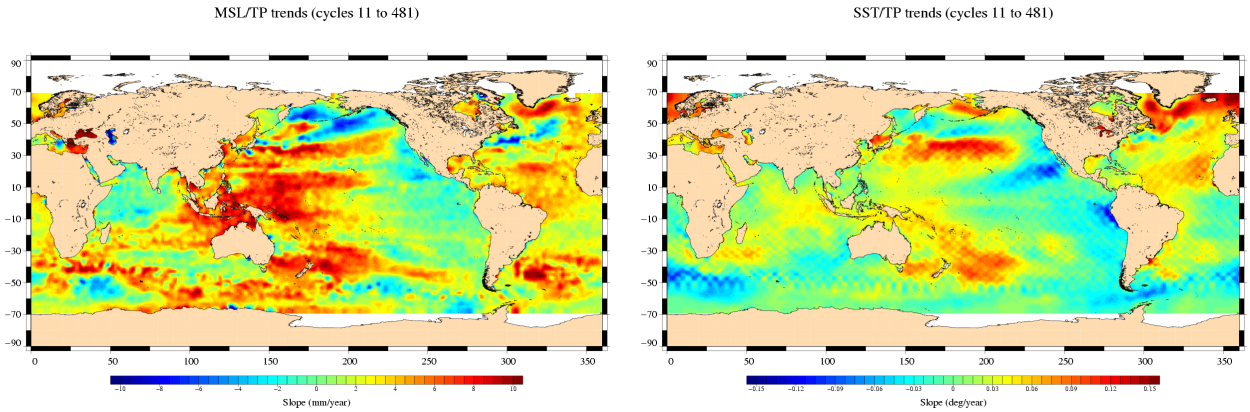

Figure 91: *T/P MSL and SST slopes over 13 years*

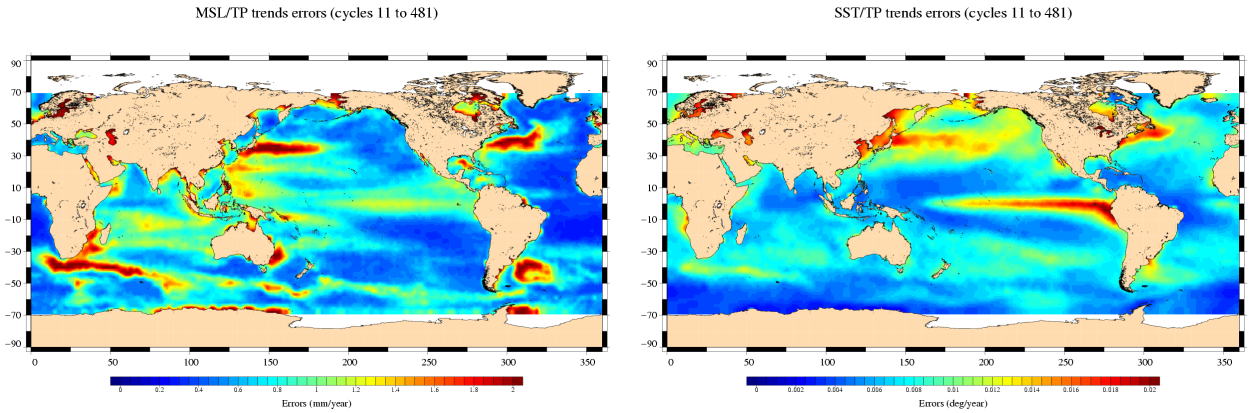

Figure 92: *Adjustment errors of T/P MSL and SST slopes over 13 years*

8.3.5 "El Niño" impact on SST and MSL slope estimations

The MSL and SST regional trends are largely impacted by inter-annual signal or oceanic phenomena such as "El Niño" for instance. The 4 maps in the figure 93 show the trend for the SST and the MSL before and after "El Niño". The first period ranges from 1992 and 1996 included, whereas the second period ranges from 1999 to 2004 included.
he MSL and SST regional trends are largely impacted by inter-annual signal or oceanic phenomena such as "El Niño" for instance. The 4 maps in the figure 93 show the trend for the SST and the MSL before and after "El Niño". The first period ranges from 1992 and 1996 included, whereas the second period ranges from 1999 to 2004 included.
MSL and SST trends are stronger for each period separetely than for the global period. In the Pacific ocean, the absolute values are greater than 20 mm/year for the MSL and 0.3 degree/year for the SST. SST and MSL maps show a strong correlation on the two period of time. But for both SST and MSL, the trends on the first period are very different from the trends of the second period. This is particularly true in tropical areas.
Finally, these maps highlight the importance of having long time series to evaluate the regional trends with a good accuracy.

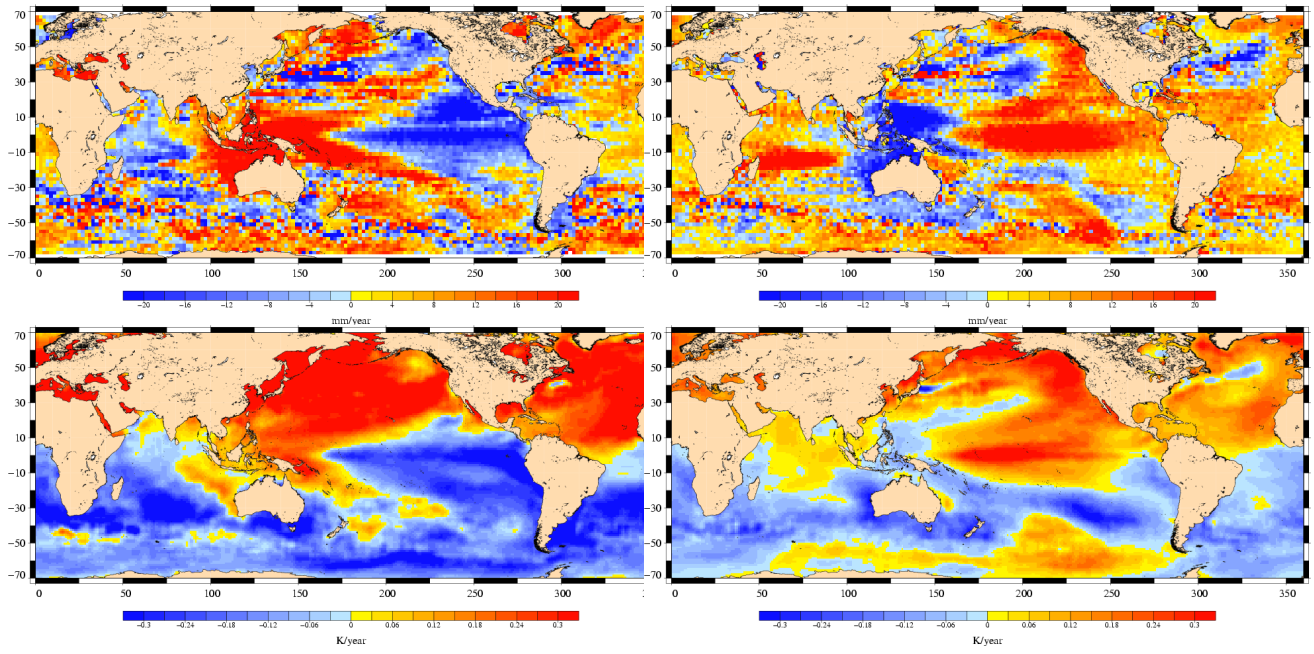

Figure 93: *Adjustment errors of T/P MSL and SST slopes over 13 years before and after "El Niño"*

9 Conclusion

4 years of Jason-1 data (GDRs 'a') are now available in a homogeneous series. The good quality of Jason-1 data has been shown in this report: main altimeter parameters have the same behaviors as T/P ones; crossover and along-track performances are very similar between both satellites; the T/PJason-1 SSH bias is stable about -14 cm. However anomalies have been detected on the JMR corrections and will be taken into account in the next GDR release. Furthermore, geographical features are observed on SSH differences between TOPEX and Jason-1. The orbit calculation can explain these geographical differences. They will be probably partly canceled using new gravity models such GRACE as shown in the dedicated section of this report.

Since the beginning of The Jason-1 mission, T/P and Jason-1 overflew the ocean over 2 parallel passes except the 21 first cycles where there were on the same pass. Thanks to this long flight configuration, performances comparisons between the both missions had be performed with success during 4 years, proving the major objective of the Jason-1 mission to continue the T/P high precision is reached. But now, the TOPEX/Poseidon mission comes to an end after more than 13 years of loyal services. It is finished since 9th October 2005, following the loss of the pitch reaction wheel. From now on, Jason-1 and T/P calibration will be only performed over the T/P period in the frame of GDRs reprocessing.

The GDR reprocessing is planned for next year 2006. GDRs 'b' will contain improvements. The major evolutions are the implementation of new geophysical corrections (tidal models, MOG2D), a new retracking algorithm (order 2 MLE4), new sea state bias correction and a new precise orbit based on a GRACE gravity model and tri-technic method. Beside it is probably planned to re-process T/P M-GDRs data with similar data. Then, performances and comparisons will be carried out using these new data in order to assess the GDRs re-processing and to assess the better consistency between Jason-1 and T/P sea surface height.

References

[1] Ablain, M., J. Dorandeu, Y. Faugère, F. Mertz, B. Soussi, F. Mercier, P. Vincent, and N. Picot. 2003a. SSALTO/CALVAL Jason-1 data quality assessment and Jason-1 / TOPEX cross-calibration using GDRs. *Paper presented at the Jason-1 and TOPEX/Poseidon Science Working Team Meeting, Arles (France), November.*

[2] Ablain, M., J. Dorandeu, Y. Faugere, F. Mertz, 2004. Jason-1 Validation and Cross-calibration activities Contract No 731/CNES/00/8435/00. Available at: http://www.jason.oceanobs.com/documents/calval/validation_report/j1/annual_report_j1_2004.pdf

[3] Ablain, M. and J. Dorandeu, 2005. TOPEX/Poseidon validation activities, 13 years of T/P data (GDR-Ms), Available at: http://www.jason.oceanobs.com/documents/calval/validation_report/tp/annual_report_tp_2005.pdf

[4] Ablain, M., S. Philipps, P. Thibaut, J. Dorandeu, and N. Picot 2005. Jason-1 GDR Quality Assessment Report. Cycle 135. SALP-RP-P2-EX-21072-CLS135, May. http://www.jason.oceanobs.com/html/calval/validation_report/j1/j1_calval_bulletin_135_fr.html

[5] Amarouche, L., P. Thibaut, O.Z. Zanife, P. Vincent, and N. Steunou. 2004. Improving the Jason-1 Ground Retracking to Better Account or Attitude Effects. *Mar. Geod.***27 (1-2): 171-197.**

[6] Arnault, S., N. Chouaib, D. Diverres, S. Jaquin, and O. Coze, 2004. Comparison of TOPEX/Poseidon and JASON Altimetry with ARAMIS In Situ Observations in the Tropical Atlantic Ocean. *Mar. Geod.***27 (1-2): 15-30.**

[7] Brown G.S., "The average impulse response of a rough surface and its application", IEEE Transactions on Antenna and Propagation, Vol. AP 25, N1, pp. 67-74, Jan. 1977.

[8] Carayon, G., N. Steunou, J. L. Courrière, and P. Thibaut. 2003. Poseidon 2 radar altimeter design and results of in flight performances. *Mar. Geod.***26(3-4): 159-165.**

[9] Carrère, L., and F. Lyard, Modeling the barotropic response of the global ocean to atmospheric wind and pressure forcing - comparisons with observations. 2003. Geophys. Res. Lett., 30(6), 1275, doi:10.1029/2002GL016473.

[10] Chambers, D. P., S. A. Hayes, J. C. Ries, and T. J. Urban. 2003. New TOPEX sea state bias models and their effect on global mean sea level. J. Geophys. Res. 108(C10): 3305.

[11] Chambers, D., P., J. Ries, T. Urban, and S. Hayes. 2002. Results of global intercomparison between TOPEX and Jason measurements and models. Paper presented at the Jason-1 and TOPEX/Poseidon Science Working Team Meeting, Biarritz (France), 10-12 June.

[12] Chambers, D. P. and B. D. Tapley, 1998: Reduction of Geoid Gradient Error in Ocean Variability from Satellite Altimetry. *Mar. Geod.*, **21, 25-39.**

[13] Choy, K, J. C. Ries, and B. D Tapley, 2004. Jason-1 Precision Orbit Determination by Combining SLR and DORIS with GPS Tracking Data. *Mar. Geod.***27(1-2): 319-331.**

[14] Desai, S. D., and B. J. Haines, 2004. Monitoring Measurements from the Jason-1 Microwave Radiometer and Independent Validation with GPS. *Mar. Geod.***27(1-2): 221-240.**

[15] Dorandeu, J., M. H. De Launay, F. Mertz and J. Stum, 2001. AVISO/CALVAL yearly report. 8 years of TOPEX/Poseidon data (M-GDRs).

[16] Dorandeu, J. and P.Y. Le Traon, 1999: Effects of Global Atmospheric Pressure Variations on Mean Sea Level Changes from TOPEX/Poseidon. *J. Atmos. Technol.,***16, 1279-1283.**

[17] Dorandeu, J, M. Ablain, Y . Faugere, B. Soussi, and J . Stum. 2002a. Global statistical assessment of Jason-1 data and Jason-1/TOPEX/Poseiodn Cross-calibration. Paper presented at the Jason-1 and TOPEX/Poseidon Science Working Team Meeting, Biarritz (France), **10-12 June.**

[18] Dorandeu, J., P. Thibaut, O. Z. Zanife, Y. Faugère, G. Dibarboure, N. Steunou, and P. Vincent. 2002b. Poseidon-1, Poseidon-2 and TOPEX noise analysis. Paper presented at the Jason-1 and TOPEX/Poseidon Science Working Team Meeting, New-Orleans (USA), **October.**

[19] Dorandeu., J., M. Ablain, P. Y. Le Traon, 2003a. Reducing Cross-track Geoid Gradient Errors around TOPEX/Poseidon and Jason-1 Nominal Tracks. Application to Calculation of Sea Level Anomalies. *J. Atmos. Oceanic Technol.,***20, 1826-1838.**

[20] Dorandeu, J., Y. Faugère, and F. Mertz. 2003b. ENVISAT data quality: Particular investigations. Proposal for ENVISAT GDR evolutions. Paper presented at the ENVISAT Ra-2 & MWR Quality Working Group meeting. **October.**

[21] Dorandeu.,J., M. Ablain, Y. Faugère, F. Mertz, 2004 : Jason-1 global statistical evaluation and performance assessment. Calibration and cross-calibration results. *Mar. Geod.***This issue.**

[22] Y.Faugere, J.Dorandeu, F.Lefevre, N.Picot and P.Femenias, 2005: Envisat ocean altimetry performance assessment and cross-calibration. Submitted in the special issue of SENSOR 'Satellite Altimetry: New Sensors and New Applications'

[23] Fu, L. L., 2002. Minutes of the Joint Jason-1 and TOPEX/Poseidon Science Working Team Meeting, Oct. 21-23, JPL Tech. Report. JPL D-25506, edited by L. Fu, USA.

[24] Gaspar, P., S. Labroue, F. Ogor, G. Lafitte, L. Marchal and M. Rafanel, 2002: Improving non parametric estimates of the sea state bias in radar altimeter measurements of sea level. *J. Atmos. Oceanic Technol.,***19, 1690-1707.**

[25] Haines, B., Y. Bar-Sever, W. Bertiger, S. Desai, P. Willis, 2004: One-Centimeter Orbit Determination for Jason-1: New GPS-Based Strategies. *Mar. Geod.***27(1-2): 299-318.**

[26] Hamming, R. W., 1977. Digital Filter. Prentice-Hall Signal Processing Series, edited by A. V. Oppenheim Prentice-Hall, Englewood Cliffs, N. J.

[27] Hernandez, F. and P. Schaeffer, 2000: Altimetric Mean Sea Surfaces and Gravity Anomaly maps intercomparisons AVI-NT-011-5242-CLS, 48 pp. CLS Ramonville St Agne.

[28] Hirose N., Fukumori I., Zlotnicki V., Ponte R. M. 2001: High-frequency barotropic response to atmospheric disturbances : sensitivity to forcing, topography, and friction, J. Geophys. Res. 106(C12), 30987-30996.

[29] Keihm, S. J., V. Zlotnicki, and C. S. Ruf. 2000. TOPEX Microwave Radiometer performance evaluation, 1992-1998, *IEEE Trans. Geosci. Rem. Sens.,***38(3): 1379-1386.**

[30] Labroue, S. and P. Gaspar, 2002: Comparison of non parametric estimates of the TOPEX A, TOPEX B and JASON 1 sea state bias. Paper presented at the Jason 1 and TOPEX/Poseidon SWT meeting, New-Orleans, 21-12 October.

[31] Labroue, S. P. Gaspar, J. Dorandeu, O.Z. Zanifé, P. Vincent, and D. Choquet. 2004. Non Parametric Estimates of the Sea State Bias for Jason 1 Radar Altimeter. *Mar. Geod.***This issue.**

[32] Lemoine, F. G., S. B. Luthcke, N. P. Zelinsky, D. S. Chinn, T. A. Williams, C. M. Cox, and B. D. Beckley. 2003. An Evaluation of Recent gravity Models Wrt to Altimeter Satellite Missions.*Paper presented at the Jason-1 and TOPEX/Poseidon Science Working Team Meeting,***Arles (France), November.**

[33] Le Traon, P.-Y., J. Stum, J. Dorandeu, P. Gaspar, and P. Vincent, 1994: Global statistical analysis of TOPEX and POSEIDON data. *J. Geophys. Res.,***99, 24619-24631.**

[34] Le Traon, P. Y., and G. Dibarboure, 2004. An Illustration of the Contribution of the TOPEX/Poseidon-Jason-1 Tandem Mission to Mesoscale Variability Studies. *Mar. Geod.***27(1-2) 3-13.**

[35] Luthcke. S. B., N. P. Zelinsky, D. D. Rowlands, F. G. Lemoine, and T. A. Williams. 2003. The 1-Centimeter Orbit: jason-1 Precision Orbit Determination Using GPS, SLR, DORIS, and Altimeter Data. *Mar. Geod.***26(3-4): 399-421.**

[36] Marshall, J. A., N. P. Zelinsky, S. B. Luthcke, K. E., Rachlin, and R. G. Williamson. 1995. The temporal and spatial characterustics of TOPEX/Poseidon radial orbit error. *J. Geophys. Res.* **100(C2):25331-25352.**

[37] Martini A., 2003: Envisat RA-2 Range instrumental correction : USO clock period variation and associated auxiliary file, Technical Note ENVI-GSEG-EOPG-TN-03-0009 Available at http://earth.esa.int/pcs/envisat/ra2/articles/USO_clock_corr_aux_file.pdfhttp://earth.esa.int/pcs/envisat/ra2/auxdata/

[38] Ménard, Y. 2003. Minutes of the Joint TOPEX/Poseidon and Jason-1 Science Working Team Meeting. CNES-SALP-CR-MA-EA-15190-CN.

[39] Obligis, E, N. Tran, and L. Eymard, 2004. An assessment of Jason-1 microwave radiometer measurements and products. *Mar. Geod.***27(1-2) 255-277.**

[40] Phaden Mc.J., April2003 : Evolution of the 2002-03 El Niño, *UCLA Tropical Meteorology and Climate Newsletter,***No57**.

[41] Picot, N., K. Case, S. Desai and P. Vincent, 2003. AVISO and PODAAC User Handbook. IGDR and GDR Jason Products, SMM-MU-M5-OP-13184-CN (AVISO), JPL D-21352 (PODAAC).

[42] Provost., C. Arnault, N. Chouaib, A. Kartavtseff, L. Bunge, and E. Sultan, 2004. TOPEX/Poseidon and Jason Equatorial Sea Surface Slope Anomaly in the Atlantic in 2002: Comparison with Wind and Current Measurements at 23W. *Mar. Geod.***27(1-2) 31-45.**

[43] Quartly, G. D., 2004. Sea State and Rain: A Second Take on Dual-Frequency Altimetry. Mar. Geod. 27(1-2) 133-152

[44] Queffeulou, P. 2004. Long Term Validation of Wave Height Measurements from Altimeters. *Mar. Geod.***This issue.**

[45] Ray, R. (1999). A Global Ocean Tide Model From TOPEX/Poseidon Altimetry/ GOT99.2 - NASA/TM-1999-209478. Greenbelt, MD, Goddard Space Flight Center/NASA: 58

[46] Ray, R. D., and B. D. Beckley, 2003. Simultaneaous Ocean Wave Measurements by the Jason and Topex Satellites, with Buoy and Model Comparisons *Mar. Geod.***26(3-4): 367-382.**

[47] Ray, R. D. 2003. Benefits of the joint T/P−Jason mission for improving knowledge of coastal tides. Paper presented at the Jason-1 and TOPEX/Poseidon Science Working Team Meeting, Arles (France), November.

[48] Ray, R.D. and R.M. Ponte, Barometric tides from ECMWF operational analyses. *Annales G*, **99, 24995-25008**, 1994.

[49] Ruf C., S. Brown, S. Keihm and A. Kitiyakara, 2002a. JASON Microwave Radiometer : On Orbit Calibration, Validation and Performance, *Paper presented at the Jason-1 and TOPEX/Poseidon Science Working Team Meeting, New-Orleans (USA),***21-23 October.**

[50] Ruf. C. S., 2002b. TMR Drift - Correction to 18 GHz Brightness Temperatures, Revisited. Report to TOPEX Project, June.

[51] Scharroo R., J. L. Lillibridge, and W. H. F. Smith, Cross-Calibration and Long-term Monitoring of the Microwave Radiometers of ERS, TOPEX, GFO, Jason-1, and Envisat, **Marine Geodesy, 27:279-297**, 2004.

[52] Tierney, C., J. Wahr, et al. 2000. Short-period oceanic circulation: implications for satellite altimetry. Geophysical Research Letters 27(9): 1255-1258

[53] Thibaut, P. O.Z. Zanifé, J.P. Dumont, J. Dorandeu, N. Picot, and P. Vincent, 2002. Data editing : The MQE criterion. Paper presented at the Jason-1 and TOPEX/Poseidon Science Working Team Meeting, New-Orleans (USA), 21-23 October.

[54] Thibaut, P. L. Amarouche, O.Z. Zanife, N. Steunou, P. Vincent, and P. Raizonville. 2004. Jason-1 altimeter ground processing look-up tables. *Mar. Geod.***This issue.**

[55] Tournadre, J. 2002. Validation of the rain flag. Paper presented at the Jason-1 and TOPEX/Poseidon Science Working Team Meeting, Biarritz (France), 10-12 June.

[56] Tran, N., D. W. Hancock III, G.S. Hayne. 2002. "Assessment of the cycle-per-cycle noise level of the GEOSAT Follow-On, TOPEX and POSEIDON." *J. Atmos. Oceanic Technol.,***19(12): 2095-2117.**

[57] Vincent, P., S. D. Desai, J. Dorandeu, M. Ablain, B. Soussi, P. S. Callahan, and B. J. Haines 2003a. Jason-1 Geophysical Performance Evaluation. *Mar. Geod.***26(3-4): 167-186.**

[58] Vincent, P., S. Desai, J. Dorandeu, M. Ablain, B. Soussi, Y. Faugère, B. Haines, N. Picot, K. Case, A. Badea, 2003b. Summary about Data Production and Quality. Paper presented at the Jason-1 and TOPEX/Poseidon Science Working Team Meeting, Arles (France), November

[59] Vincent, P., J.P. Dumont, N. Steunou, O.Z. Zanife, P. Thibaut, and J. Dorandeu. 2003c. Jason-1 I/GDR science processing: ground retracking improvements. Paper presented at the European Geophysical Society meeting, Nice, April.

[60] Zanife, O. Z., P. Vincent, L. Amarouche, J. P. Dumont, P. Thibaut, and S. Labroue, 2003. Comparison of the Ku-band range noise level and the relative sea-state bias of the Jason-1, TOPEX and Poseidon-1 radar altimeters. *Mar. Geod.***26(3-4): 201-238.**